NASA CONTRACTOR REPORT

NASA CR-693

THEORETICAL INVESTIGATION OF THE ABSORPTIVE PROPERTIES OF SMALL PARTICLES AND HEAVY-ATOM GASES

by N. L. Krascella

Prepared by
UNITED AIRCRAFT CORPORATION
East Hartford, Conn.
for

NATIONAL AERONAUTICS AND SPACE ADMINISTRATION • WASHINGTON, D. C. • JANUARY 1967

THEORETICAL INVESTIGATION OF THE ABSORPTIVE PROPERTIES OF SMALL PARTICLES AND HEAVY-ATOM GASES

By N. L. Krascella

Prepared under Contract No. NASw-847 by
UNITED AIRCRAFT CORPORATION
East Hartford, Conn.

for

NATIONAL AERONAUTICS AND SPACE ADMINISTRATION

For sale by the Clearinghouse for Federal Scientific and Technical Information
Springfield, Virginia 22151 – Price $2.50

FOREWORD

An exploratory experimental and theoretical investigation of gaseous nuclear rocket technology is being conducted by the United Aircraft Corporation Research Laboratories under Contract NASw-847 with the joint AEC-NASA Space Nuclear Propulsion Office. The Technical Supervisor of the Contract for NASA is Captain W. A. Yingling (USAF). Results of the investigation conducted during the period between September 15, 1965 and September 15, 1966 are described in the following six reports (including the present report) which comprise the required fourth Interim Summary Technical Report under the Contract:

1. Krascella, N. L.: Theoretical Investigation of the Absorptive Properties of Small Particles and Heavy-Atom Gases. NASA CR-693, 1967. (Unclassified) (present report)

2. Kinney, R. B.: Theoretical Effect of Seed Opacity and Turbulence on Temperature Distributions in the Propellant Region of a Vortex-Stabilized Gaseous Nuclear Rocket (U). NASA CR-694, 1967. (report classified Confidential)

3. Kesten, A. S., and N. L. Krascella: Theoretical Investigation of Radiant Heat Transfer in the Fuel Region of a Gaseous Nuclear Rocket Engine. NASA CR-695, 1967. (Unclassified)

4. Roback, R.: Theoretical Performance of Rocket Engines Using Gaseous Hydrogen in the Ideal State at Stagnation Temperatures up to 20,000 R. NASA CR-696, 1967. (Unclassified)

5. Latham, T. S.: Nuclear Criticality Study of a Specific Vortex-Stabilized Gaseous Nuclear Rocket Engine (U). NASA CR-697, 1967. (report classified Confidential)

6. McLafferty, G. H., H. E. Bauer, and D. E. Sheldon: Preliminary Conceptual Design Study of a Specific Vortex-Stabilized Gaseous Nuclear Rocket Engine (U). NASA CR-698, 1967. (report classified Confidential)

Theoretical Investigation of the Absorption Properties of Small Particles and Heavy-Atom Gases

TABLE OF CONTENTS

Theoretical Investigation of the Absorptive Properties of Small Particles and Heavy-Atom Gases

SUMMARY

A theoretical investigation was conducted to determine the spectral and mean absorption characteristics of solid and gaseous elemental materials which might be utilized to control the transfer of radiant energy in the propellant region of a gaseous nuclear rocket engine. Spectral extinction, absorption and scattering parameters were calculated, based on the Mie theory, for spherical molybdenum, niobium, tantalum and cadmium particles having radii of 0.01, 0.05, 0.10, and 0.50 μ. Similar calculations were made for spherical tungsten particles at five temperatures between 1600 K (2880 R) and 2400 K (4320 R). The tungsten calculations were based on analytically extrapolated refractive indices for wavelengths between 0.1 and 30 μ at each temperature. The Rosseland mean absorption parameter of spherical tungsten particles having a radius of 0.05 μ was calculated for temperatures between 1000 K (1800 R) and 5600 K (10,080 R). In addition, the spectral absorption parameters and normal spectral reflectivities of bulk aluminum, cadmium, carbon, cobalt, hafnium, iridium, iron, molybdenum, niobium, nickel, palladium, platinum, silicon, tantalum, thallium, titanium, tungsten, vanadium, and zirconium were calculated. The bulk absorption parameters apply to seeds in the form of thin plates and are generally higher than those for seeds in the form of spherical particles. Average reflectivities for normally incident radiation, determined by weighting the normal spectral reflectivities with respect to the black-body radiation function, were computed for aluminum, copper, gold, nickel, silver and tungsten.

The spectral absorption coefficients and Rosseland mean opacity of gaseous tungsten were re-evaluated using the UARL heavy-atom model with a modified oscillator strength distribution function. Additional average local line spacing and local line intensities for materials which might be used as gaseous seed agents were calculated. These materials included neutral iron, silicon, uranium, and vanadium as well as singly ionized niobium, tungsten, and vanadium.

CONCLUSIONS

1. Theoretical estimates of the spectral absorption parameters of thin plates and spherical particles indicate that thin plates are in general more effective as possible propellant seeding agents in gaseous-core nuclear rocket engines.

2. The effect of temperature on the spectral extinction and absorption parameters of spherical tungsten particles (based on the Mie theory using analytically extrapolated refractive index data) is small.

3. The differences between measured and calculated refractive index data of tungsten from various sources do not have an appreciable effect on the absorption parameter of spherical tungsten particles at wavelengths below approximately 2 μ.

4. At wavelengths less than approximately 0.6 μ, most materials studied to date are more effective absorbers of radiation than tungsten when both are in particle form. At wavelengths greater than approximately 0.6μ, all materials studied (except carbon) have absorption parameters of about the same magnitude.

5. Selection of the best seed material for gaseous nuclear rockets requires information on the spectral absorption characteristics of vaporized seed as well as for the same seed in particulate form. Because insufficient information is available on the characteristics of vaporized seed, it is not possible to choose between various seed materials at the present time.

INTRODUCTION

The control of radiation through gaseous media by the addition of small solid or liquid particles or opaque gases is of interest in numerous advanced rocket engine designs such as the gaseous-core nuclear rocket engine concept described in Ref. 1. In this concept, energy generated by nuclear fission in a central plasma is transferred to the surrounding propellant, usually hydrogen, principally by the mechanism of thermal radiation. The propellant must be sufficiently opaque to insure an adequate propellant temperature rise and to prevent excessive radiation from reaching the walls of the thrust chamber. Hydrogen, however, is essentially transparent at temperatures below approximately 8000 K (14,400 R) (Ref. 2). Thus the propellant region must be seeded with opaque materials to insure adequate absorption of the radiation at temperatures up to about 8000 K (14,400 R).

Small particles, low-ionization-potential metal vapors, and various polyatomic gases have been examined theoretically and experimentally as possible seeding agents for the propellant region (Refs. 3 through 8). Small-sized solid or liquid particles exhibit essentially continuous spectral absorption characteristics as contrasted with the discrete spectral absorption characteristics exhibited by low-ionization-potential metal vapors and polyatomic gases. Theoretical studies of the absorption properties of small-size solid particles at UARL (Refs. 7 and 8) have been based on the Mie theory (Refs. 9 and 10) which describes the spectral extinction, absorption, and scattering of radiation by spherical particles as a function of particle size and the wavelength of the incident radiation. Although Mie calculations have been made for many seed materials of interest using available complex index of refraction data (Refs. 7 and 8), new refractive index data is continuously being published in the literature. Therefore, additional calculations of particle absorption characteristics using recent index of refraction information are required to insure selection of the most effective seeds for gaseous nuclear rocket engines.

The gaseous states of various heavy-atom materials which might be used as solid-particle seeding agents generally exhibit spectra with dense line structures (Ref. 11). If the lines in these gases are sufficiently broadened by collisions with hydrogen molecules and atoms, a nearly continuous absorption spectrum will result in the bound-bound spectral region. The analytical model employed in Ref. 12 to calculate the spectral absorption coefficients of gases with dense line structures assumes that the line density decreases linearly as the wave number increases. However, experimental evidence noted in Ref. 12 and in this report indicates that the line density per unit wavelength may vary in an irregular manner from one part of the spectrum to another. Similarly, the oscillator strength per unit wave number assumed in the heavy-atom model for the bound-bound spectral region is not in complete agreement with that inferred from experimental

spectral line intensity data cited in Ref. 12 and in later sections of this report. Therefore, additional information is required to determine the effect of line density distribution and oscillator strength distribution on the spectral and mean absorption properties.

In view of the foregoing discussion, the objectives of this study are twofold: to continue the examination of the absorptive properties of various solid materials; and to modify the heavy-atom model used in calculating spectral and mean absorption properties of gases to enable more accurate assessment of these properties in the bound-bound spectral region.

PROPERTIES OF SOLID SEEDS

Spectral absorption coefficients and reflectivities of bulk solid materials may be calculated if the complex refractive index is known as a function of wavelength. Similarly, the spectral extinction, absorption, and scattering properties of small particles with spherical symmetry may be calculated using the Mie theory (Refs. 9 and 10) if the requisite complex refractive index data are available. A continuing effort over an extended period has been expended at UARL to evaluate the absorptive properties of small spherical particle seeds (Refs. 7 and 8) as the requisite refractive index data have become available. In Table I, the pertinent physical properties of all materials investigated to date are listed. Table II is a list of UARL references which include various data and results applicable to seed materials previously studies. The figure numbers in Table II refer to graphical data and results for seed materials discussed in this report.

Complex Refractive Indices

The complex refractive indices required in the computation of the absorptive and reflective properties of the solid materials investigated are graphically shown in Figs. 1 through 8. The materials investigated are tungsten, molybdenum, niobium, thallium, and cadmium.

The real and imaginary parts of the complex refractive index of tungsten were calculated in the wavelength range between 0.1 and 30μ at temperatures of 1600 K (2800 R), 1800 K (3240 R), 2000 K (3600 R), 2200 K (3690 R) and 2400 K (4320 R). Computation of the data over the extended wavelength range was effected by means of a modified free-electron model described in Ref. 13. The model parameters were determined from refractive indices experimentally measured at wavelengths between approximately 0.3 and 0.8μ at the five temperatures listed above (Ref. 13). The calculated results for tungsten are given in Figs. 1 and 2 for each of the temperatures. It should be noted that the temperature variation of the real and imaginary parts of the refractive indices is small. In Figs. 3 and 4, refractive index data for tungsten from different literature sources (Refs. 13 and 14) are compared for two temperatures, 300 K (540 R) and 1600 K (2800 R). In Figs. 5 through 8, complex refractive index data are given for molybdenum (Ref. 17) at a temperature of 2210 K (3978 R), niobium (Ref. 15) at 2003 K (3605 R) and for thallium (Ref. 16) and cadmium (Ref. 16) at 300 K (540 R).

Optical Properties of Spherical Particles

Spectral extinction, absorption, and scattering parameters were calculated for each of the materials listed in the preceeding section using the UARL Mie theory

machine program (Ref. 7) for spherical particles with radii of 0.01, 0.05, 0.1, and 0.5μ. Typical spectral extinction and absorption parameters for spherical tungsten particles at a temperature of 1600 K (2800 R) are shown as a function of wavelength for the four specified particle radii in Fig. 9. The absorption parameter for the bulk material, is also shown in Fig. 9 where, according to Ref. 10:

$$b_0' = 4\pi k/\lambda \tag{1}$$

In this expression, k is the imaginary part of the refractive index and λ is the wavelength of the incident radiation. The spectral absorption parameter for bulk material is uniformly more effective than that for spherical particles over the entire wavelength range, which suggests that thin plates of tungsten or other materials might be more useful as seeding agents than spherical particles. A discussion of the physical size requirements for these thin plates is given in the section entitled "Optical Properties of Bulk Materials."

The effect of temperature on the spectral extinction and absorption parameters of spherical tungsten particles (radius = 0.05μ) is illustrated in Fig. 10 for wavelengths of 0.1, 1.0, 10, and 30μ. These results are based on the computed refractive indices shown in Figs. 1 and 2 (Ref. 13). It is observed that temperature has a negligible effect on the extinction and absorption parameters of spherical tungsten particles. In Fig. 11, the spectral absorption parameters of spherical tungsten particles (radius = 0.05μ) based on different sources of refractive index data are compared as a function of wavelength.

The extinction and absorption parameters of spherical molybdenum particles at a temperature of 2210 K (3978 R), niobium at 2003 K (3605 R), and thallium and cadmium at 300 K (540 R) are graphically illustrated in Figs. 12 through 15 as a function of wavelength for particle radii of 0.01, 0.05, 0.10, and 0.5μ. The results are typical of Mie calculations for other materials with the exception of the deep minimums at a wavelength of approximately 0.1μ for thallium (see Fig. 14) and at a wavelength of approximately 0.12μ for cadmium (see Fig. 15).

The curves in Figs. 16, 17, and 18 summarize the results of Mie calculations of spectral absorption parameters for spherical particles (radius = 0.05μ) as a function of wavelength for all materials investigated to date. These results are based on complex refractive index data from Refs. 8, 15, and 17 through 29. The absorption parameters for spherical tungsten particles are plotted in all figures for comparison. The spectral absorption parameters of most materials studied exceed or are at least approximately equal to the spectral absorption parameter of tungsten (see Figs. 16, 17, and 18). However, tungsten is important as a prospective seeding agent in gaseous-core nuclear rocket engines because it has a very high boiling-point temperature and is essentially nonreactive with high-temperature hydrogen.

The spectral absorption parameter results for spherical tungsten particles (radius = 0.05μ) given in Fig. 19 were used to estimate the Rosseland mean opacity parameter of tungsten as a function of temperature. The Rosseland mean opacity parameter, b_R, is given by:

$$b_R = \frac{\int_0^\infty (dB_\omega/dT)\, d\omega}{\int_0^\infty \frac{(dB_\omega/dT)}{b_a\left(1 - e^{-hc\omega/k'T}\right)}\, d\omega} \qquad (2)$$

where B_ω is the spectral black-body function; ω, the wave number; T, the temperature; and h, c, and k' are the usual physical constants. The integration indicated in Eq. (2) is performed over the limits $\omega = 0$ to ∞; therefore, the spectral absorption parameter results for spherical tungsten particles given in Fig. 19 by the solid curve (based on refractive index data of Ref. 13 at a temperature of 1600 K) were extrapolated for wave numbers greater than 100,000 cm^{-1} ($\lambda < 0.1\mu$) as shown. Similar spectral absorption parameter results (Refs. 7 and 11) based on the refractive index data of Ref. 14 are illustrated in Fig. 19 by a dashed curve. These spectral absorption coefficient results were extrapolated above a wave number of 25,000 cm^{-1} ($\lambda < 0.4\mu$) as indicated in the figure. The area under the solid curve (proportional to the total oscillator strength) is approximately ten times the area under the dashed curve. The oscillator strength (approximately 2.0) represented by the normalized area under the solid curve in Fig. 19 is, therefore, approximately equal to that for gaseous tungsten seed using the heavy-atom model described in later sections of this report. The corresponding Rosseland mean opacity parameters, based on both sets of spectral absorption parameter results in Fig. 19, are shown for comparison in Fig. 20 for spherical tungsten particles having a radius of 0.05μ. The increase in the magnitude of the Rosseland mean opacity parameter shown by the solid curve over that exhibited by the dashed curve in Fig. 20 is primarily attributable to the increase in oscillator strength associated with the two corresponding areas under the spectral absorption parameter curves shown in Fig. 19.

Optical Properties of Bulk Materials

Absorption

The spectral absorption parameter for bulk tungsten exceeds that for spherically symmetrical particles of any size (see Fig. 9) and suggests the possibility, as indicated previously, that small thin plates of tungsten or other materials might be used for seeding in the transparent propellant region. In view of this result, the spectral absorption parameters for thin plates of all materials investigated to date at UARL were computed (see Eq. (1)) and are compared in Figs. 21 through 23. The calculations were based on the refractive index data from Refs. 8, 13, and 15 through 27. In Fig. 21, the spectral absorption parameter for tungsten plates is shown as a function of wavelength based on complex refractive index data

from different sources. Similarly, computed results are illustrated in Figs. 22 and 23 for other materials and include the tungsten results to enable comparison.

Comparison of the results in Figs. 22 and 23 for thin plates with corresponding results for spherical particles in Figs. 16 through 18 indicates that the absorption parameters of thin plates are greater than those for spherical particles for any given material at all wavelengths. At a wavelength of 1.0μ, the ratio of the absorption parameter for thin plates to that for spherical particles of the same material varies from approximately 2 to 117. At a wavelength of 10μ, this ratio varies from approximately 420 to 1460 for the various materials considered.

The reason for the low value of absorption parameter for spherical particles at long wavelengths is that the radiation does not "see" particles which are small relative to the wavelength (see, for example, Fig. 1 of Ref. 7). Effective cross-sectional areas for absorption equal to or greater than the physical cross-sectional area of a spherical particle require a particle radius approximately equal to or greater than the wavelength of the radiation. Therefore, by analogy, it would be expected that the width and height of thin plates (i.e., the dimension normal to the direction of propagation of the radiation) should be equal to or greater than the wavelength in order to obtain the advantages of the high absorption parameters indicated by comparing the results shown in Figs. 22 and 23 with those shown in Figs. 15 through 18. If these thin plates are to be effective in absorbing radiation at wavelengths up to 10μ, the width and height of the plates must be equal to or greater than approximately 10μ (3.94×10^{-4} in.).

Large diameter spherical particles are inefficient absorbers of short wavelength radiation because much of the volume is "hidden" behind the front of the particle. A similar limitation applies to thin plates. The effectiveness of a thin plate as an absorber decreases rapidly once the intensity of the incident radiation has been reduced to a magnitude of $1/e$ its initial value. A typical absorption parameter for tungsten plates at short wavelengths is of the order of 10^5 cm^2/gm, therefore, this $1/e$ factor would be achieved in a plate having a "thickness" of approximately 10^{-5} gm/cm^2. Since the density of tungsten is approximately 20 gm/cm^3, the corresponding plate thickness would be about 5×10^{-7} cm (0.005μ or 50 Å).

Although any single small plate might be aligned such that it would provide little absorption of incident radiation, the number density of plates would be so high that statistically the plates can be considered randomly oriented. For example, there would be approximately 10^7 plates in a cubic centimeter if the thickness of the plates were $5 \times 10^{-3}\mu$ and their height and width were 10μ. The effectiveness of a randomly oriented plate would be approximately half that of a plate which was positioned perpendicular to the direction of the incident radiation. However, absorption parameters for thin plates are greater than those for spherical particles by a factor considerably greater than 2, thus thin plates nominally 50 Å thick would be superior to spherical particles as seeding agents.

The discussion in the preceding paragraphs has considered only the absorbing characteristics of thin plates. In addition, these plates would scatter a certain fraction of the incident radiation (for example, see discussion of reflectivities in following sections). The scattering of radiation from a system of randomly oriented thin plates would be analogous to the scattering of radiation by spherical particles. In general, the scattering process increases the path length for absorption of the photons passing through the seeded region. Thus an enhancement of the effective absorbing ability of spherical particles or thin plates will result.

Reflection

It is anticipated that the seed density in the propellant region of a gaseous nuclear rocket engine will be such as to reduce the radiant flux by two or more orders of magnitude relative to the flux incident on the propellant region. However, a flux of only 10^{-2} times the incident flux might still be sufficient to result in a very large heat deposition rate at the surface of the cavity wall if all of the radiation incident on the wall were absorbed. This wall heating rate would be substantially reduced if the walls were made of a reflecting material. The reflectivity of a material is related to its complex index of refraction. For light incident at an angle, ϕ, relative to a normal to the surface of the material, the reflectivity is given by (see Ref. 28):

$$r_\phi = \frac{1}{2}\left(r_p^\phi + r_s^\phi\right) \tag{3}$$

where

$$r_s^\phi = \frac{a^2 + b^2 - 2a\cos\phi + \cos^2\phi}{a^2 + b^2 + 2a\cos\phi + \cos^2\phi} \tag{4}$$

$$r_p^\phi = r_s^\phi \left\{ \frac{a^2 + b^2 - 2a\sin^2\phi\tan\phi + \sin^2\phi\tan^2\phi}{a^2 + b^2 + 2a\sin^2\phi\tan\phi + \sin^2\phi\tan^2\phi} \right\} \tag{5}$$

$$a^2 = \frac{n^2 - k^2 - \sin^2\phi}{2} + \frac{1}{2}\sqrt{(n^2 - k^2 - \sin^2\phi)^2 + 4n^2k^2} \tag{6}$$

$$b^2 = \frac{n^2 k^2}{a^2} \tag{7}$$

where n is the real part and k is the imaginary part of the refractive index. The spectral reflectivity for normally incident light ($\phi = 0$) is given by:

$$r_o = \frac{(n-1)^2 + k^2}{(n+1)^2 + k^2} \tag{8}$$

Equation (8) was used to compute the normal reflectivities for all materials studied (see Table II) and the resulting data are presented in Figs. 24 through 27. The computations were based on the refractive index data from Refs. 8 and 13 through 27. As is evident from the curves, aluminum has the highest reflectivity over a wide wavelength range.

The normal spectral reflectivities calculated using the refractive index data of Refs. 1, 13, and 24 are shown in Fig. 28. These results were used to compute average reflectivities defined by the following equation:

$$\bar{R} = \frac{\int_{0.1}^{12} B_\lambda r_o \, d\lambda}{\int_{0.1}^{12} B_\lambda \, d\lambda} \tag{9}$$

where B_λ is the Planck black-body function and λ is the wavelength. The average reflectivities for normally incident radiation are graphically shown in Fig. 29 as a function of the black-body radiating temperature.

Comparison of Solid Seed Materials

The selection of the most efficient material as a seeding agent for the propellant region in a gaseous-core nuclear rocket engine is dependent upon a number of criteria, for example: compatibility or reactivity with hot hydrogen, temperature at which the particle melts or vaporizes; and the cross section for thermal neutron absorption. With regard to chemical reactivity with hot hydrogen, information in Ref. 29 indicates that materials such as graphite, which react rapidly with hydrogen at high temperature, are not useful as seed materials.

A correlation of boiling-point temperatures with the absorption parameters of 0.05μ-radius particles for each material investigated is shown in Fig. 30. (Boiling-point temperature data was obtained from Ref. 30.) For materials which absorb weakly as a gas, it is necessary to have as high a boiling-point temperature as

possible. However, for materials which absorb strongly in the gas phase, the boiling-point temperature is of less significance. For example, the information in Ref. 11 indicates that materials such as tungsten which have complex spectral line structures as gases are probably as valuable as absorbers in gaseous form as in solid form. Therefore, information on the absorbtivity of each material in gaseous form is needed as well as the information presented in Fig. 30 in order to permit a choice between various materials on the basis of boiling-point temperature.

The absorption parameters of 0.05μ-radius particles for various materials considered are shown in Fig. 31 as a function of the respective thermal neutron cross sections (from Ref. 31). It is obviously advantageous to employ materials with as low a thermal neutron cross section as possible.

OPTICAL PROPERTIES OF GASEOUS SEEDS

Seeding of the relatively transparent propellant region of a gaseous-core nuclear rocket engine may be accomplished in part by the use of a material such as tungsten in the form of small spherical particles or thin plates at temperatures up to the boiling point (approximately 5600 K for tungsten). At temperatures above the boiling point, evaporated particle seeds will absorb radiation at high wave numbers (short wavelengths) by bound-free transitions and at low wave numbers (long wavelengths) by bound-bound transitions which give rise to spectral lines. In some gases, lines in the bound-bound region are few in number and are relatively widely spaced, thus spectral "windows" between the widely spaced lines occur. Conversely, heavy-atom gases usually have dense line structures over wide spectral regions. Although there are small windows between each of these lines in a heavy-atom gas, these windows will be substantially eliminated due to line broadening by perturbing species such as electrons and hydrogen atoms or molecules. The preliminary calculations of Ref. 11 indicate that the spectral lines in a heavy-atom gas will be essentially overlapped in the propellant region of a gaseous nuclear rocket engine if the line spacing is approximately 50 cm^{-1} or less.

The analytical heavy-atom model of Ref. 12, employed in Ref. 11 to calculate the spectral and mean absorption properties of heavy-atom gaseous seeds, assumes line density and oscillator strength distributions in disagreement with line density and oscillator strength distributions inferred from experimental line spacing and intensity data quoted in Ref. 11 and later sections of this report. The following section of this report describes a modification made to the oscillator strength distribution function for tungsten in order to match more closely the calculated tungsten line spectra to measured results. Also discussed is information on line spacing and line intensities for heavy-atom elements other than tungsten which might be used as gaseous seeds.

Tungsten

Heavy-Atom Model

As a prerequisite in the modification of the heavy-atom model to account for discrete line effects, experimental line spacing and intensity data for the neutral tungsten atom (Ref. 32) reported in Ref. 11 were re-examined. Similar data for singly ionized tungsten from Ref. 33 were also examined. These data are shown in Fig. 32 (average line spacing per 1000 cm^{-1} interval as a function of wavelength) and Fig. 33 (relative total line intensity as a function of wavelength) for both species. It should be noted that the results shown in Figs. 32 and 33 may be biased in that lines outside the indicated wavelength range (between approximately 10,000 cm^{-1} and 57,000 cm^{-1}) undoubtedly exist but have not been examined or

reported. Therefore, local average line spacing at the wavelength extremes shown in Fig. 32 are probably too large. The line intensity data shown in Fig. 33 (probably underestimated at the wavelength extremes for the reason cited above) were used as a guide in the modification of the heavy-atom model.

The heavy-atom model used to estimate spectral absorption coefficients and Rosseland mean opacity has been described in Refs. 11 and 12. A "continuum" type oscillator strength distribution, dfc/dE, as a function of photon energy, E, is used to prescribe the strength of a transition (absorption) from a given ground state in the work of Ref. 12. Schematically the continuum oscillator strength distribution function is shown by the dashed curve in Fig. 34. Mathematically this function is given by:

$$\left(\frac{dfc}{dE}\right)_{i,j} = \begin{cases} \dfrac{2AX_{i,j}^{2}}{(E_{i,j}^{o})^{3}} & 0 \le E < E_{i,j}^{o} \\ \dfrac{2AX_{i,j}^{2}}{E^{3}} & E_{i,j}^{o} \le E \end{cases} \qquad (10)$$

where $E_{i,j}^{o}$ is the cut-off energy, $X_{i,j}$ is the ionization potential from energy level j, E is the photon energy and A is a constant. Equation (10) is normalized such that

$$\int_{0}^{\infty}\left(\frac{dfc}{dE}\right)_{i,j} dE = n' = 2.0 \qquad (11)$$

where n' is the total oscillator strength.

The modified oscillator strength distribution ("band" distribution) used in the current study of heavy-atom gas absorptive properties is shown schematically in Fig. 34 by the solid curve and is given mathematically as follows:

$$\left(\frac{df_b}{dE}\right)_{i,j} = b_i\left[\sum_{j} a_{i,j}\sin^{2}\left\{m_i\,\pi\left(\frac{X_{i,j}-E}{X_{i,j}}\right)\right\} + d_i\right] \qquad (12)$$

where $a_{i,j}$ are the arbitrary amplitudes (may be zero or finite), m_i the number of peaks and d_i a constant of arbitrary magnitude. The normalization factor, b_i, is adjusted such that Eq. (11) applies. The oscillator strength in the bound-free spectral region is the same as in Eq. (10); that is:

$$\int_{x_{i,j}}^{\infty} \left(\frac{df_b}{dE}\right)_{i,j} dE = \int_{x_{i,j}}^{\infty} \left(\frac{df_c}{dE}\right)_{i,j} dE = A = 8.2 \times 10^{-2} \qquad (13)$$

Spectral and Mean Absorption

The quantities $a_{i,j}$, m_i, and d_i in Eq. (12) were adjusted until the major features of the experimental intensity data for neutral tungsten were approximately reproduced. Values of these constants subsequently incorporated as part of the heavy-atom model used to estimate the spectral absorption coefficients and Rosseland mean opacity of gaseous tungsten are given in Table III.

In Fig. 35 a comparison is made of the theoretical spectral absorption coefficients obtained using both the "band" and "continuum" oscillator strength distribution functions in the heavy-atom model and the relative experimental intensity data from Ref. 35. (Note that each curve is normalized with respect to its maximum.) As is evident from Fig. 35, the continuum oscillator strength distribution function appears to overestimate the spectral absorption coefficient at wave numbers less than approximately 20,000 cm^{-1}. Conversely, above a wave number of approximately 30,000 cm^{-1} the spectral properties appear to be underestimated. Although the band oscillator strength distribution function, given by Eq. (12), does not reproduce all details of the experimental data, the theoretical absorption results are in essential agreement with the major features exhibited by the normalized experimental intensities. In Fig. 36 the spectral absorption coefficients between wave numbers of 1000 and 200,000 cm^{-1} are shown for tungsten gas at temperatures of 6000 K (10,800 R) and 10,000 K (18,000 R). The solid line was calculated using the band oscillator strength distribution function and the dashed curve using the continuum oscillator strength distribution function. The total area under each curve, which is proportional to the total oscillator strength, is identical. The nearly linear increase in spectral absorption between wave numbers of 1000 and 10,000 cm^{-1} for the band oscillator strength distribution function is attributed to the constant value of $(df_b/dE)_{i,j} = d_i$ ($d_i = 0.001$ for all i - see Table III). The relative uniform magnitude of the peaks in the spectral absorption (solid curve) at a temperature of 10,000 K (18,000 R) as compared to those at 6000 K (10,800 R) is due to an increased contribution to the absorption at the higher temperature from higher ionization species. At wave numbers greater than approximately 110,000 cm^{-1}, the two calculations (solid and dashed curves) give coincident results. Wave numbers greater than approximately 110,000 cm^{-1} represent the bound-free transition region of singly-ionized tungsten which is treated in the same fashion with either oscillator strength distribution function (see Fig. 34).

These results and similar spectral results at other temperatures were used to compute the Rosseland mean opacity of tungsten which is graphically illustrated for two partial pressures in Fig. 37. As is evident in Fig. 37, use of a band oscillator strength distribution function in the heavy-atom model reduces the Rosseland mean opacity at temperatures greater than 10,000 K (18,000 R) by approximately an order of magnitude. Below a temperature of about 9000 K (16,200 R), the band oscillator strength distribution function results in a Rosseland mean opacity which decreases in magnitude as the temperature is decreased (see solid curve in Fig. 37): the continuum oscillator strength distribution function results in a Rosseland mean opacity which increases in magnitude as the temperature is decreased (see dashed curve in Fig. 37). At a temperature of 6000 K (10,800 R), the ratio of the Rosseland mean opacity based on the continuum approximation to that based on the band approximation is about 80 as compared to approximately 10 at a temperature of 16,000 K (28,800 R). Since the low absorption in the ultraviolet and infrared regions of the spectrum may be due to incomplete experimental data in these regions (see preceding discussion), there is no guarantee that the band distribution is superior to the continuum distribution in these regions. Additional experimental data with regard to the spectral properties of heavy-atom gaseous seed materials is obviously required.

Line Spacing and Intensities in Other Heavy-Atom Elements

Additional local average line spacing and relative total line intensities were calculated from experimental data reported in the current literature for several species other than tungsten as a prerequisite to the examination of these species as possible gaseous seeds. In Fig. 38 local average line spacing is plotted as a function of wave number for neutral iron (Ref. 32), silicon (Ref. 34), and uranium (Ref. 35). Similar data are shown in Fig. 39 for neutral and singly-ionized niobium (Ref. 36) and in Fig. 37 for neutral (Ref. 37) and singly-ionized (Ref. 38) vanadium. As pointed out in the case of tungsten, these data may not be indicative of actual average local spacing at low or high wave numbers because measurements in the far ultraviolet and far infrared appear to be lacking for most elements.

Relative line intensities are shown in Fig. 41 for neutral iron, in Fig. 42 for neutral silicon, and in Fig. 43 for neutral uranium. In Fig. 44 relative line intensities are shown for both neutral and singly-ionized niobium; in Fig. 45 for neutral and singly-ionized vanadium. The data in Figs. 44 and 45 suggest that the niobium and vanadium systems might be useful as seeding agents because the relatively high intensities over large spectral regions infers a correspondingly high gas phase opacity.

REFERENCES

1. Weinstein, H. and R. Ragsdale: The Coaxial Flow Reactor- A Gaseous Nuclear-Rocket Concept. ARS Reprint 1518-60, presented at the ARS 15th Annual Meeting, Washington, D. C., December 1960.

2. Krascella, N. L.: Tables of the Composition, Opacity, and Thermodynamic Properties of Hydrogen at High Temperatures. UAC Research Laboratories Report B-910168-1 prepared under Contract NAS 3-3382, September 1963. (Also issued as NASA Report NASA SP-3005)

3. Lanzo, C. D. and R. G. Ragsdale: Experimental Determination of Spectral and Total Transmissivities of Clouds of Small Particles. NASA Technical Note D-1405, September 1962.

4. Lanzo, C. D. and R. G. Ragsdale: Heat Transfer to a Seeded Flowing Gas from an Arc Enclosed by A Quartz Tube. NASA Technical Memorandum X-52005, June 1964.

5. Marteney, P. J. and N. L. Krascella: Theoretical and Experimental Investigations of Spectral Opacities of Mixtures of Hydrogen and Diatomic Gases. Air Force Systems Command Report RTD-TDR-63-1102 prepared by UAC Research Laboratories under Contract AF 04(611)-8189, November 1963.

6. Marteney, P. J.: Experimental Investigation of the Opacity of Small Particles. UAC Research Laboratories Report C-910092-2 prepared under Contract NASw-847, September 1964. (Also issued as NASA Report CR-211.)

7. Krascella, N. L.: Theoretical Investigation of the Absorption and Scattering Characteristics of Small Particles, UAC Research Laboratories Report C-910092-1 prepared under Contract NASw-847, September 1964. (Also issued as NASA Report CR-210.)

8. Marteney, P. J., N. L. Krascella, and W. G. Burwell: Experimental Refractive Indices and Theoretical Small-Particle Spectral Properties of Selected Metals. UAC Research Laboratories Report D-910092-6 prepared under Contract NASw-847, September 1965.

9. Mie, G.: Annalen der Physik, Vol. 30, 1919.

10. Van de Hulst, H. C.: Light Scattering by Small Particles. John Wiley and Sons, 1957.

11. Krascella, N. L.: Theoretical Investigation of the Opacity of Heavy-Atom Gases. UAC Research Laboratories Report D-910092-4 prepared under Contract NASw-847, September 1965.

12. Krascella, N. L.: Theoretical Investigation of the Spectral Opacities of Hydrogen and Nuclear Fuel. Air Force Systems Command Report RTD-TDR-63-1101 prepared by UAC Research Laboratories under Contract AF 04(611)-8189, November 1963.

13. Larrabee, R. D.: The Spectral Emissivity and Optical Properties of Tungsten. Technical Report 328, Research Laboratory of Electronics, Massachusetts Institute of Technology, Cambridge, Massachusetts, May 1957.

14. Roberts, S.: Optical Properties of Nickel and Tungsten and Their Interpretation According to Drude's Formula. Physical Review, Vol. 114, No. 1, April 1959.

15. Martin, W. S., E. M. Duchane, and H. H. Blau, Jr.: Measurements of Optical Constants at High Temperatures. Journal of the Optical Society of America, Vol. 55, No. 12, December 1965.

16. Jelinek, T. M., et al: Optical Constants of Vacuum Evaporated Films of Cd and Tl in the Vacuum Ultraviolet. Journal of the Optical Society of America, Vol. 56, No. 2, February 1966.

17. Waldron, J. P. and D. W. Juenker: Optical Properties of Clean Molybdenum. Journal of the Optical Society of America, Vol. 54, No. 2, February 1964.

18. Gray, D. E.: American Institute of Physics Handbook. McGraw-Hill Book Company, New York, 1963.

19. Philipp, H. R. and E. A. Taft: Optical Constants of Silicon in the Region 1 to 10 ev. Physical Review, Vol. 120, No. 1, October 1960.

20. Saski, T. and K. Ishiguro: Optical Constants of Silicon in the Extreme Ultraviolet Region. Physical Review, Vol. 127, No. 4, August 1962.

21. Brattain, W. H. and H. B. Briggs: Optical Constants of Germanium in the Infrared and Visible. Physical Review, Vol. 75, No. 11, June 1949.

22. Kirillova, M. M. and B. A. Charikov: Study of the Optical Properties of Transition Metals. Optics and Spectroscopy, Vol. 17, No. 2, August 1964.

23. Kirillova, M. M. and B. A. Charikov: Optical Properties of Titanium in the Quantum Transition Range. Physics of Metals and Metallography, Vol. 15, No. 2, 1963.

24. Stull, V. R. and G. N. Plass: Emissivity of Dispersed Carbon Particles. Journal of the Optical Society of America, Vol. 50, No. 2, February 1960.

25. Yolken, H. T. and J. Kruger: Optical Constants of Iron in the Visible Region. Journal of the Optical Society of America, Vol. 55, No. 7, July 1965.

26. Roberts, S.: Interpretation of the Optical Properties of Metal Surfaces. Physical Review, Vol. 100, No. 6, December 1955.

27. Bolotin, G. A., et al: Optical Properties of Titanium and Vanadium in the Infrared Range of the Spectrum. Physics of Metals and Metallography, Vol. 13, No. 6, 1962.

28. Jenkins, F. A. and H. E. White: Fundamental of Optics. McGraw-Hill Book Company, New York, 1950.

29. Roback, R.: Thermodynamic Properties of Coolant Fluids and Particle Seeds for Gaseous Nuclear Rockets. UAC Research Laboratories Report C-910092-3 prepared under Contract NASw-847, September 1964. (Also issued as NASA CR-212.)

30. Nesmeyanov, A. N.: Vapor Pressure of the Chemical Elements. Elsevier Publishing Company, New York, 1963.

31. Hughes, D. J. and J. A. Harvey: Neutron Cross Sections. U. S. Atomic Energy Commission, Brookhaven National Laboratory, McGraw-Hill Book Company, New York, 1955.

32. Meggers, W. F., C. H. Corliss, and B. F. Scribner: Tables of Spectral-Line Intensities. National Bureau of Standards Monograph 32 - Part I, December 1961.

33. Laun, D. D.: Second Spectrum of Tungsten (W II). Journal of Research of the National Bureau of Standards, Vol. 68 A, No. 2, March - April 1964.

34. Kiess, C. C.: Extension and Revision of the Arc Spectrum of Silicon. Journal of Research of the National Bureau of Standards, Vol. 21, August 1938.

35. Kiess, C. C., et al: Preliminary Description and Analysis of the First Spectrum of Uranium. Journal of Research of the National Bureau of Standards, Vol. 37, July 1946.

36. Humphreys, C. J., and W. F. Meggers: Term Analysis of the First Two Spectra of Columbium. Journal of Research of the National Bureau of Standards, Vol. 34, June 1945.

37. Meggers, W. F. and H. N. Russell: Term Analysis of the First Spectrum of Vanadium (VI). Journal of Research of the National Bureau of Standards, Vol. 17, July 1936.

38. Meggers, W. F. and C. E. Moore: Description and Analysis of the Second Spectrum of Vanadium (VII). Journal of Research of the National Bureau of Standards, Vol. 25, July 1940.

LIST OF SYMBOLS

a	Reflectivity function defined by Eq. (6)
$a_{i,j}$	Amplitude factor for oscillator strength distribution function in heavy-atom model
a_{ω}^{*}	Spectral absorption coefficient with stimulated emission, cm^{-1}
a_R	Rosseland mean opacity, cm^{-1}
A	Constant used in heavy atom model = $4/9\pi\sqrt{3}$
b	Reflectivity function defined by Eq. (7)
b_a	Absorption parameter, cm^2/gm
b_a'	Absorption parameter for bulk material, see Eq. (1), cm^2/gm
b_e	Extinction parameter, cm^2/gm
b_i	Normalization factor for oscillator strength distribution function in heavy-atom model
b_R	Rosseland mean absorption parameter, cm^2/gm
b_S	Scattering parameter, cm^2/gm
B_ω, B_λ	Planck black-body function, erg/cm-sec or erg/cm^2-sec-μ
C	Velocity of light = 2.9987×10^{10} cm/sec
d_i	Constant for oscillator strength distribution function in heavy-atom model
E	Photon energy, ev
$E_{i,j}^{o}$	Cut-off energy for oscillator strength distribution function in heavy-atom model, ev
f_b	"Band"oscillator strength distribution function used in heavy-atom model
f_c	"Continuum" oscillator strength distribution function used in heavy-atom model

h	Planck constant, 6.6237×10^{-27} erg sec
i	Subscript denoting an ionization species in heavy-atom model
j	Quantum number denoting an energy level in heavy-atom model
k'	Boltzmann constant, 1.3802×10^{-16} erg/K
k	Imaginary part of the refractive index
m_i	Number of peaks for oscillator strength distribution function in heavy-atom model
n	Real part of the refractive index
n'	Total oscillator strength used in heavy-atom model
N	Complex refractive index = $n - ik$
r_o	Normal spectral reflectivity
r_p^{ϕ}	Reflectivity for light with electric vector parallel to the plane of incidence
r_s^{ϕ}	Reflectivity for light with electric vector normal to the plane of incidence
r_{ϕ}	Reflectivity for unpolarized light incident at an angle ϕ with respect to the normal to the surface
R	Particle radius, μ
$\bar{R}$	Average normal reflectivity
S	Local average line spacing, cm^{-1}
T	Temperature, deg K or deg R
T_{BB}	Black-body radiating temperature, deg K or deg R
$X_{i,j}$	Ionization potential from jth level in heavy-atom model, ev

LIST OF SYMBOLS (cont'd)

λ	Wavelength, μ
ρ	Density, gm/cm^3
ϕ	Angle between the normal to a surface and the direction of propogation of incident light.
ω	Wave number, cm^{-1}

TABLE I

SELECTED PHYSICAL PROPERTIES OF ELEMENTAL MATERIALS INVESTIGATED

Seed Material	Symbol	Temperatures - Ref. 30				Mass Density Ref. 30		Thermal Neutron Cross Section Ref. 31 Barns
		Melting Point		Boiling Point				
		Deg K	Deg R	Deg K	Deg R	gm/cm^3	lb/ft^3	
Aluminum	Al	932	1678	2621	4718	2.70	168	0.230
Cadmium	Cd	594	1069	1043	1877	2.13	133	2550
Carbon	C	4200-s	7560-s	-	-	2.00	125	0.003
Cobalt	Co	1768	3182	2528	4550	8.90	555	37.0
Copper	Cu	1356	2441	3150	5670	8.92	557	3.69
Gold	Au	1336	2405	3120	5616	19.30	1204	98
Hafnium	Hf	2250	4050	5960	10728	13.30	830	105
Iridium	Ir	2727	4909	4450	8010	22.40	1398	430
Iron	Fe	1812	3262	3045	5481	7.86	490	2.53
Molybdenum	Mo	2890	5202	5100	9180	10.20	636	2.5
Niobium	Nb	2770	4986	5115	9207	8.55	534	1.1
Nickel	Ni	1728	3110	2415	4347	8.90	555	4.6
Palladium	Pd	1823	3281	3385	6093	11.97	747	8.0
Platinum	Pt	2043	3677	3980	7164	21.45	1338	8.1
Rhenium	Re	3453	6215	5915	10647	20.53	1281	84
Rhodium	Rh	2239	4030	3940	7092	12.40	774	150
Silicon	Si	1683	3029	2890	5202	2.40	151	0.13
Silver	Ag	1234	2221	2436	4385	10.50	655	62
Tantalum	Ta	3270	5886	5565	10017	16.60	1036	21.3
Thallium	Tl	577	1039	1745	3141	11.85	739	3.3
Titanium	Ti	1963	3533	3443	6197	4.50	281	5.6
Tungsten	W	3650	6570	5645	10161	19.30	1204	19.2
Uranium	U	1406	2531	4135	7443	18.70	1167	7.68
Vanadium	V	2190	3942	3273	5891	5.96	372	5.1
Zirconium	Zr	2125	3825	4598	8276	6.40	398	0.18

TABLE II

INDEX OF FIGURES AND UARL REFERENCES FOR ELEMENTAL MATERIALS INVESTIGATED

Figure numbers refer to current report
References indicate other UARL reports concerning the listed subjects

Seed Material	Symbol	Refractive Index		Extinction or Absorption Parameter			Rosseland Mean Opacity Parameter		Normal Reflectivities		Line Spacing		Line Intensities	
				Spherical Particles		Thin Plates			Spectral	Average				
		Fig.	Ref.	Fig.	Ref.	Fig.	Fig.	Ref.	Fig.	Fig.	Fig.	Ref.	Fig.	Ref.
Aluminum	Al		7	17	7	23			27, 28	29				
Cadmium	Cd	8		15, 16		22			26					
Carbon	C		7	17	6, 7	23			26, 28					
Cobalt	Co		7, 8	18	7, 8	23			26			11		
Copper	Cu								28	29				
Gold	Au								28	29				
Hafnium	Hf		8	17	8	22			25			11		11
Iridium	Ir		7	17	7	23			27			11		
Iron	Fe		8	17	8	22			25		38	11	41	
Molybdenum	Mo	5	7, 8	12, 16, 17	7, 8	22			25			11		11
Niobium	Nb	6		13, 17		22			25	29	39	11	44	11
Nickel	Ni		8	16	8	22			27, 28	29				
Palladium	Pd		7	16	7	22			25			11		
Platinum	Pt		7	17	7	23			26			11		
Rhenium	Re		7		7							11		
Rhodium	Rh		7		7							11		
Silicon	Si		7	16	7	22			26		38	11	42	
Silver	Ag								28	29				
Tantalum	Ta		7		7							11		
Thallium	Tl	7		14, 16		22			26					
Titanium	Ti		7, 8	18	7, 8	23			27					
Tungsten	W	1-4	7, 8	9-11, 16-19	6, 7, 8	21, 22, 23	20	8	24, 28	29	32	11	33, 35	11
Uranium	U										38		43	
Vanadium	V		8	18	7, 8	23			27		40	11	45	
Zirconium	Zr		8	18	7, 8	23			27			11		

TABLE III

CONSTANTS USED IN HEAVY-ATOM MODEL OSCILLATOR STRENGTH DISTRIBUTION FUNCTION FOR GASEOUS TUNGSTEN SEEDS

See Eq. (12) and Fig. 34

i	Ionization Species	Number of Peaks m_i	Amplitudes*							Ionization Potentials (ev)	d_i
			$a_{i,7}$	$a_{i,8}$	$a_{i,9}$	$a_{i,10}$	$a_{i,11}$	$a_{i,12}$	$a_{i,13}$		
1	W^0	18	0.95	1.0	0.92	0.61	0.63	0.88	0.23	7.98	0.001
2	W^+	18	0.95	1.0	0.92	0.61	0.63	0.88	0.23	14.00	0.001
3	W^{++}	18	0.95	1.0	0.92	0.61	0.63	0.88	0.23	24.10	0.001
4	W^{+++}	18	0.95	1.0	0.92	0.61	0.63	0.88	0.23	35.40	0.001

(*NOTE: $a_{i,1}$ THROUGH $a_{i,6}$ AND $a_{i,14}$ THROUGH $a_{i,18} = 0$)

EFFECT OF WAVELENGTH ON THE REAL PART OF THE THEORETICAL REFRACTIVE INDEX OF TUNGSTEN AT TEMPERATURES BETWEEN 1600 AND 2400 DEG K

$N = n - ik$

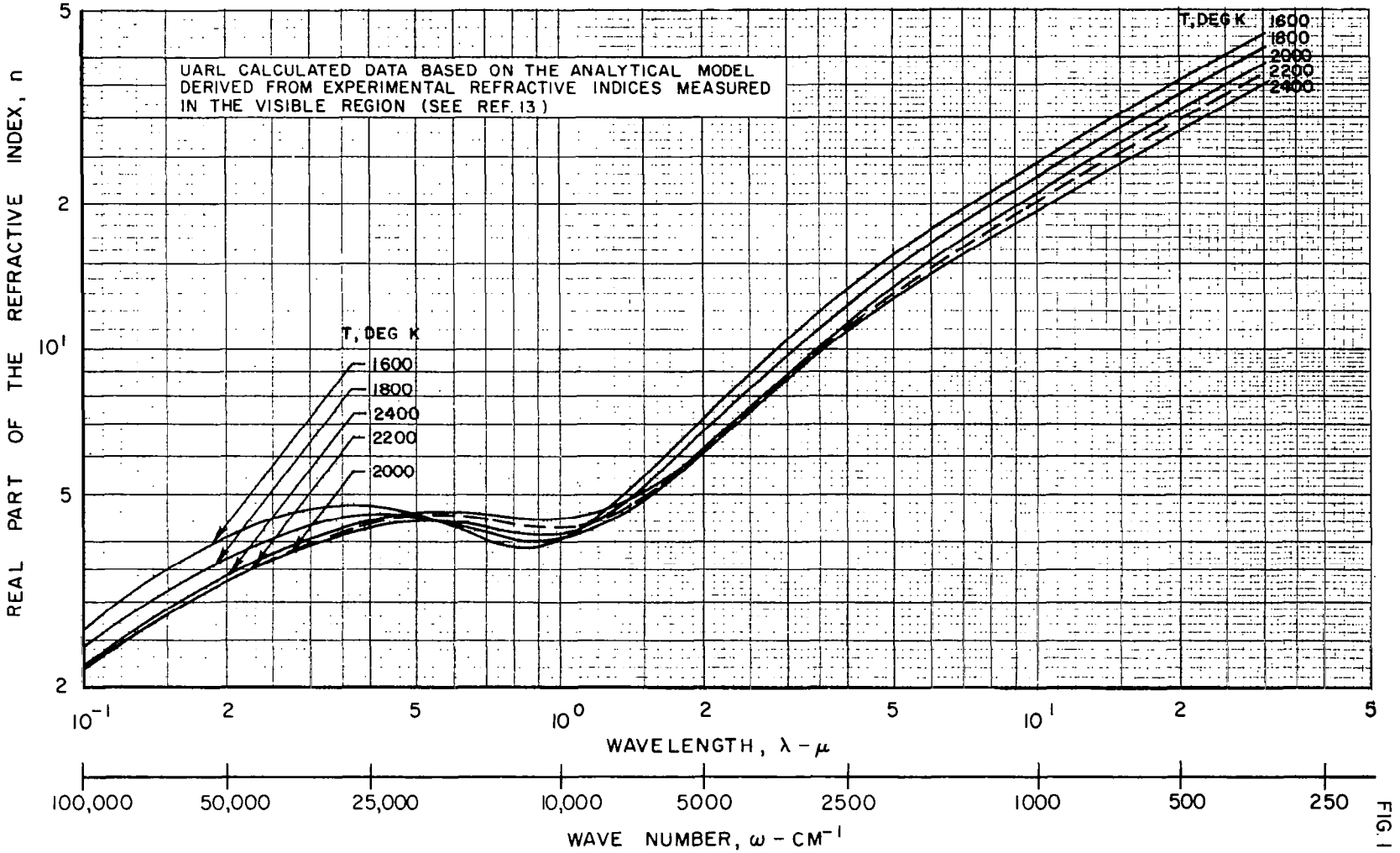

FIG. 1

EFFECT OF WAVELENGTH ON THE IMAGINARY PART OF THE THEORETICAL REFRACTIVE INDEX OF TUNGSTEN AT TEMPERATURES BETWEEN 1600 AND 2400 DEG K

$N = n - ik$

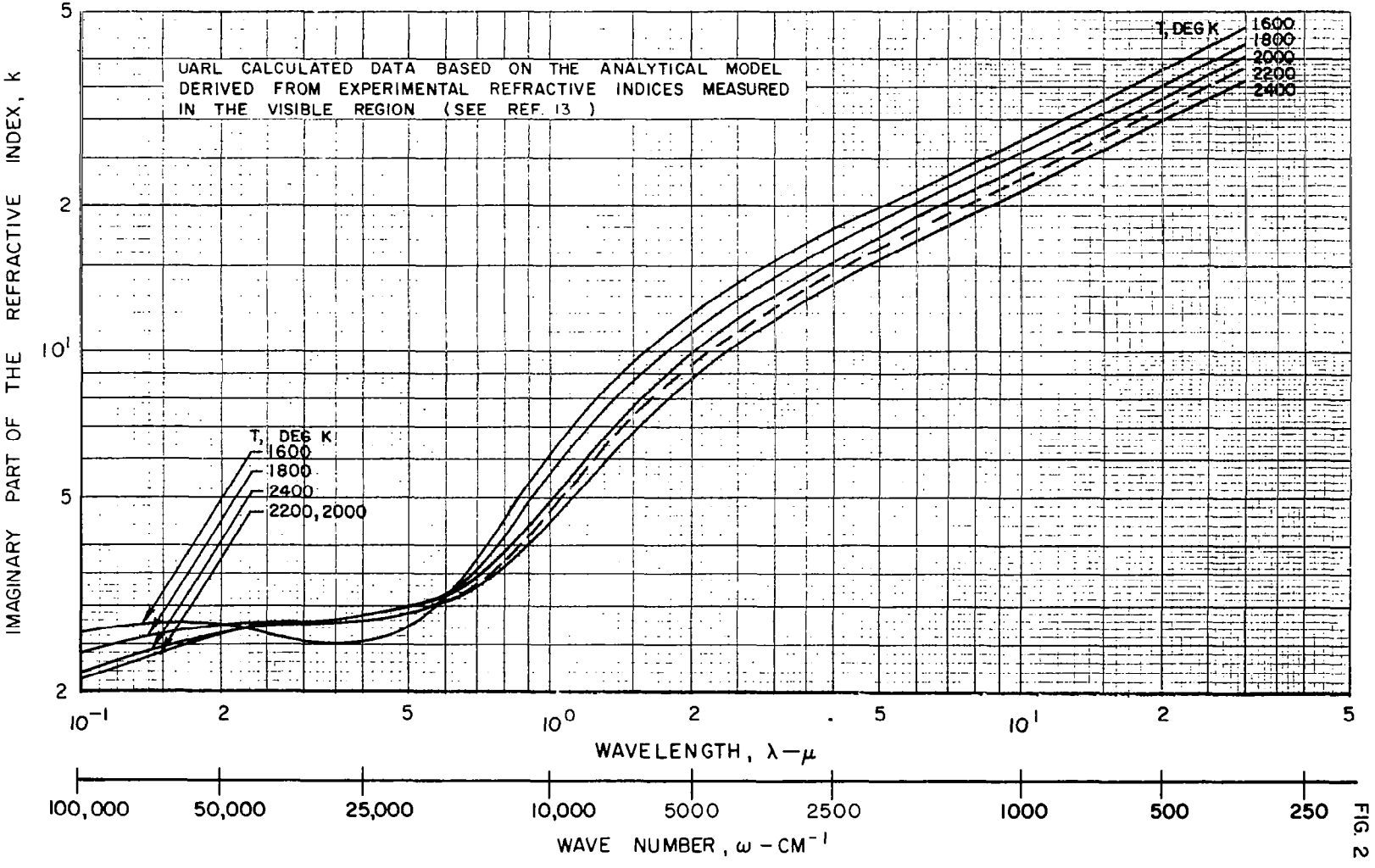

FIG. 2

COMPARISON OF THE REAL PART OF THE REFRACTIVE INDEX DATA OF TUNGSTEN OBTAINED FROM DIFFERENT SOURCES

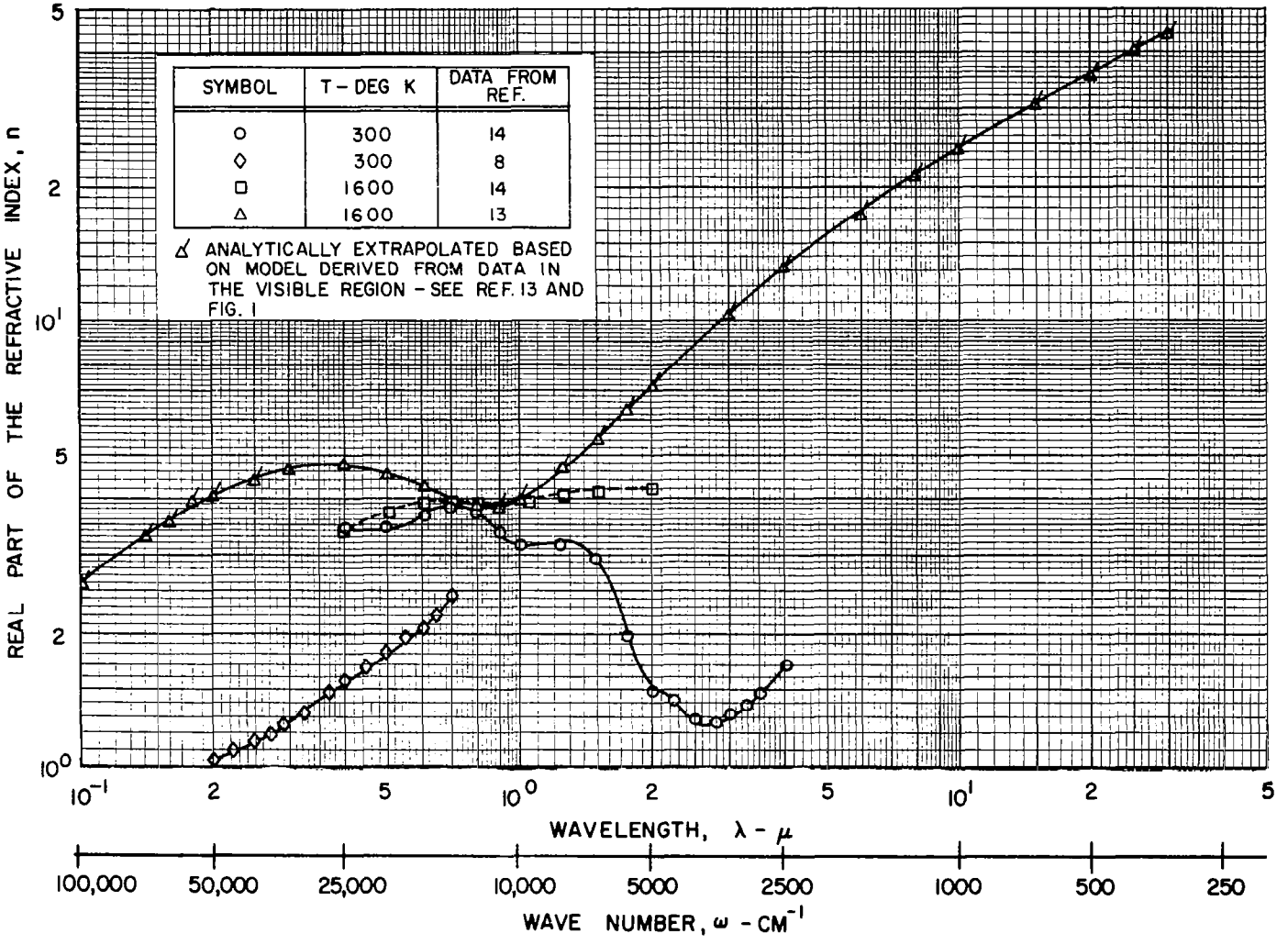

FIG. 3

COMPARISON OF THE IMAGINARY PART OF THE REFRACTIVE INDEX DATA OF TUNGSTEN OBTAINED FROM DIFFERENT SOURCES

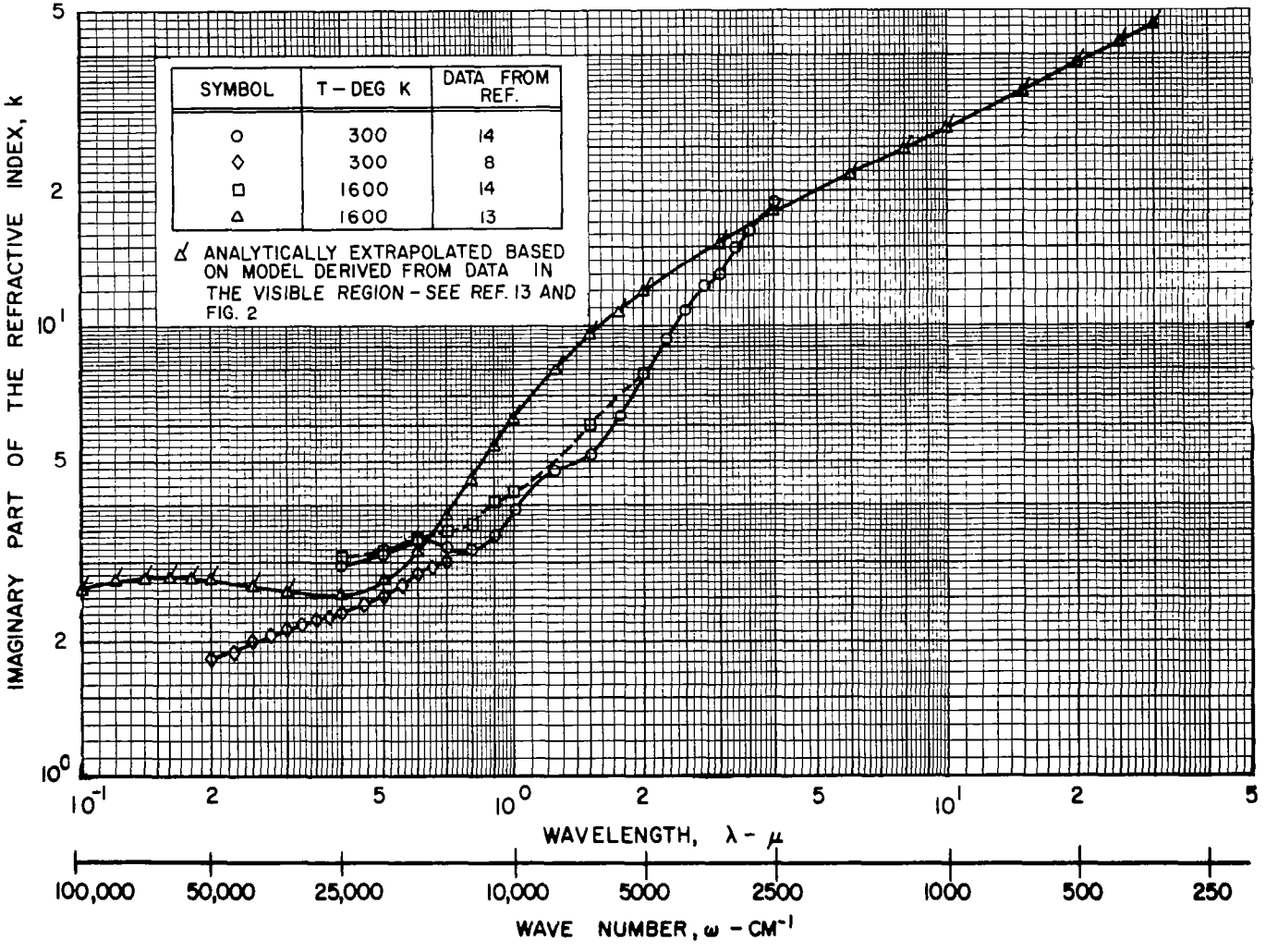

FIG. 4

FIG. 5

EFFECT OF WAVELENGTH ON THE REAL AND IMAGINARY PARTS OF THE REFRACTIVE INDEX OF MOLYBDENUM

T = 2210K (3978 R)
N = n − ik

O INDICATES POINTS WHICH WERE OBTAINED FROM REF. 15 AND WHICH WERE USED IN THE MIE THEORY CALCULATIONS

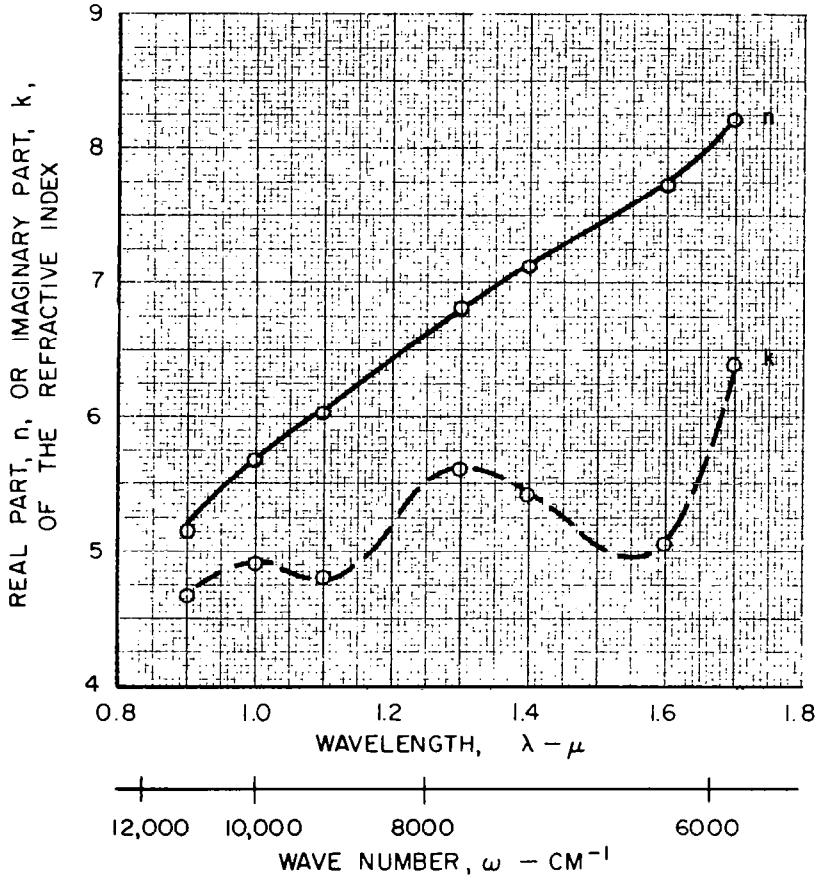

FIG. 6

EFFECT OF WAVELENGTH ON THE REAL AND IMAGINARY PARTS OF THE REFRACTIVE INDEX OF NIOBIUM

T = 2003K (3605 R)
N = n − ik

O INDICATES POINTS WHICH WERE OBTAINED FROM REF. 15 AND WHICH WERE USED IN THE MIE THEORY CALCULATIONS

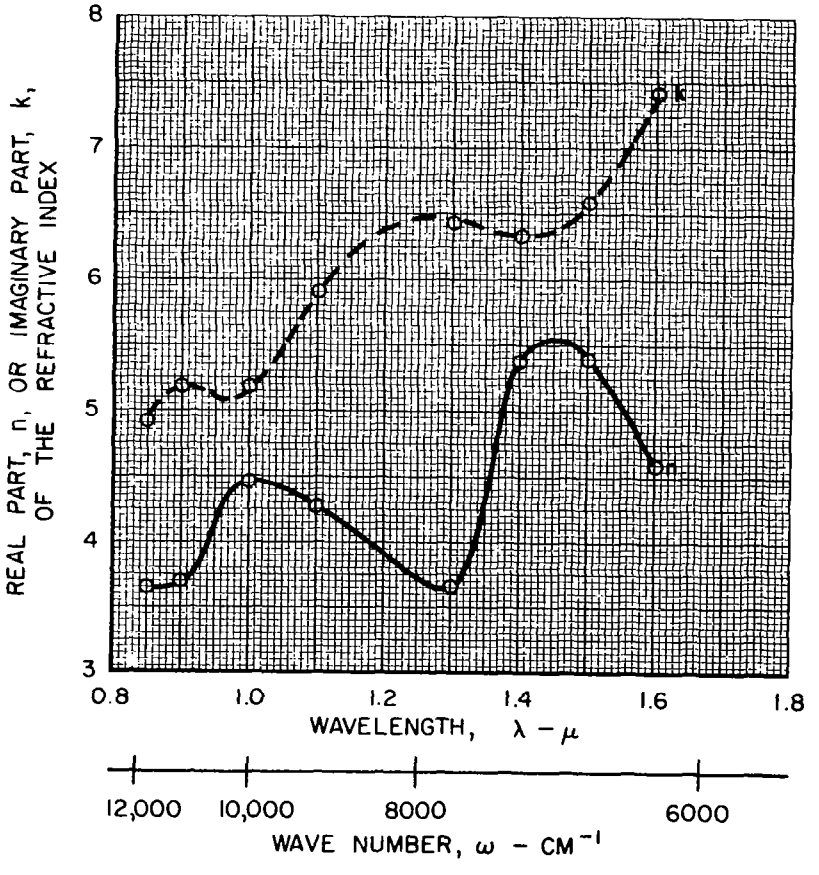

FIG. 7

EFFECT OF WAVELENGTH ON THE REAL AND IMAGINARY PARTS OF THE REFRACTIVE INDEX OF THALLIUM

T = 300K (540 R)
N = n-ik

O INDICATES POINTS WHICH WERE OBTAINED FROM REF. 16 AND WHICH WERE USED IN THE MIE THEORY CALCULATIONS

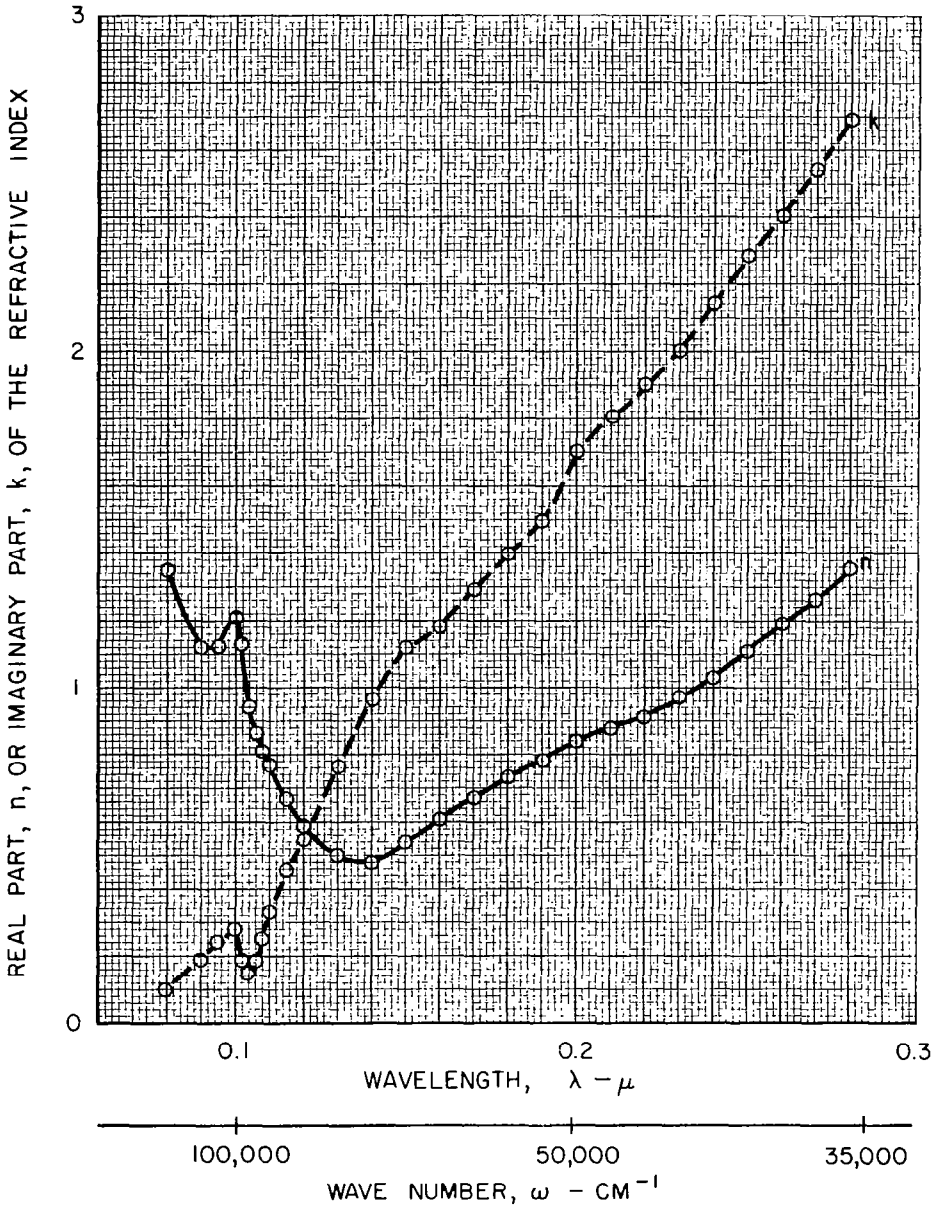

EFFECT OF WAVELENGTH ON THE REAL AND IMAGINARY PARTS OF THE REFRACTIVE INDEX OF CADMIUM

T = 300K (540 R)
N = n - ik

O INDICATES POINTS WHICH WERE OBTAINED FROM REF. 16
AND WHICH WERE USED IN THE MIE THEORY CALCULATIONS

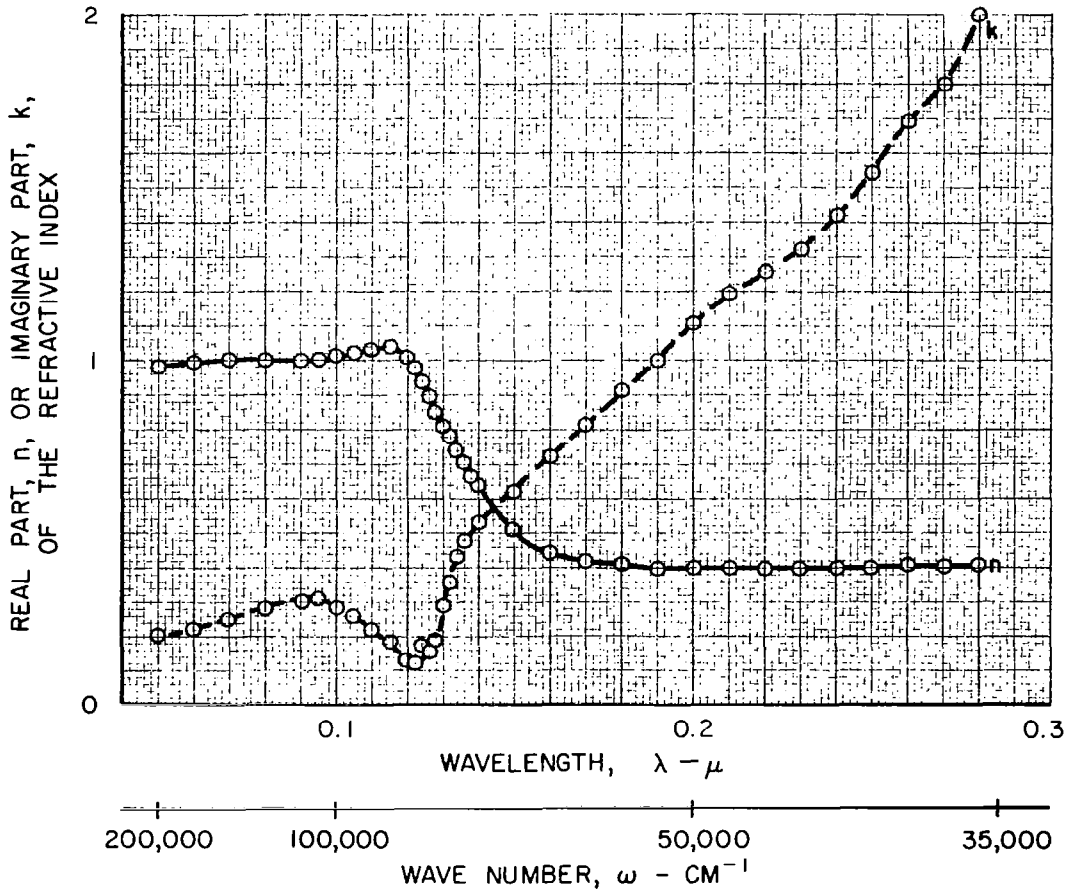

FIG. 9

EFFECT OF WAVELENGTH ON THE EXTINCTION AND ABSORPTION CHARACTERISTICS OF TUNGSTEN PARTICLES AND THIN PLATES AT A TEMPERATURE OF 1600 DEG K

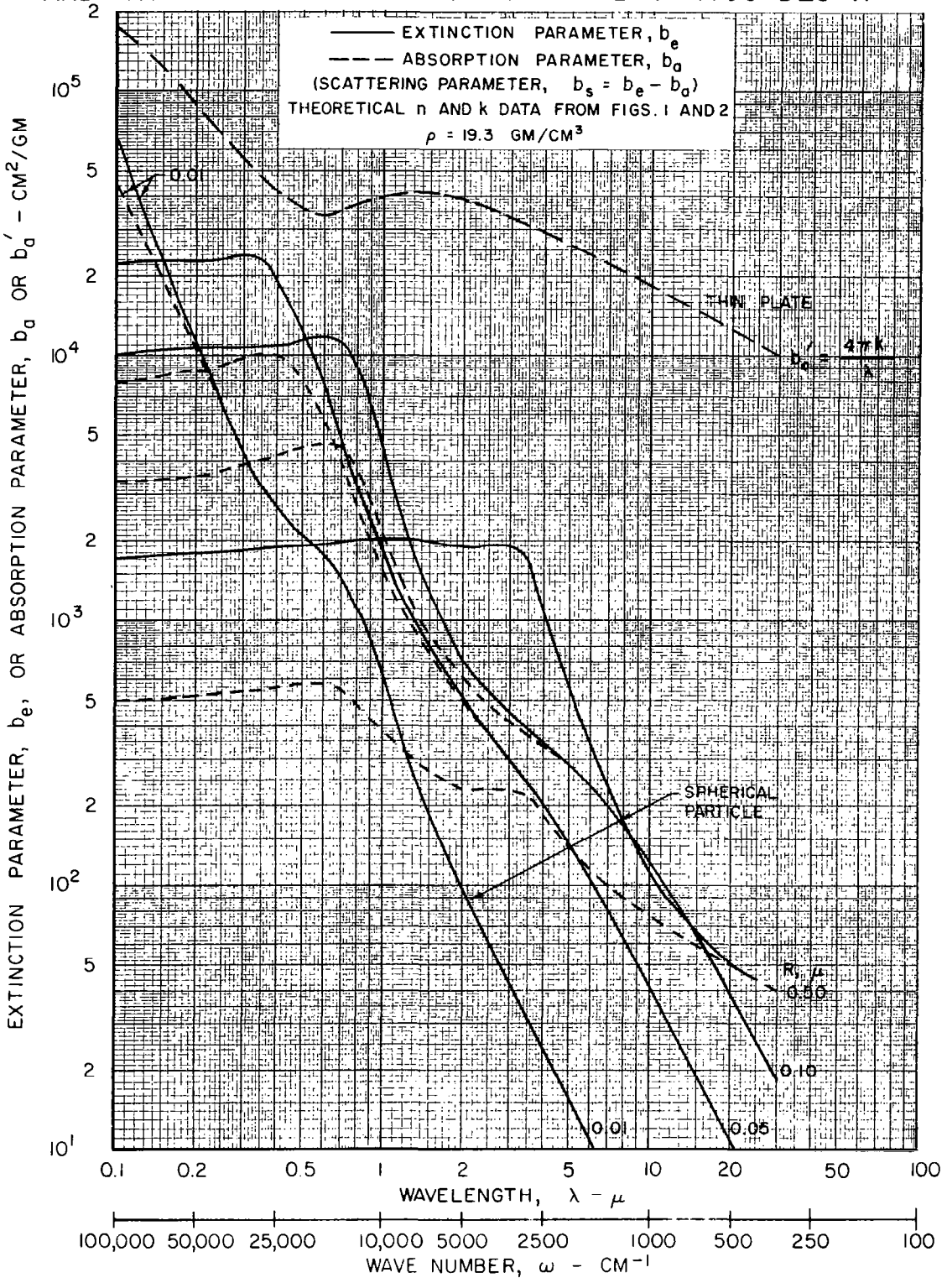

FIG. 10

EFFECT OF TEMPERATURE ON THE EXTINCTION AND ABSORPTION PARAMETERS OF SPHERICAL TUNGSTEN PARTICLES

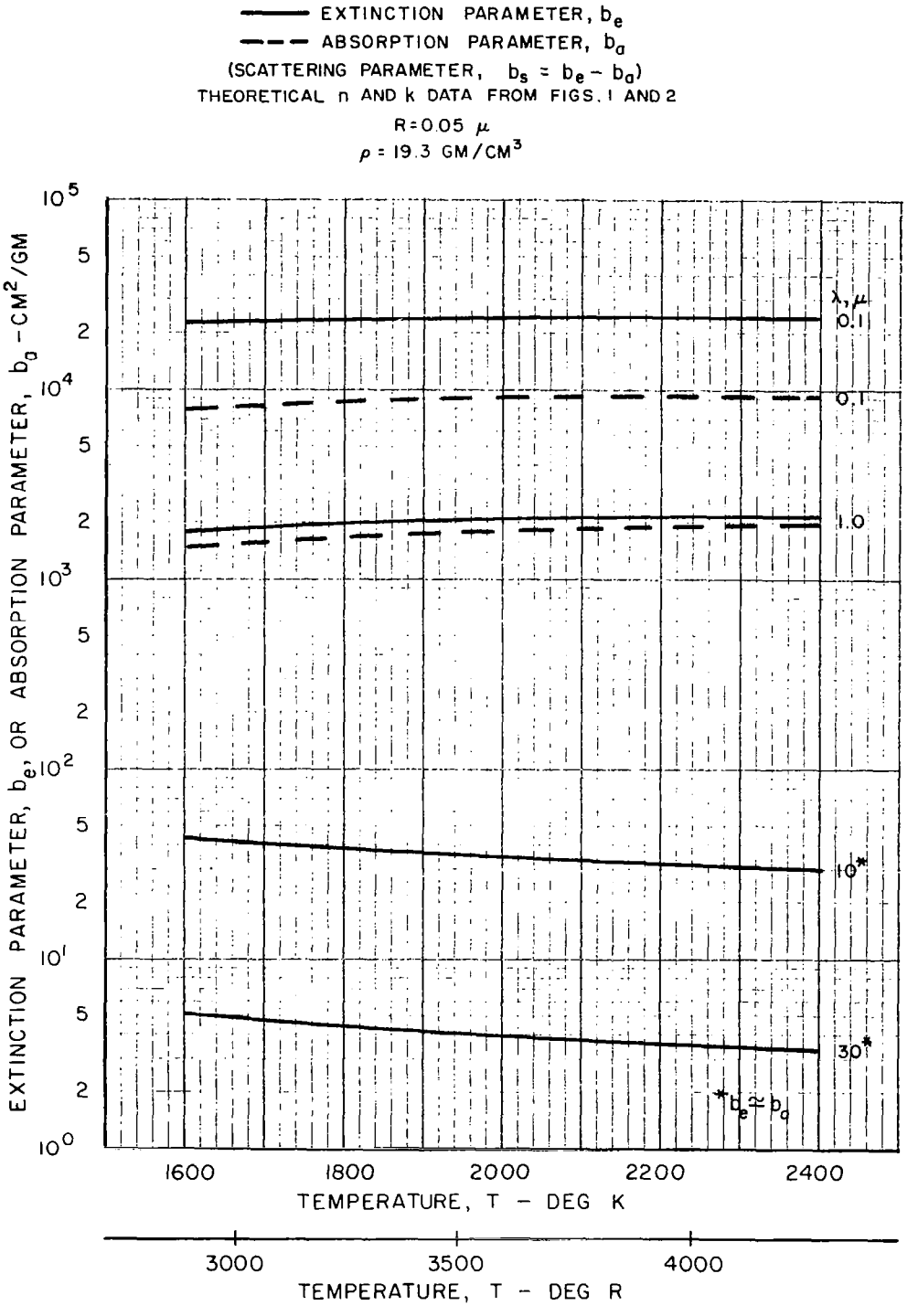

FIG. 11

COMPARISON OF THE ABSORPTION PARAMETER OF SPHERICAL TUNGSTEN PARTICLES BASED ON REFRACTIVE INDEX DATA FROM DIFFERENT SOURCES

TYPICAL n AND k DATA IN FIGS. 3 AND 4
$R = 0.05\mu$
$\rho = 19.3\ GM/CM^3$

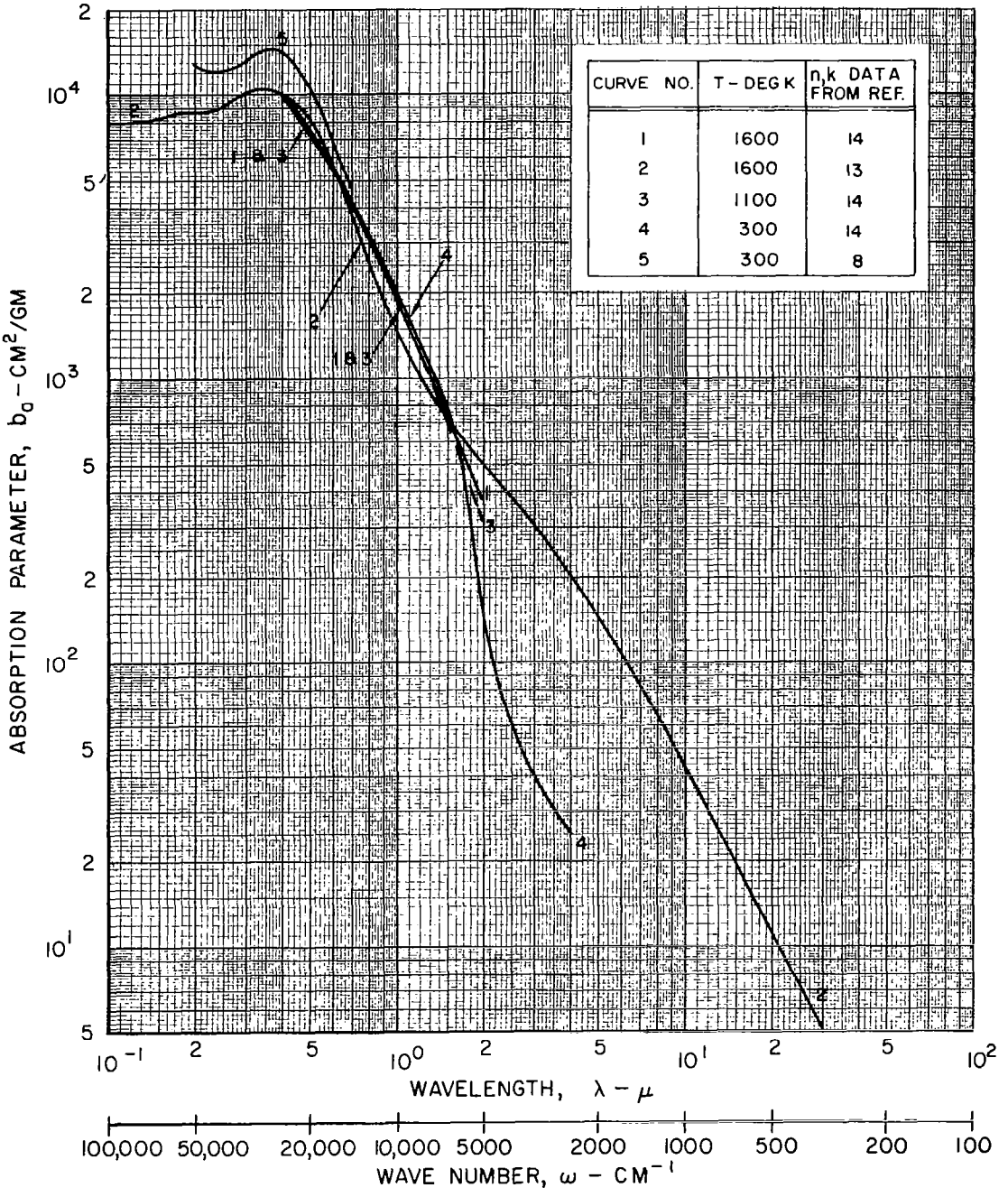

FIG. 12

EFFECT OF WAVELENGTH ON THE EXTINCTION AND ABSORPTION PARAMETERS OF SPHERICAL MOLYBDENUM PARTICLES

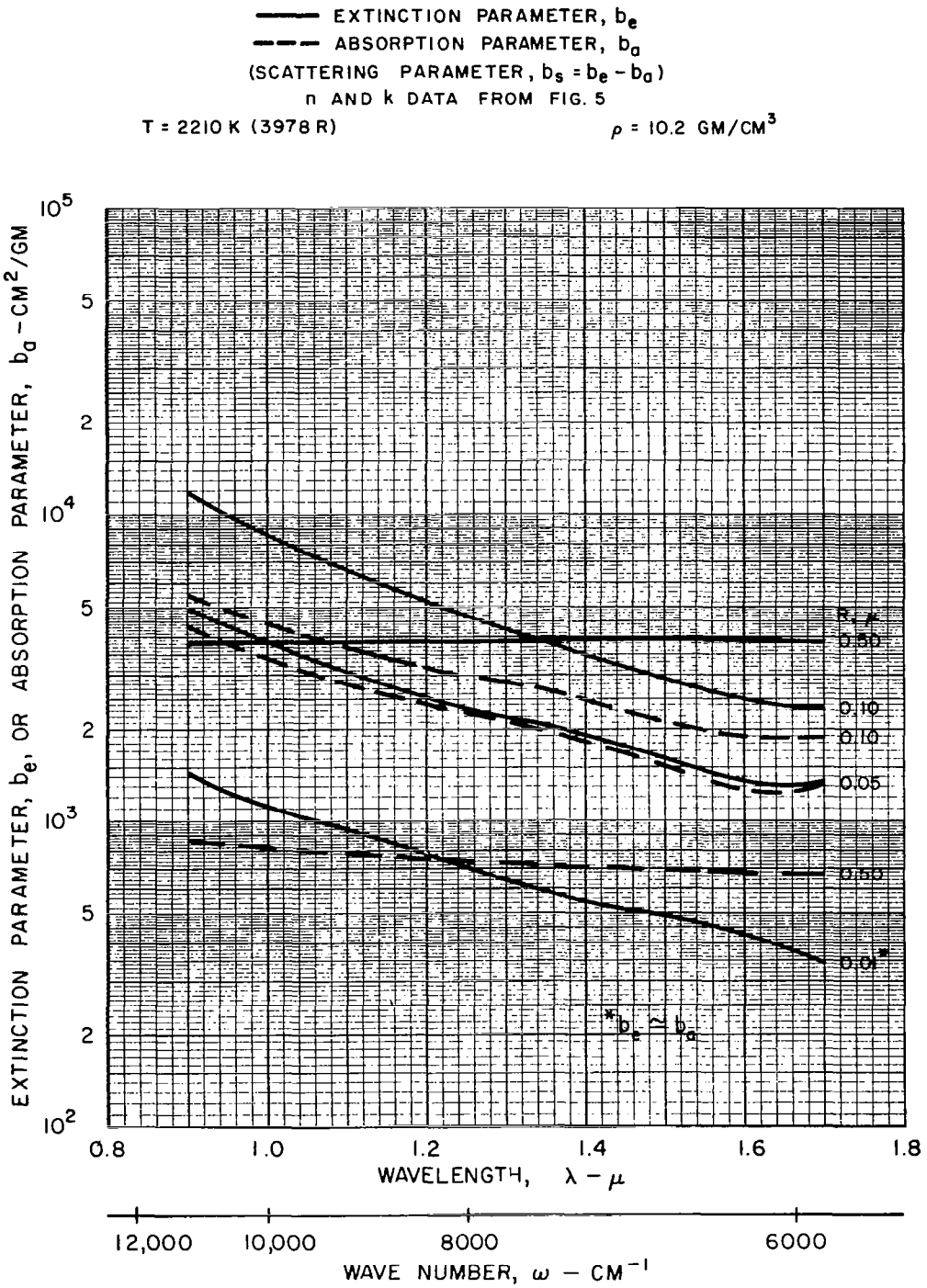

FIG. 13

EFFECT OF WAVELENGTH ON THE EXTINCTION AND ABSORPTION PARAMETERS OF SPHERICAL NIOBIUM PARTICLES

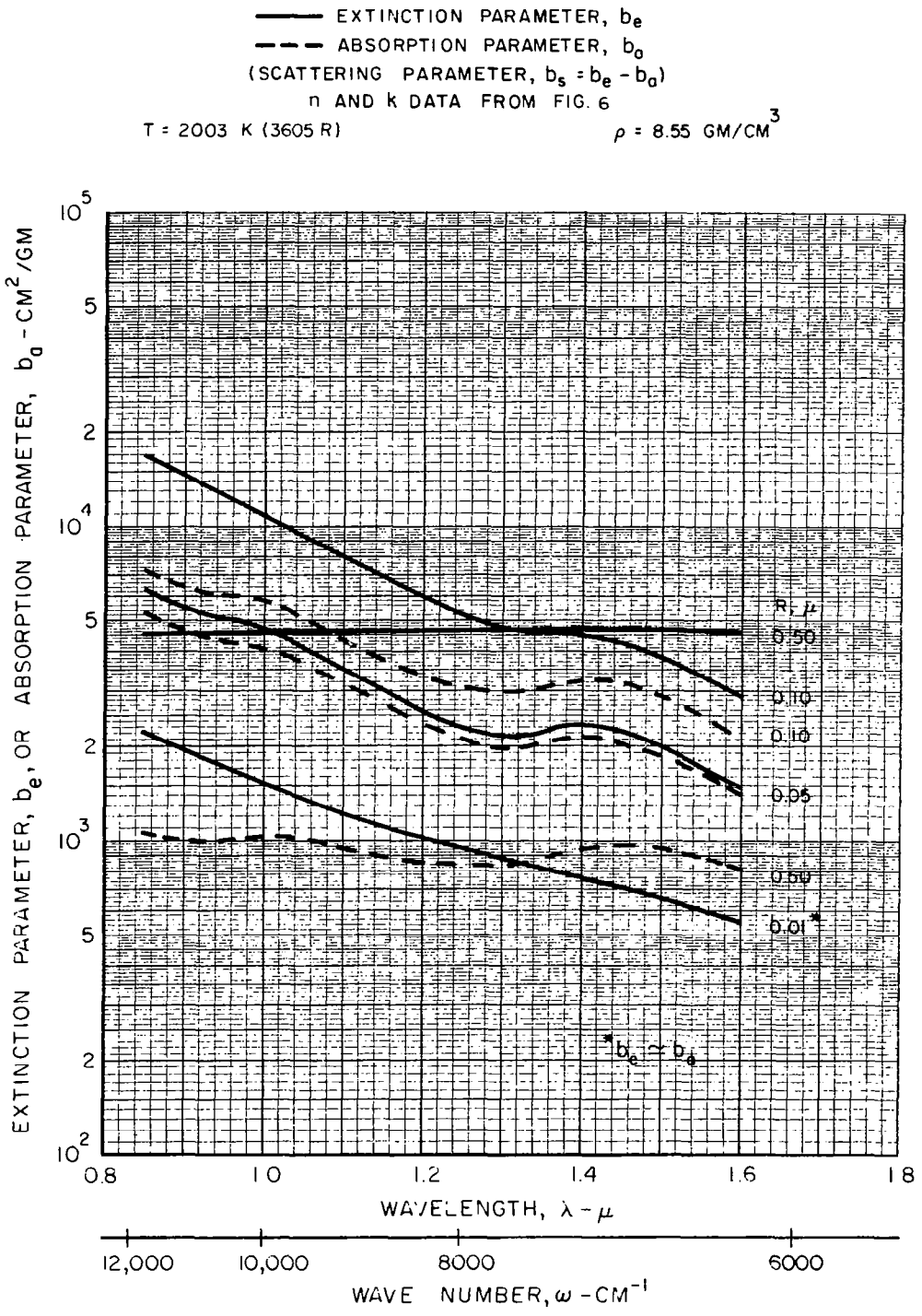

FIG. 14

EFFECT OF WAVELENGTH ON THE EXTINCTION AND ABSORPTION PARAMETERS OF SPHERICAL THALLIUM PARTICLES

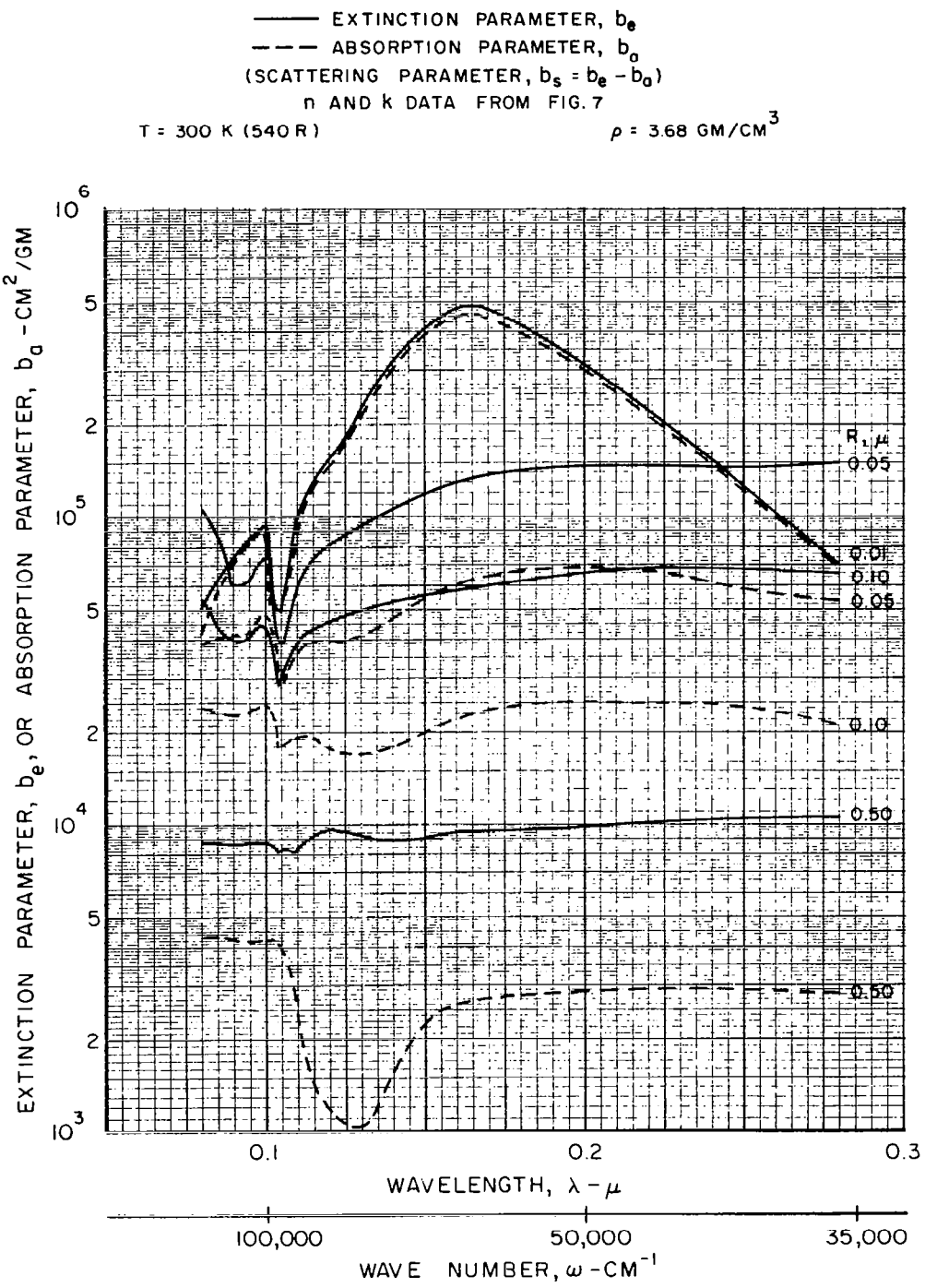

FIG. 15

EFFECT OF WAVELENGTH ON THE EXTINCTION AND ABSORPTION PARAMETERS OF SPHERICAL CADMIUM PARTICLES

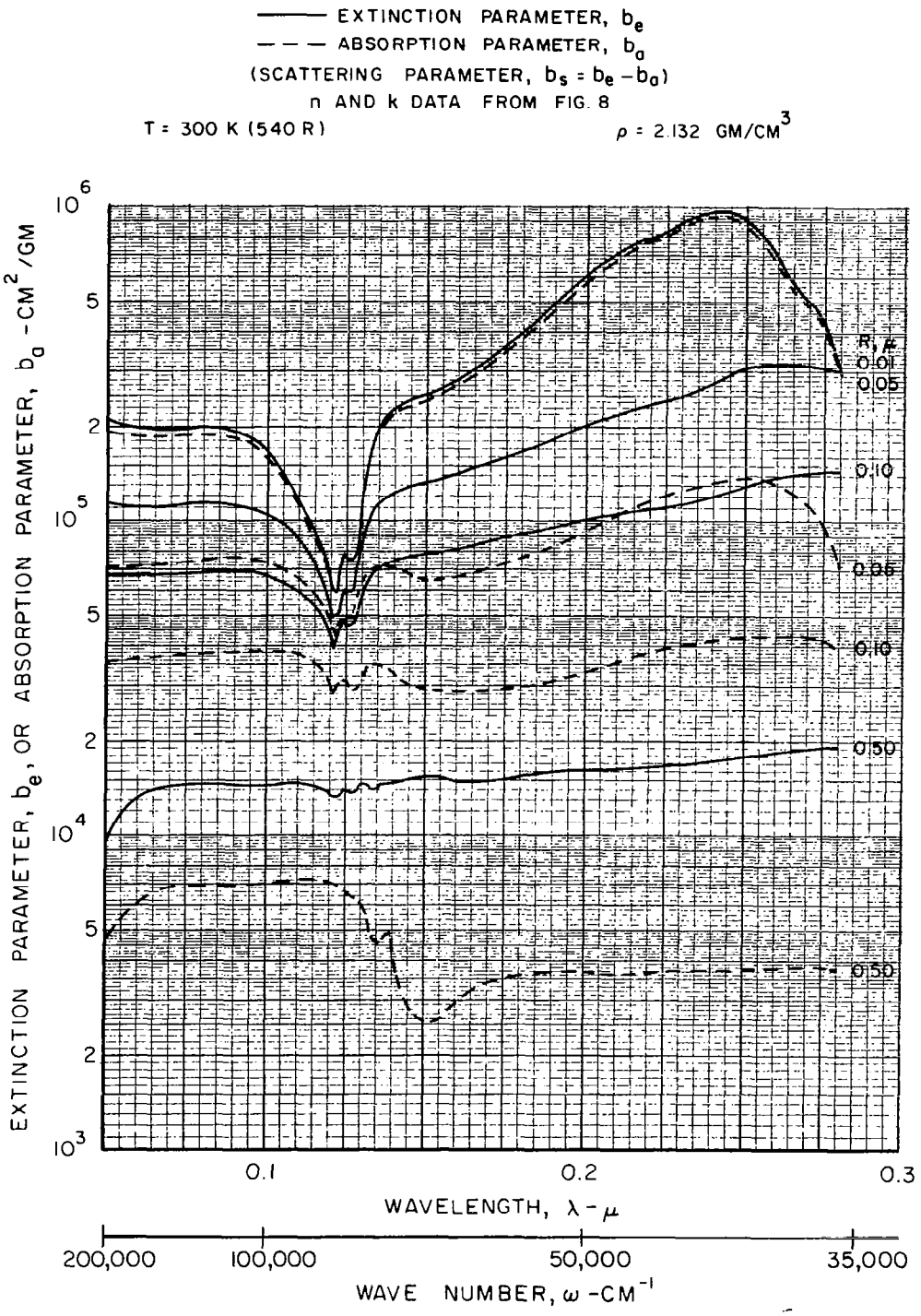

FIG. 16

COMPARISON OF THE EFFECT OF WAVELENGTH ON THE ABSORPTION PARAMETERS OF SPHERICAL CADMIUM, MOLYBDENUM, NICKEL, PALLADIUM, SILICON, THALLIUM AND TUNGSTEN PARTICLES

MATERIAL	TEMPERATURE DEG K	n & k DATA FROM REF.
CADMIUM	300	16
MOLYBDENUM	298	17*
MOLYBDENUM	300	8
NICKEL	300	8
PALLADIUM	298	18
SILICON	300	19, 20, 21
THALLIUM	300	16
TUNGSTEN	1600	13

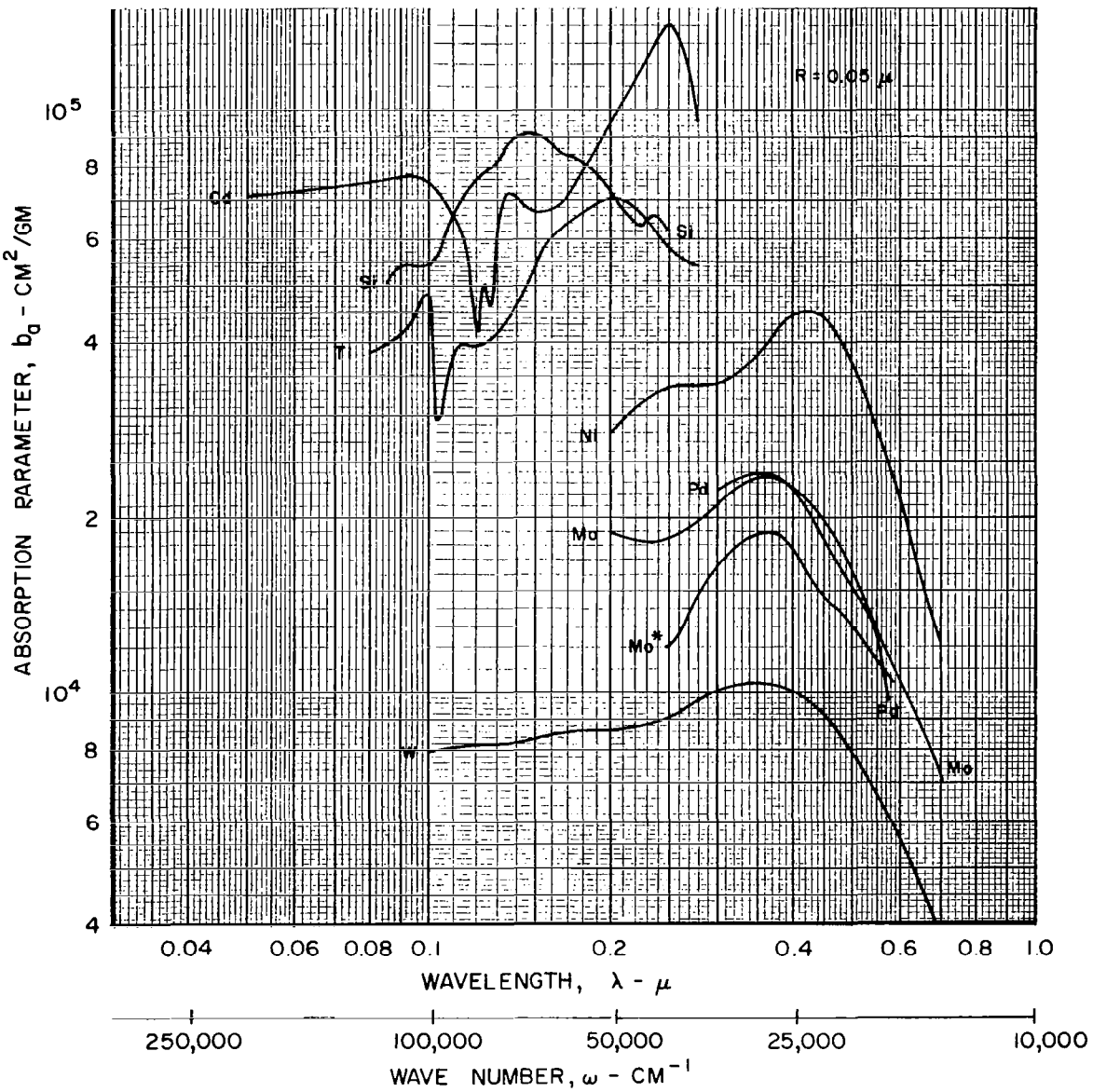

FIG. 17

COMPARISON OF THE EFFECT OF WAVELENGTH ON THE ABSORPTION PARAMETERS OF SPHERICAL ALUMINUM, CARBON, HAFNIUM, IRIDIUM IRON, MOLYBDENUM, NIOBIUM, PLATINUM AND TUNGSTEN PARTICLES

R = 0.05 μ

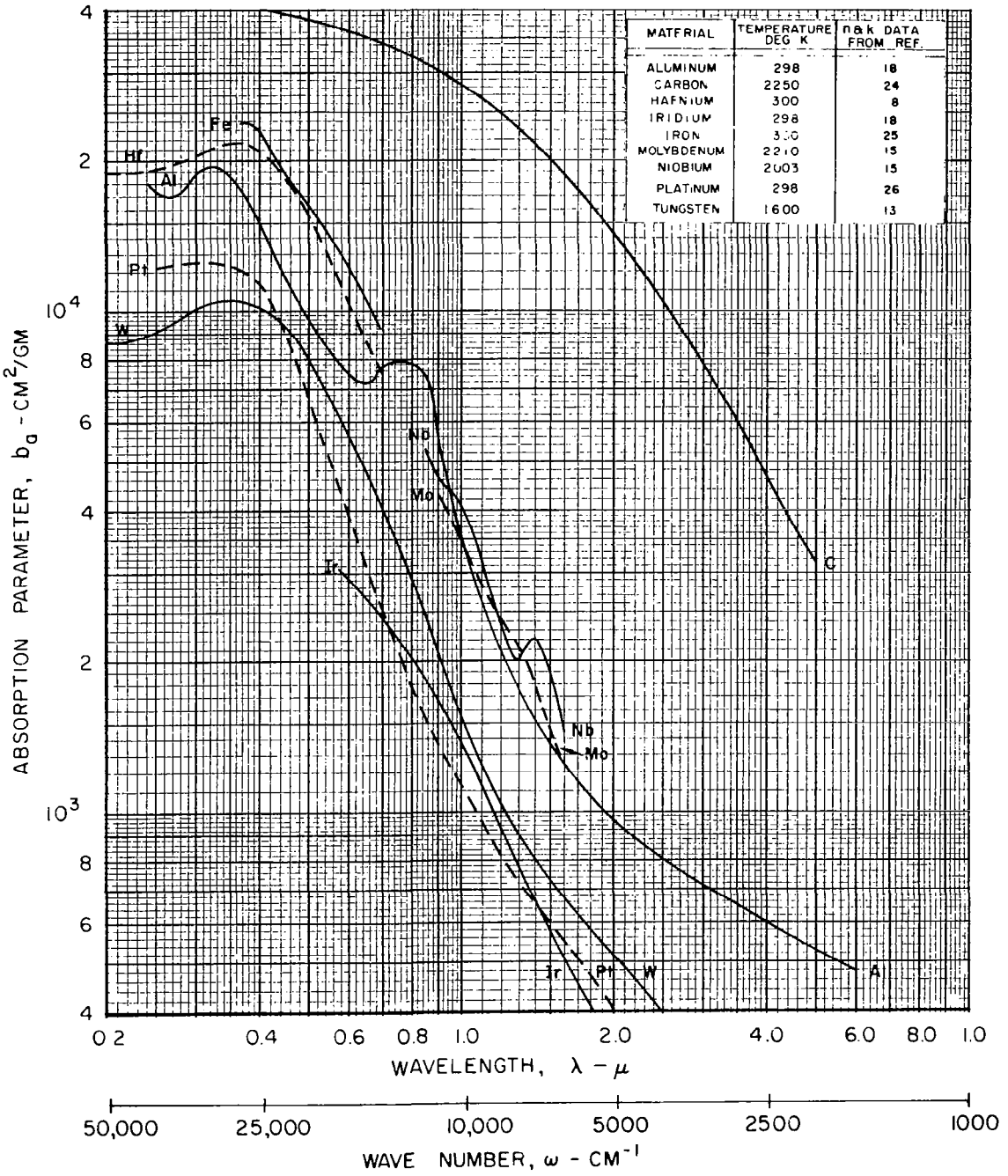

FIG. 18

COMPARISON OF THE EFFECT OF WAVELENGTH ON THE ABSORPTION PARAMETERS OF SPHERICAL COBALT, TITANIUM, TUNGSTEN, VANADIUM AND ZIRCONIUM PARTICLES

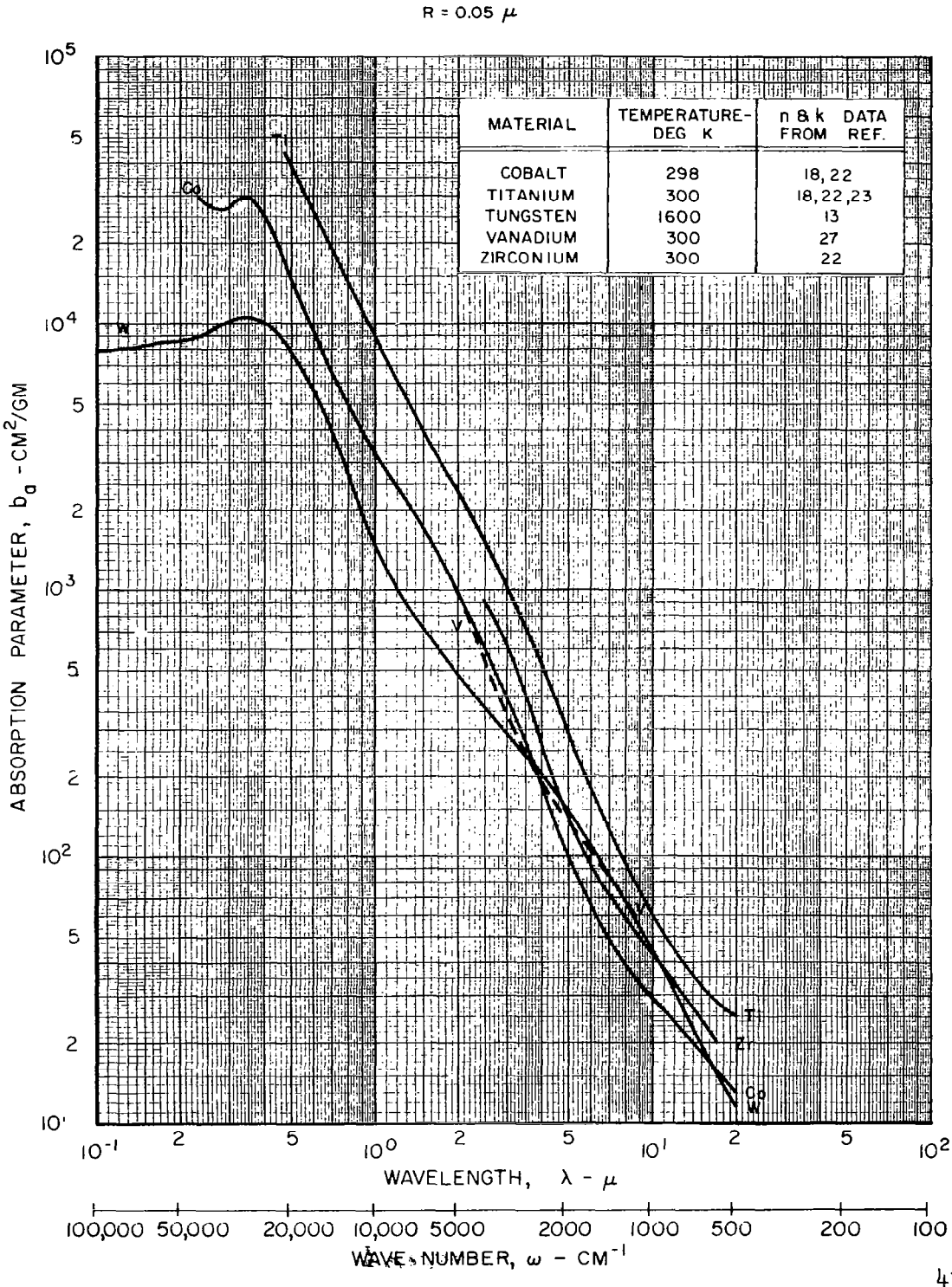

FIG. 19

COMPARISON OF EFFECT OF WAVE NUMBER ON THE ABSORPTION PARAMETER OF SPHERICAL TUNGSTEN PARTICLES COMPUTED FOR DIFFERENT SETS OF REFRACTIVE INDEX DATA

$R = 0.05\,\mu$

$\rho = 19.3$ GM/CM^3

——— b_a DATA BASED ON n AND k FROM REF. 13 (SEE FIGS. 3 AND 4) EXTRAPOLATED FOR $\omega > 1.0 \times 10^5$ CM^{-1} (TOTAL OSCILLATOR STRENGTH ~ 2.0)

– – – – b_a DATA BASED ON n AND k FROM REF. 14 (SEE FIGS. 3 AND 4) EXTRAPOLATED FOR $\omega > 2.5 \times 10^4$ CM^{-1} AND FOR $\omega < 4.0 \times 10^3$ (TOTAL OSCILLATOR STRENGTH ~ 0.208)

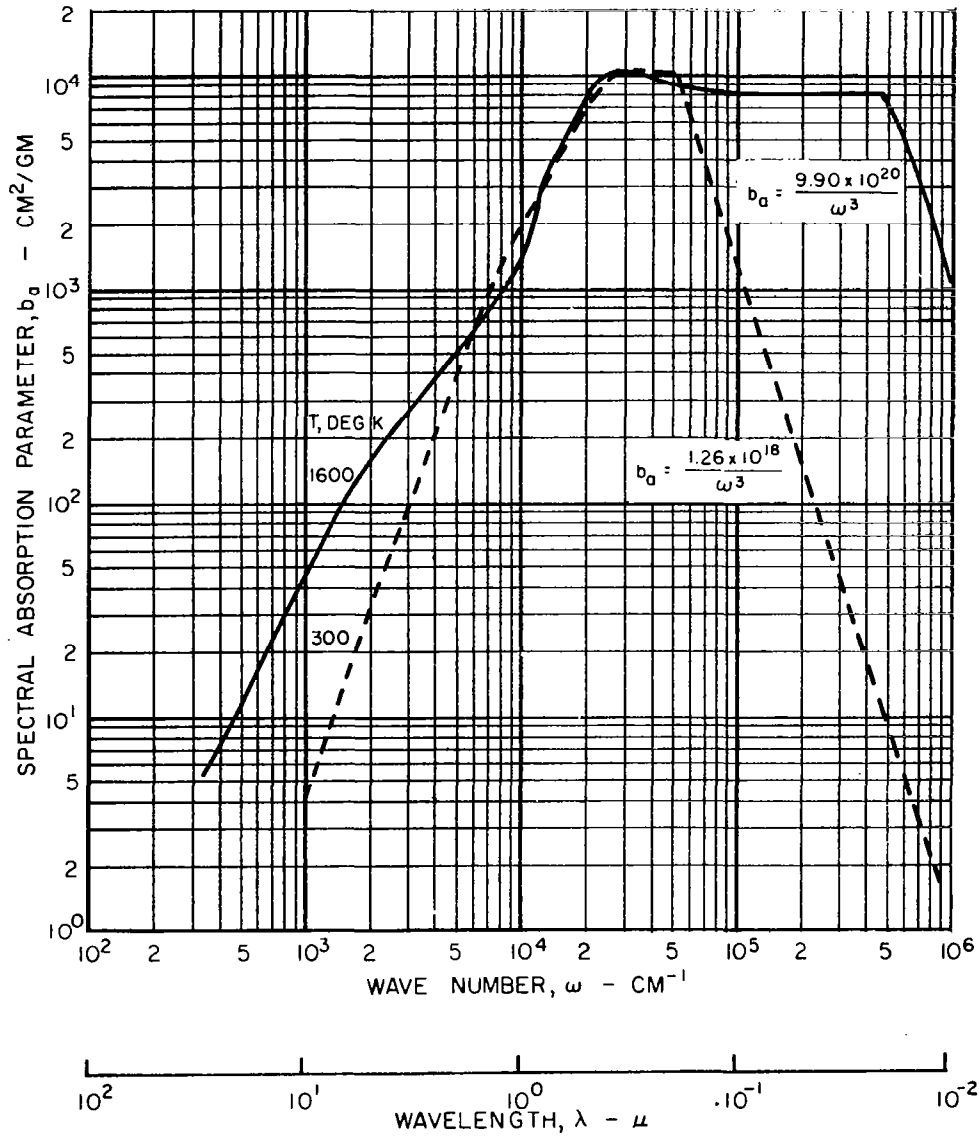

FIG. 20

EFFECT OF TEMPERATURE ON THE ROSSELAND MEAN OPACITY PARAMETER OF SPHERICAL TUNGSTEN PARTICLES

R = 0.05 μ
SEE FIG. 19 FOR SPECTRAL ABSORPTION PARAMETERS

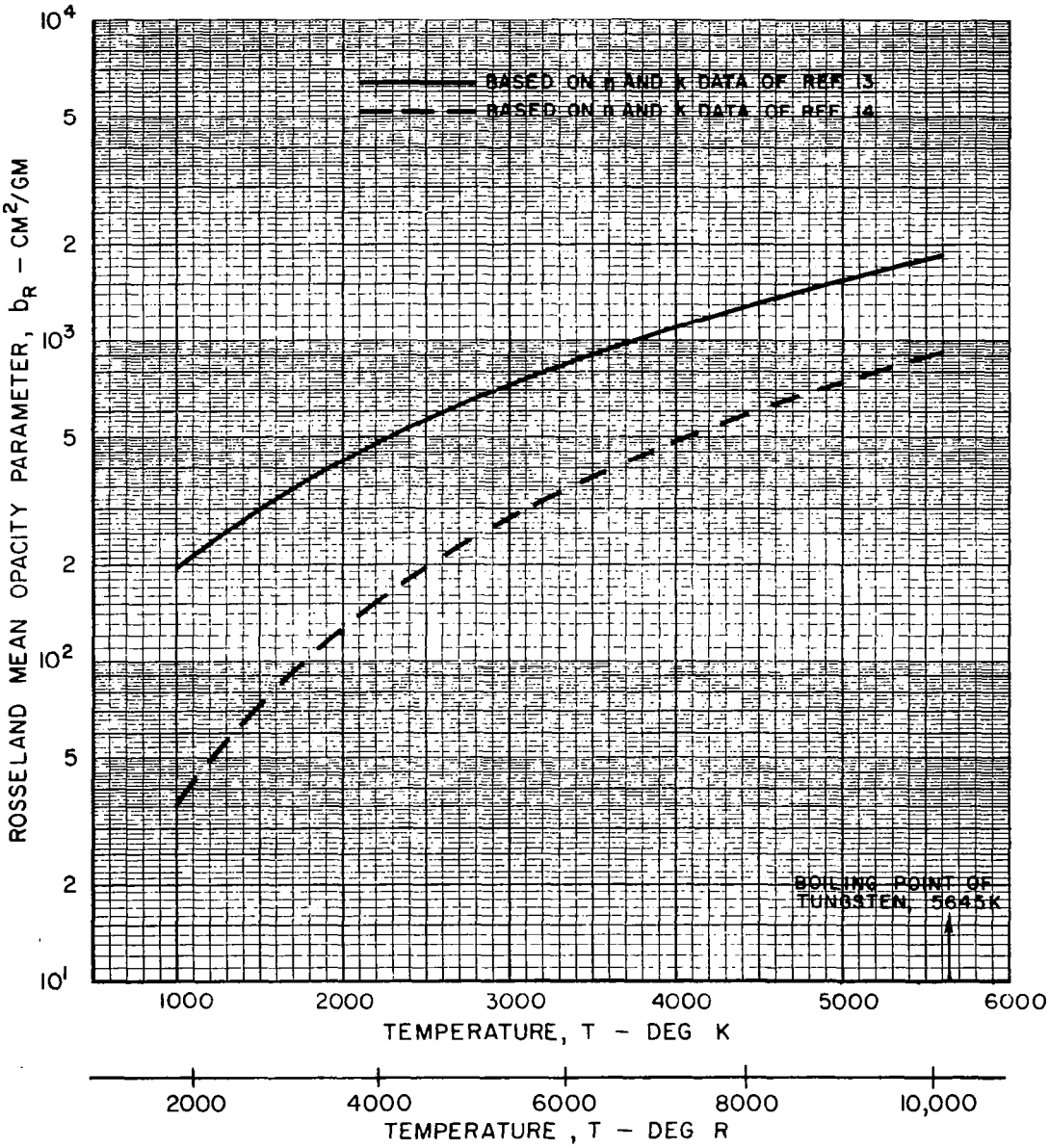

EFFECT OF TEMPERATURE ON THE ABSORPTION PARAMETER OF THIN TUNGSTEN PLATES BASED ON REFRACTIVE INDEX DATA FROM DIFFERENT SOURCES

$b_a' = 4\pi k/\lambda$

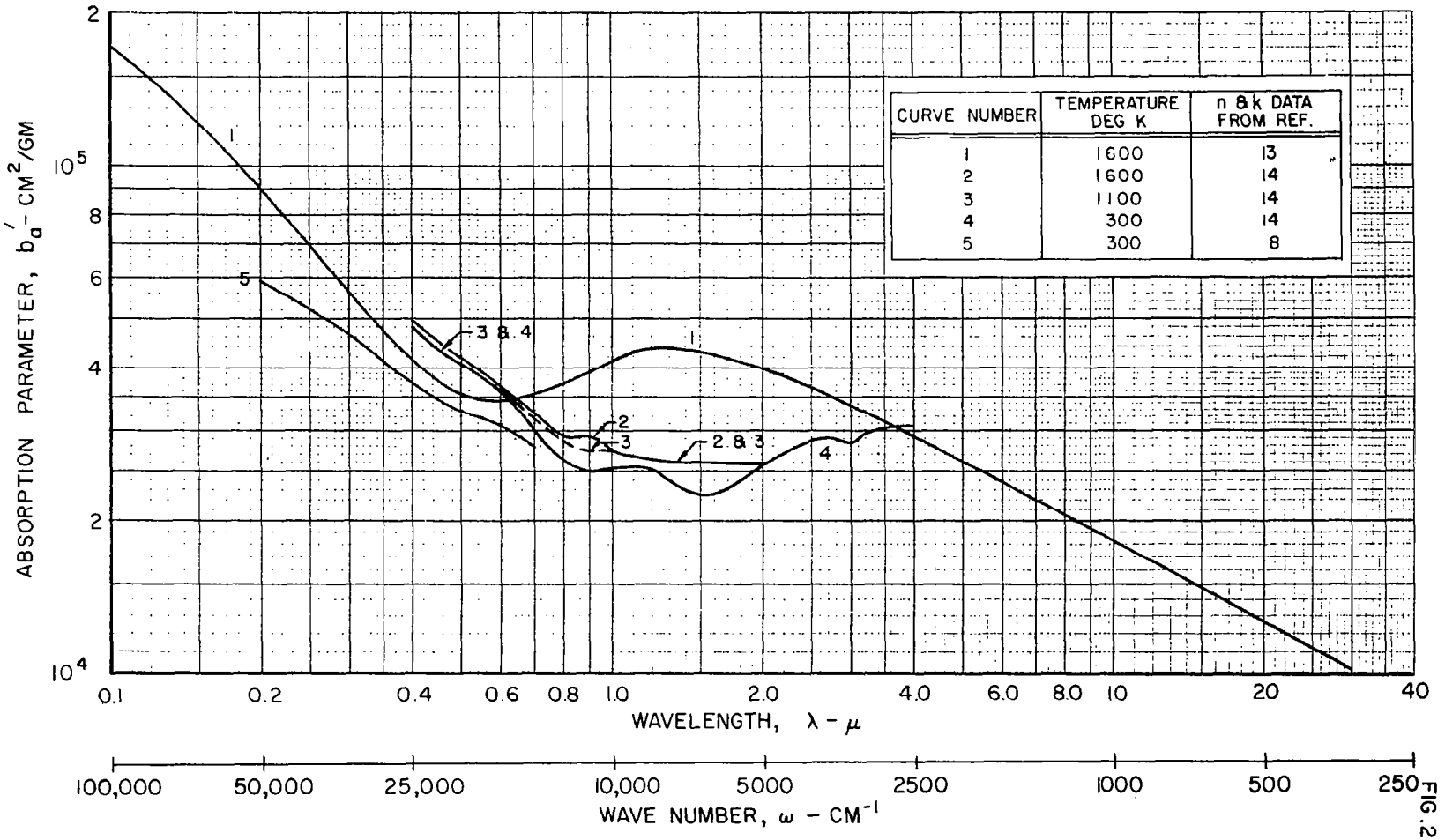

FIG. 21

FIG. 22

EFFECT OF WAVELENGTH ON THE ABSORPTION PARAMETER OF THIN CADMIUM, HAFNIUM, IRON, MOLYBDENUM, NICKEL, NIOBIUM, SILICON, THALLIUM AND TUNGSTEN PLATES

MATERIAL	TEMPERATURE DEG K	n&k DATA FROM REF.
CADMIUM	300	16
HAFNIUM	300	8
IRON	300	25
MOLYBDENUM	300	17
MOLYBDENUM	300	8*
MOLYBDENUM	2210	15**
NICKEL	300	8
NIOBIUM	2003	15
PALLADIUM	298	18
SILICON	300	19,20,21
THALLIUM	300	16
TUNGSTEN	1600	13

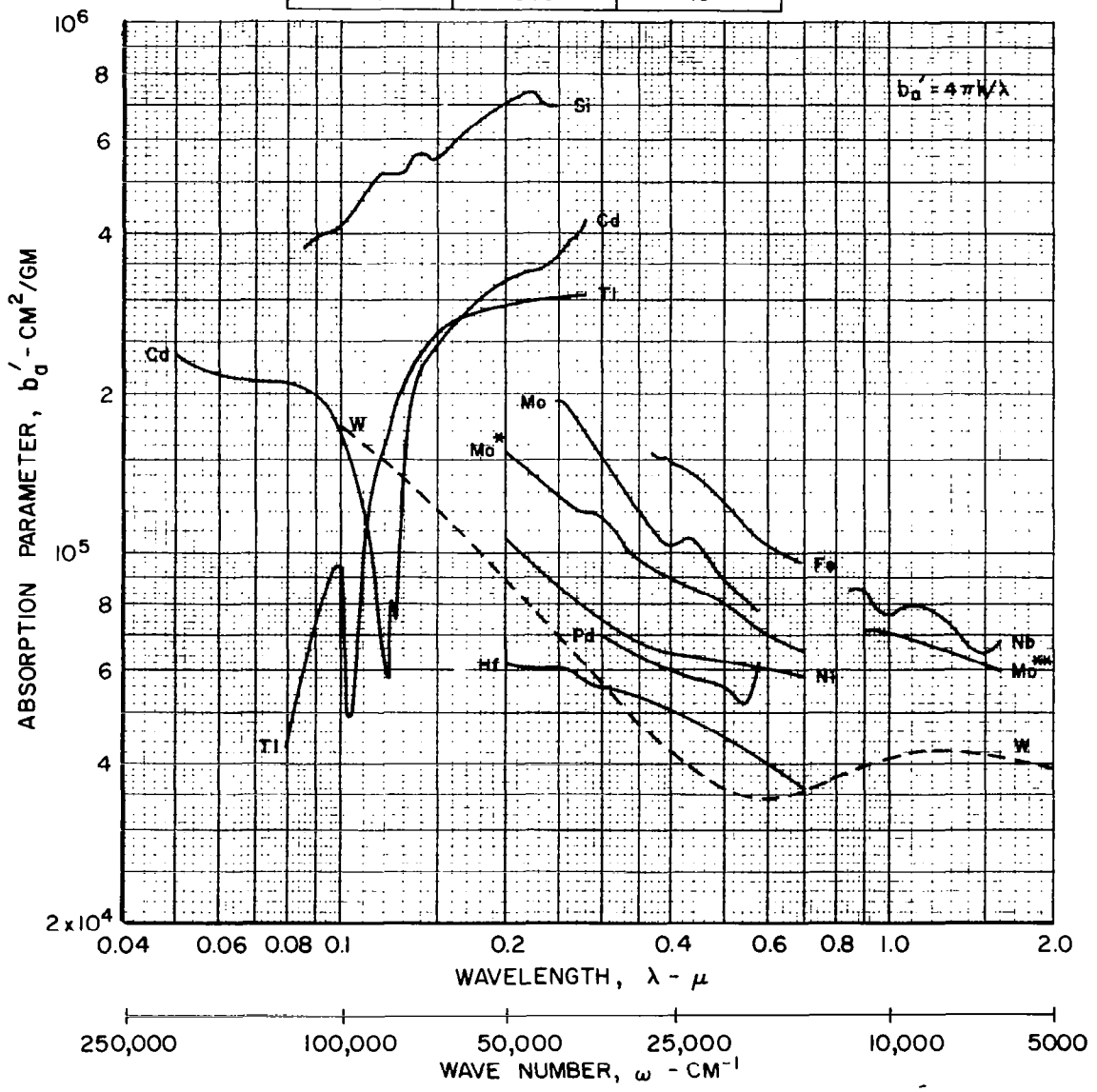

EFFECT OF WAVELENGTH ON THE ABSORPTION PARAMETER OF THIN ALUMINUM, CARBON, COBALT, IRIDIUM, PLATINUM, TITANIUM, TUNGSTEN, VANADIUM AND ZIRCONIUM PLATES

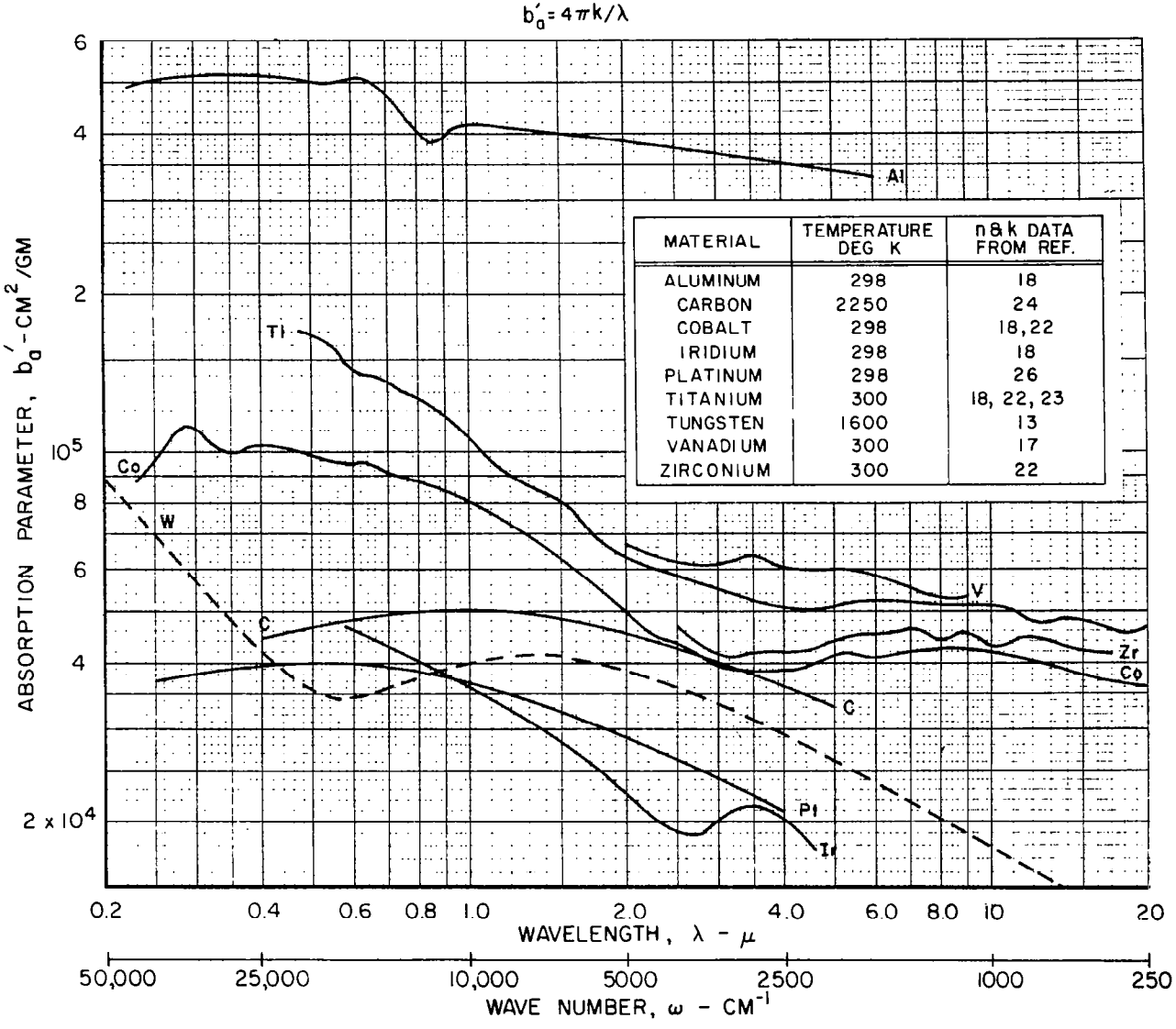

MATERIAL	TEMPERATURE DEG K	n & k DATA FROM REF.
ALUMINUM	298	18
CARBON	2250	24
COBALT	298	18, 22
IRIDIUM	298	18
PLATINUM	298	26
TITANIUM	300	18, 22, 23
TUNGSTEN	1600	13
VANADIUM	300	17
ZIRCONIUM	300	22

FIG. 23

FIG. 24

EFFECT OF WAVELENGTH ON THE NORMAL REFLECTIVITY OF TUNGSTEN BASED ON REFRACTIVE INDEX DATA FROM DIFFERENT SOURCES

CURVE NUMBER	TEMPERATURE DEG K	n&k DATA FROM REF.
1	300	8
2	300	14
3	1600	14
4	1100	14
5	1600	13

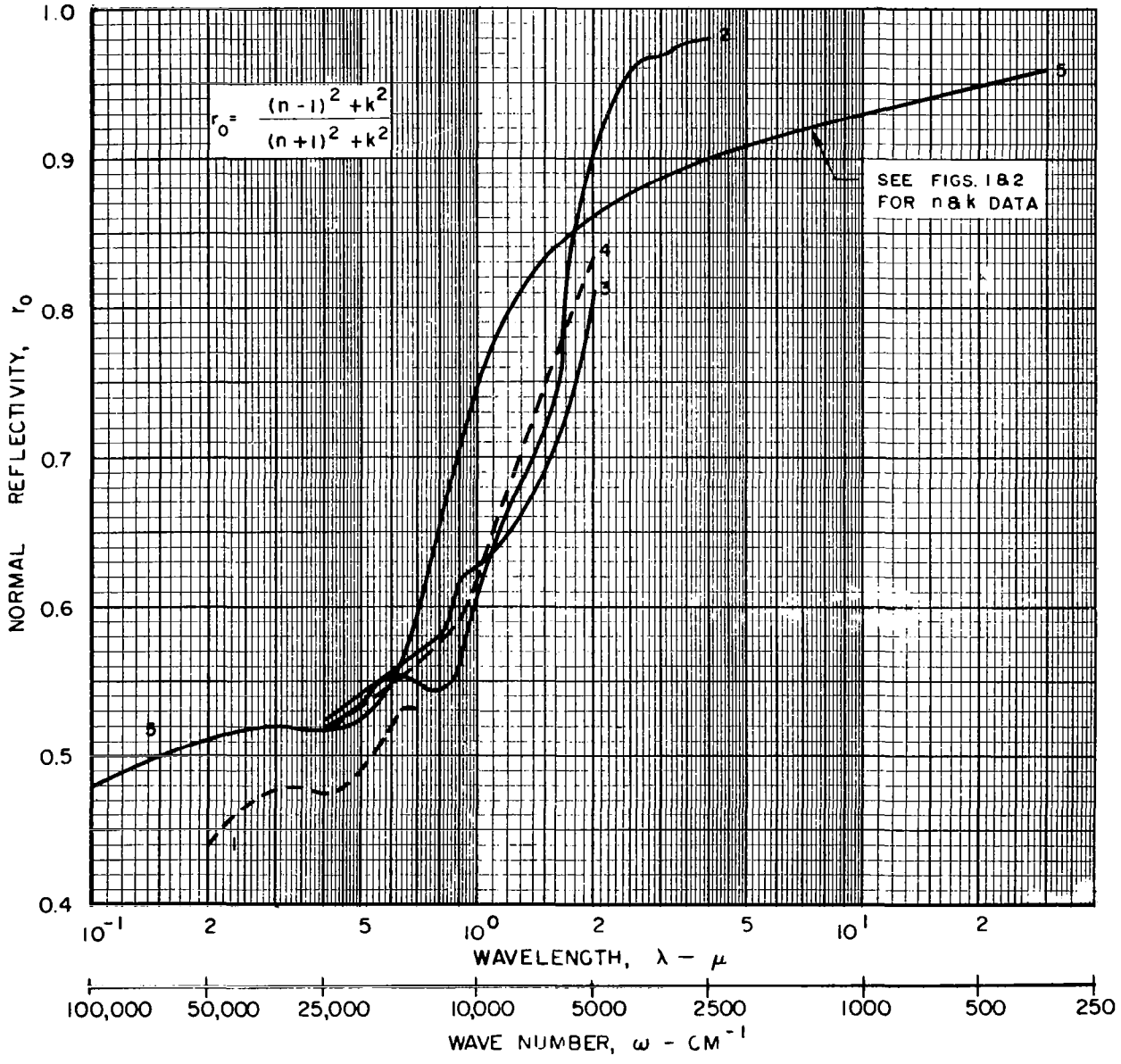

FIG. 25

EFFECT OF WAVELENGTH ON THE NORMAL REFLECTIVITIES OF HAFNIUM, IRON, MOLYBDENUM, NIOBIUM AND PALLADIUM

MATERIAL	TEMPERATURE DEG K	n&k DATA FROM REF.
HAFNIUM	300	8
IRON	300	25
MOLYBDENUM	300	8
MOLYBDENUM	300	17*
MOLYBDENUM	2210	15**
NIOBIUM	2003	15
PALLADIUM	298	18

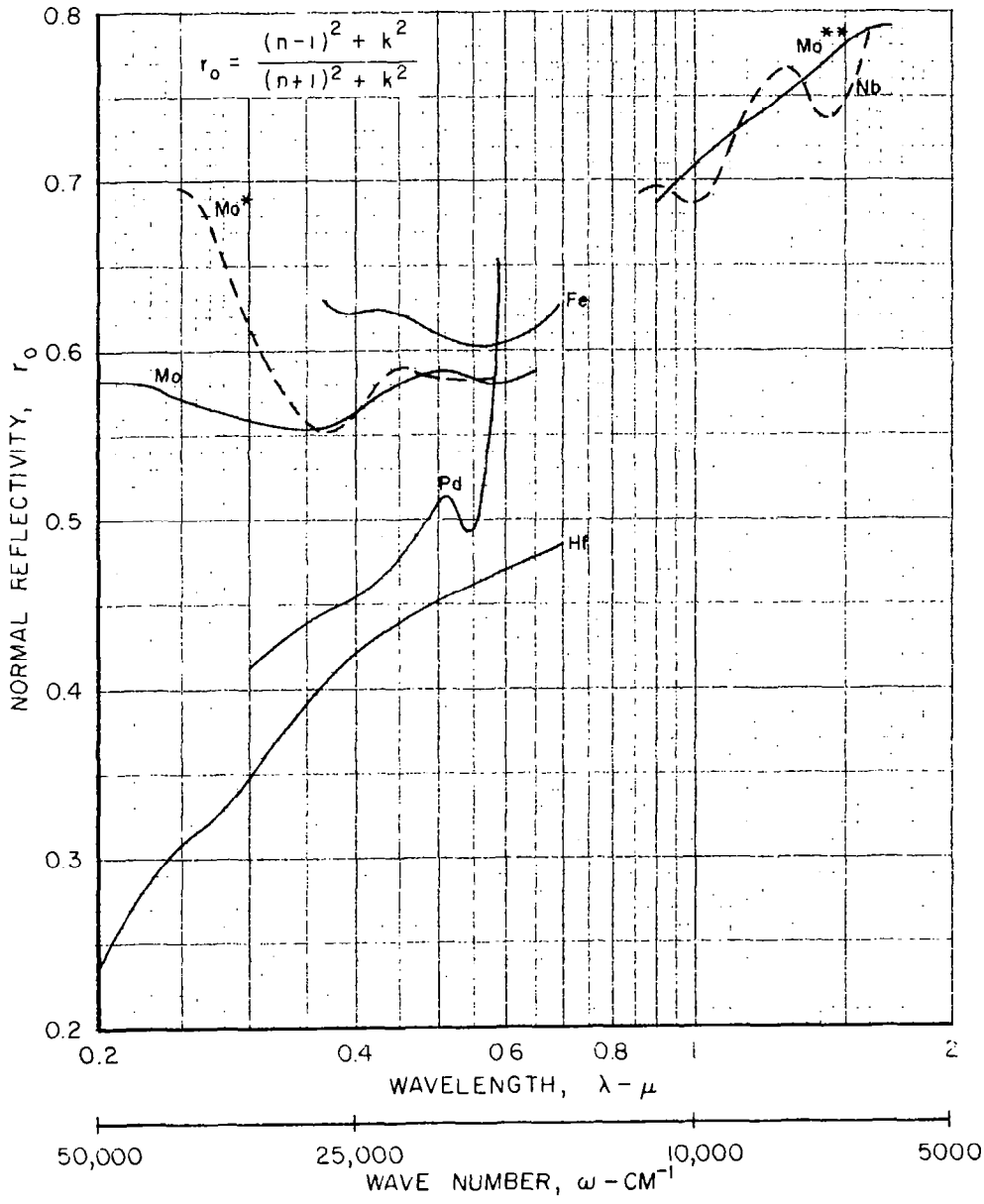

EFFECT OF WAVELENGTH ON THE NORMAL REFLECTIVITIES OF CADMIUM, CARBON, COBALT, PLATINUM, SILICON AND THALLIUM

$$r_0 = \frac{(n-1)^2 + k^2}{(n+1)^2 + k^2}$$

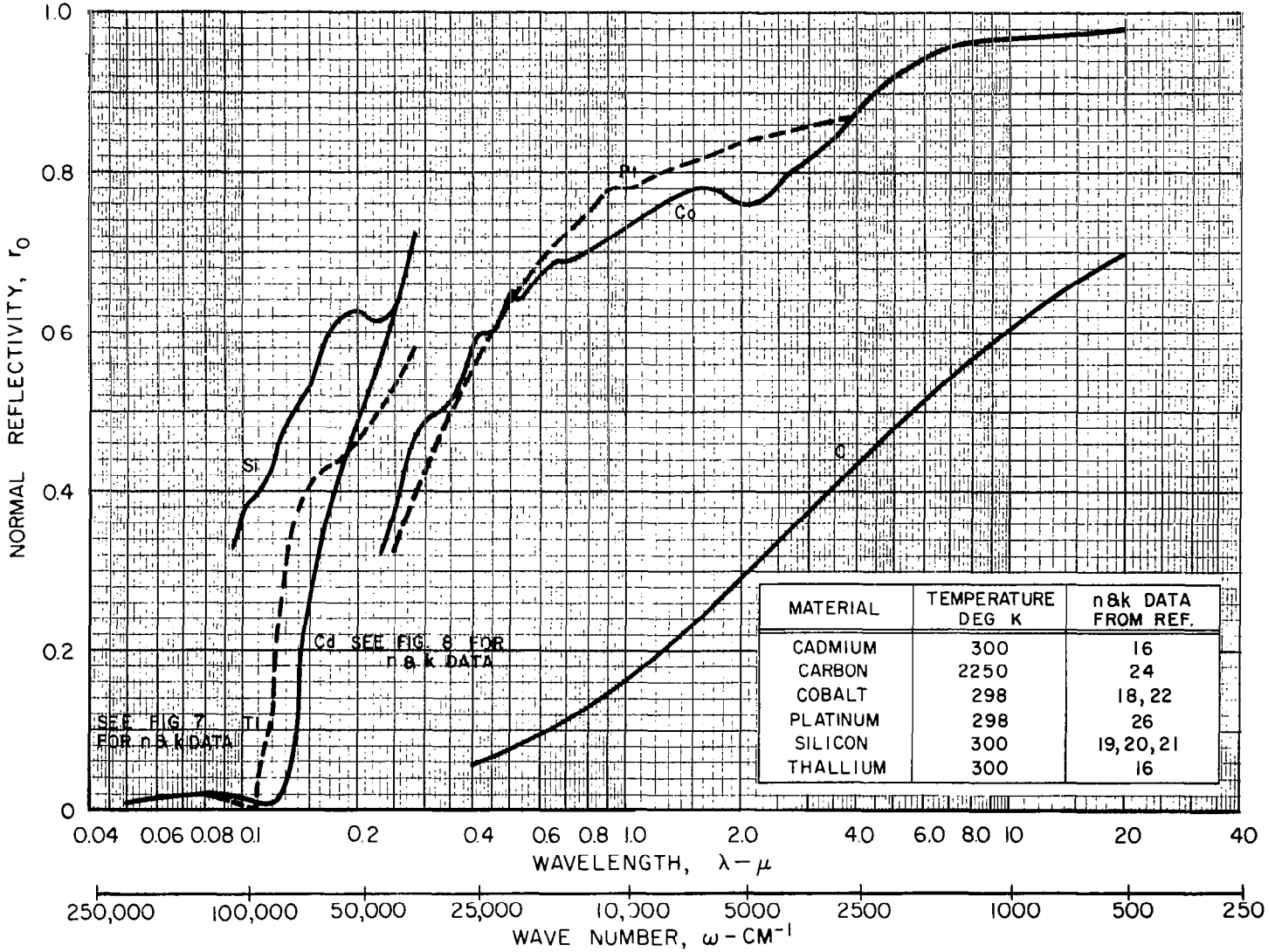

MATERIAL	TEMPERATURE DEG K	n & k DATA FROM REF.
CADMIUM	300	16
CARBON	2250	24
COBALT	298	18, 22
PLATINUM	298	26
SILICON	300	19, 20, 21
THALLIUM	300	16

FIG. 26

EFFECT OF WAVELENGTH ON THE NORMAL REFLECTIVITIES OF ALUMINUM, IRIDIUM , NICKEL, TITANIUM, VANADIUM AND ZIRCONIUM

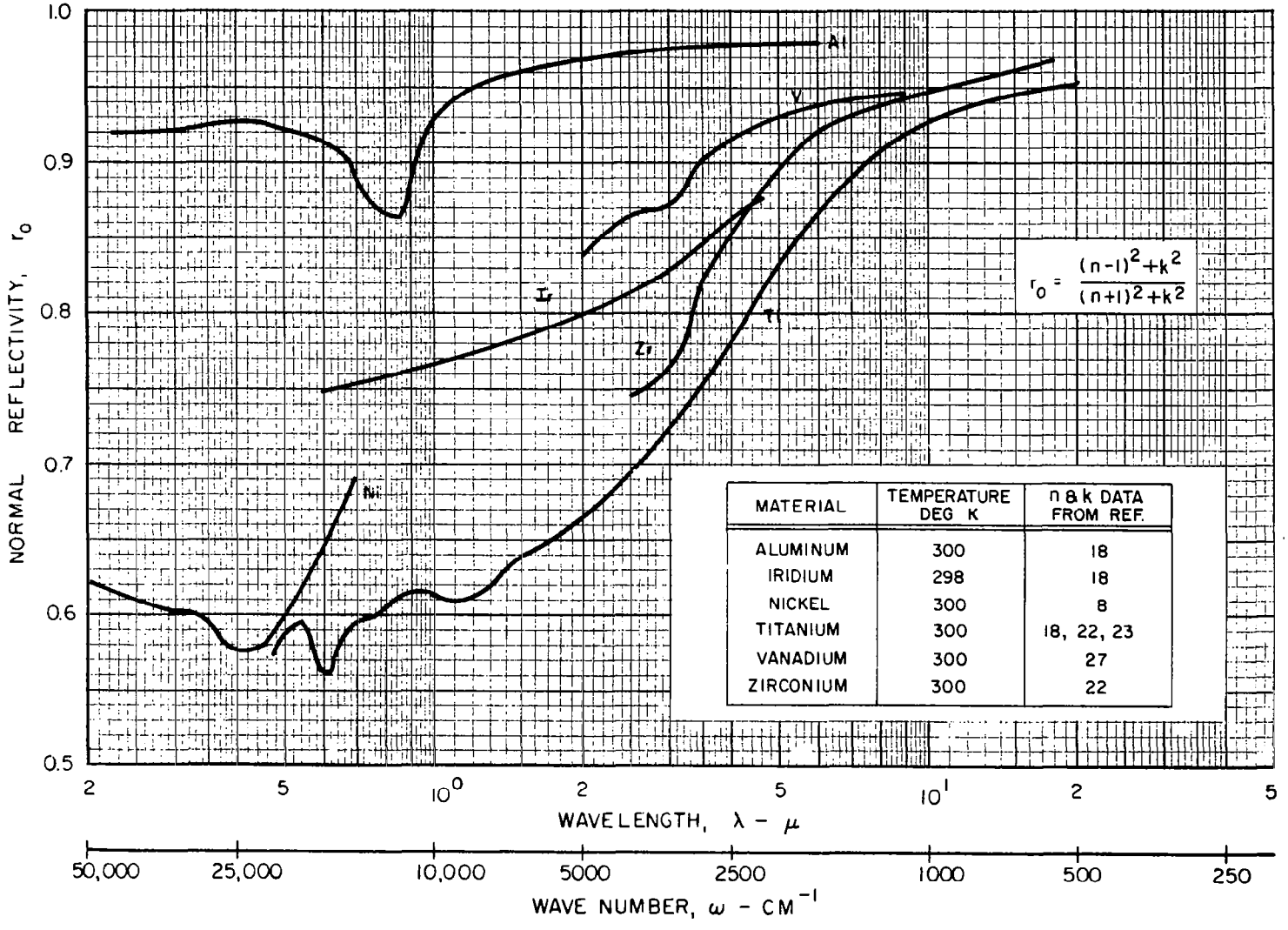

MATERIAL	TEMPERATURE DEG K	n & k DATA FROM REF.
ALUMINUM	300	18
IRIDIUM	298	18
NICKEL	300	8
TITANIUM	300	18, 22, 23
VANADIUM	300	27
ZIRCONIUM	300	22

FIG. 27

NORMAL SPECTRAL REFLECTIVITIES EMPLOYED IN CALCULATION OF AVERAGE REFLECTIVITIES

SOLID LINES INDICATE DATA FROM REFERENCE GIVEN IN TABLE BELOW
DASHED LINES INDICATE EXTRAPOLATED VALUES
SYMBOLS INDICATE WAVELENGTHS USED AS INPUT FOR CALCULATING AVERAGE REFLECTIVITIES (SEE FIG. 29)

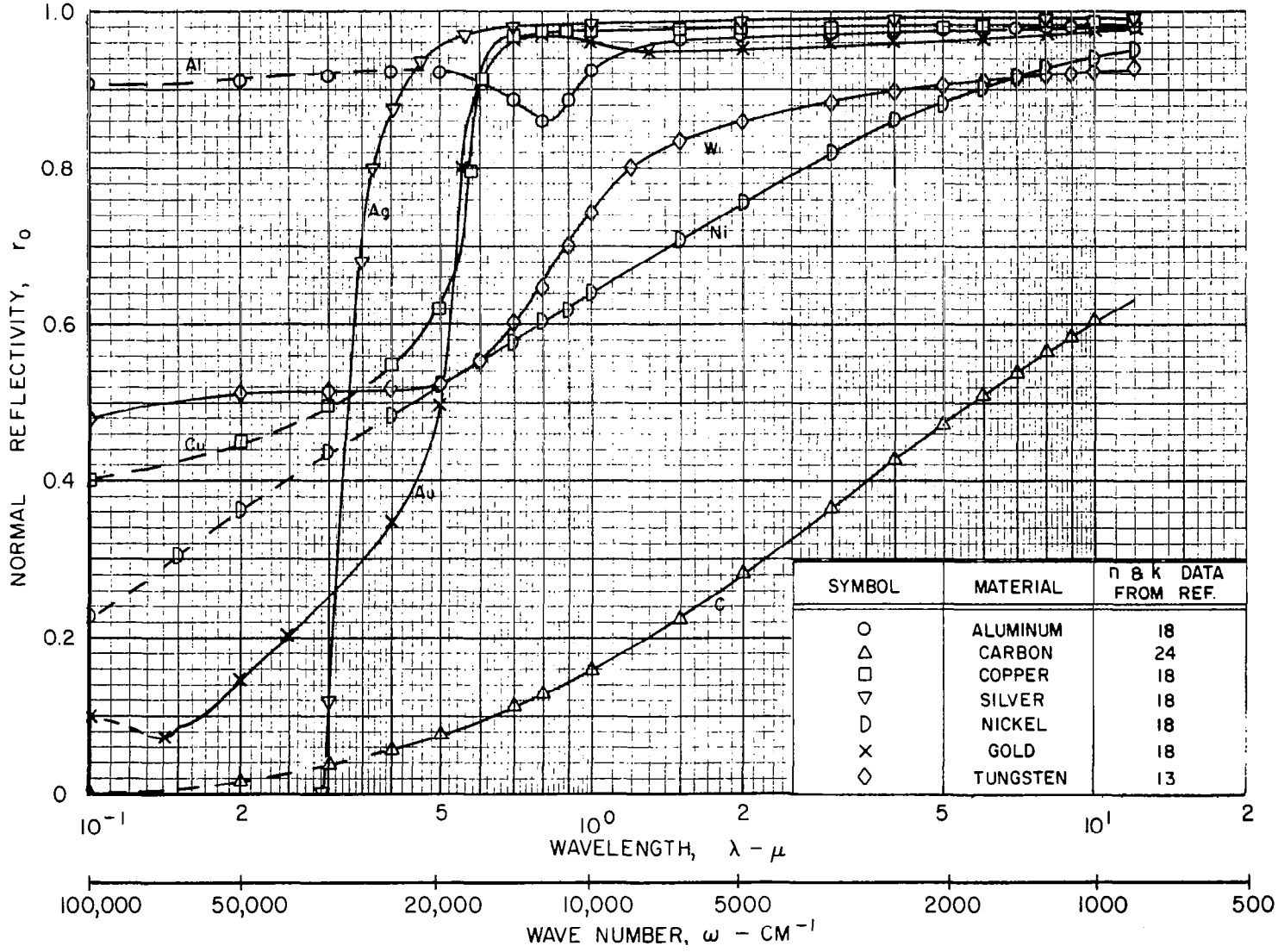

SYMBOL	MATERIAL	n & k DATA FROM REF.
○	ALUMINUM	18
△	CARBON	24
□	COPPER	18
▽	SILVER	18
D	NICKEL	18
×	GOLD	18
◇	TUNGSTEN	13

FIG. 28

EFFECT OF BLACK-BODY RADIATING TEMPERATURE ON AVERAGE REFLECTIVITY OF SEVERAL MATERIALS

$$\overline{R} = \int_{\lambda=0.1}^{\lambda=12} B_\lambda r_0 d_\lambda \Big/ \int_{\lambda=0.1}^{\lambda=12} B_\lambda d_\lambda$$

NORMAL SPECTRAL REFLECTIVITIES USED AS INPUT FOR CALCULATING AVERAGE REFLECTIVITIES GIVEN IN FIG. 28

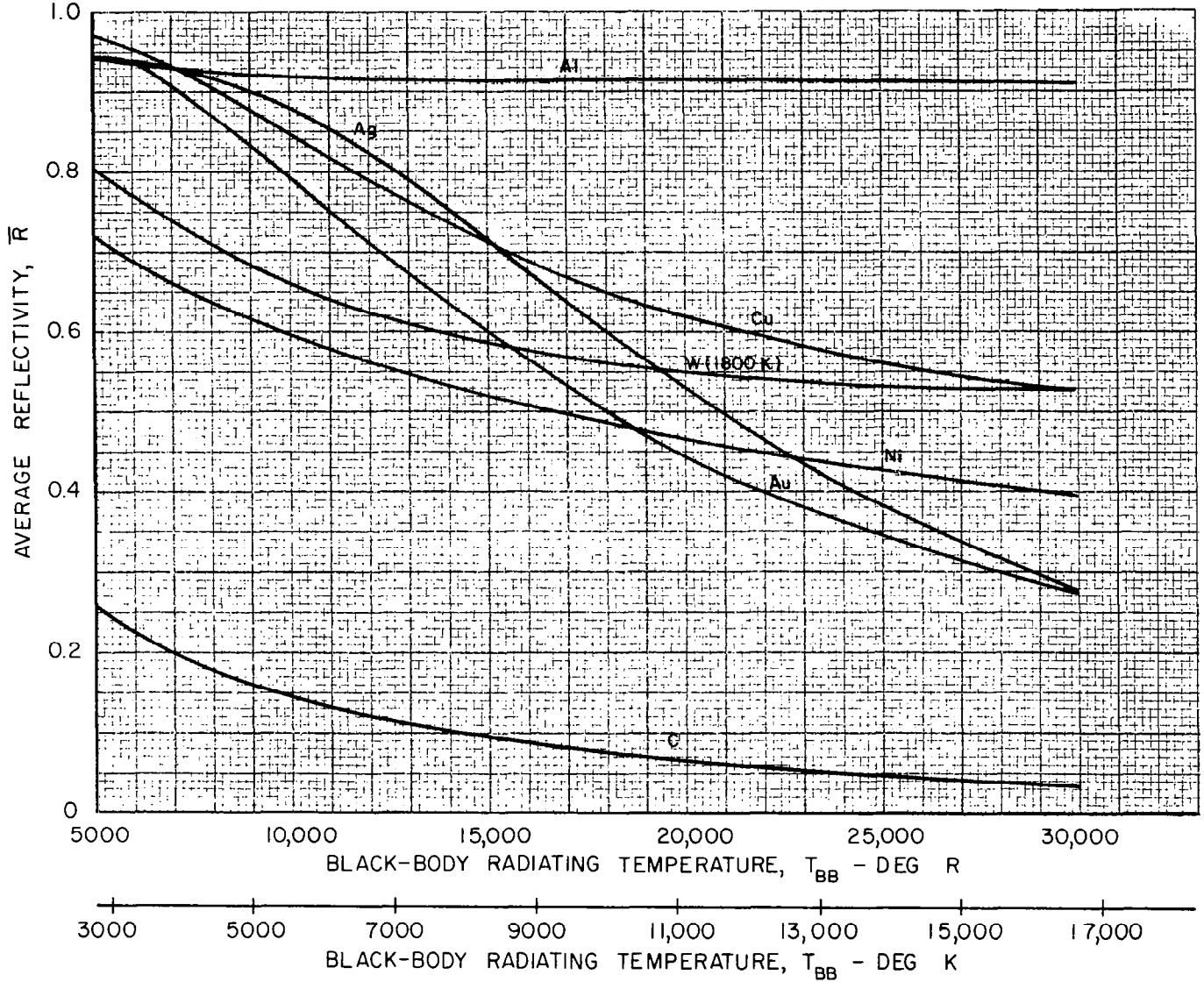

FIG. 29

FIG. 30

CORRELATION BETWEEN BOILING-POINT TEMPERATURES AND THE ABSORPTION PARAMETERS OF VARIOUS SPHERICAL PARTICLES INVESTIGATED

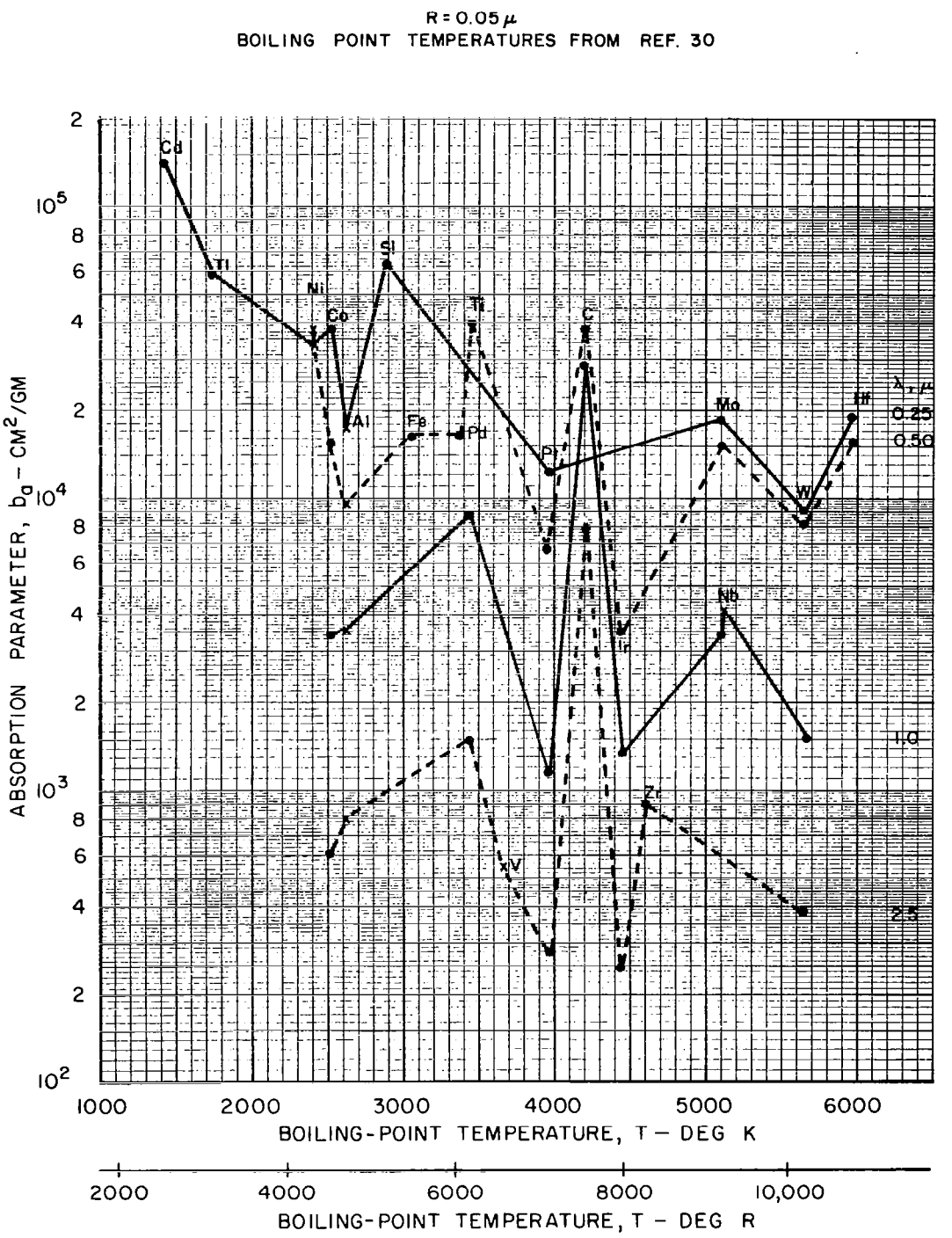

CORRELATION BETWEEN THERMAL NEUTRON CROSS SECTIONS AND THE ABSORPTION PARAMETERS OF VARIOUS SPHERICAL PARTICLES INVESTIGATED

R = 0.05 μ

THERMAL NEUTRON CROSS SECTIONS FROM REF. 31

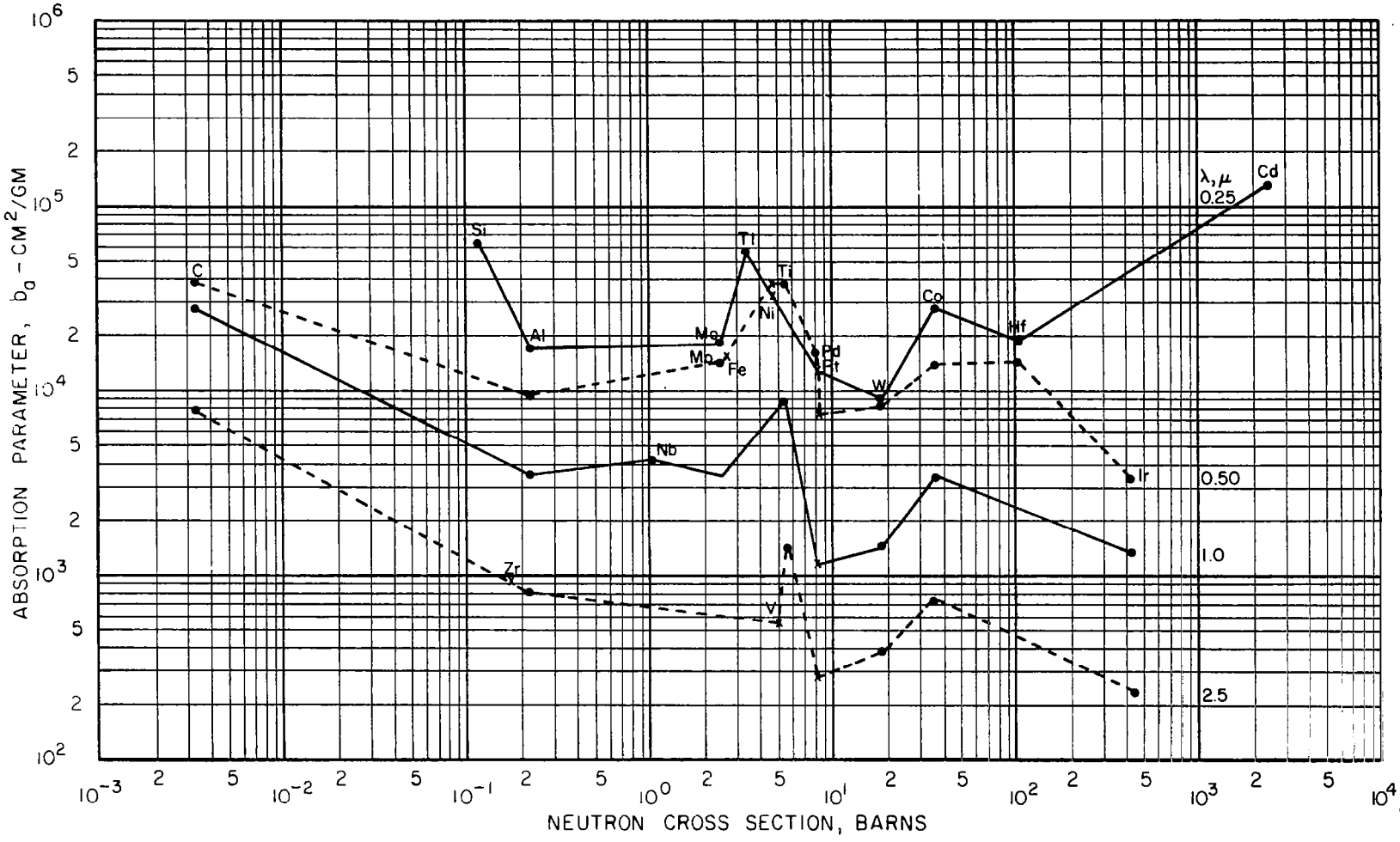

FIG. 31

FIG. 32

LOCAL AVERAGE SPACING IN 1000 CM^{-1} INTERVALS CALCULATED FROM EXPERIMENTAL LINE STRUCTURES OF TUNGSTEN I AND TUNGSTEN II

$$S = \frac{1}{\text{NUMBER OF LINES PER 1000 } CM^{-1} \text{ INTERVAL}}$$

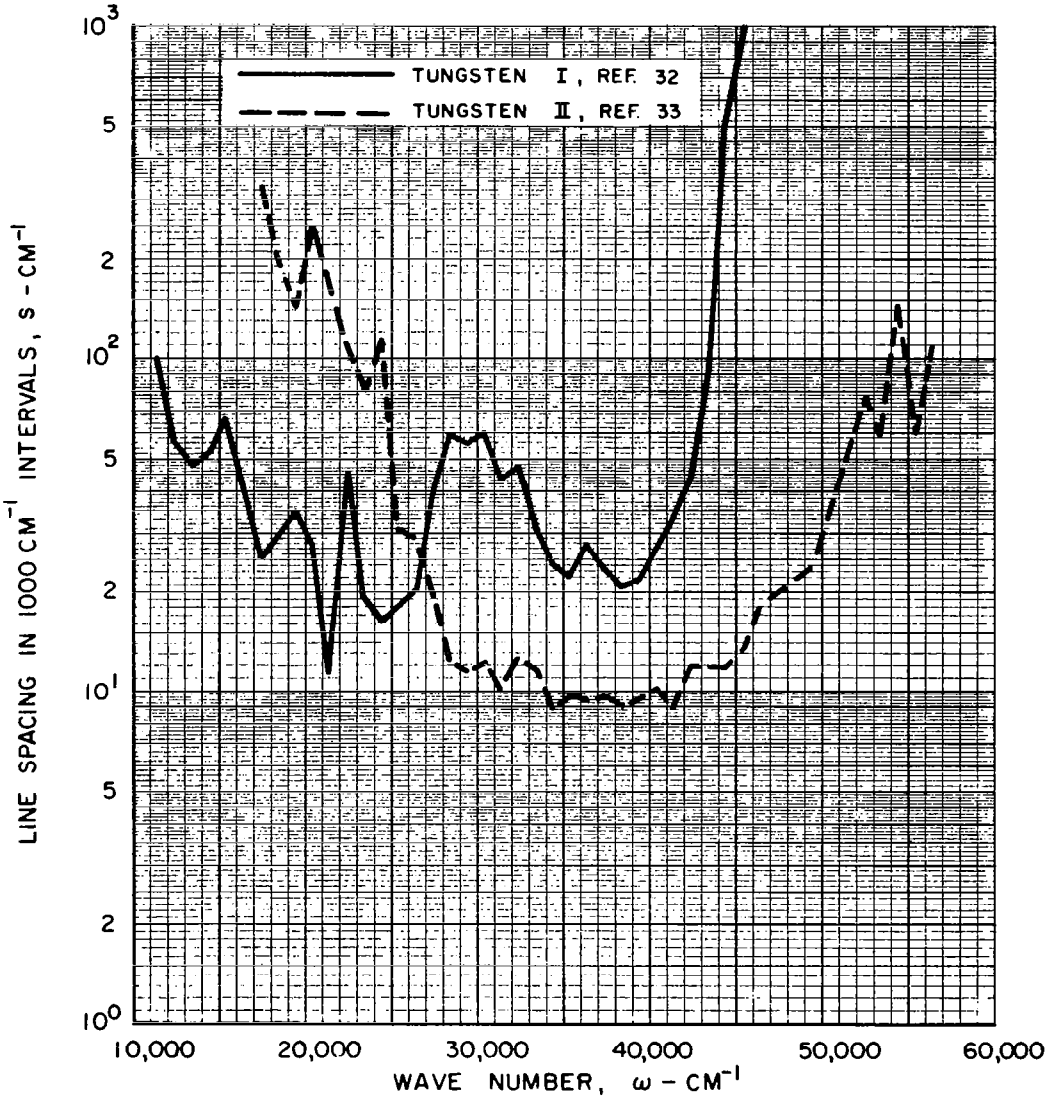

RELATIVE TOTAL LINE INTENSITY PER 1000 CM^{-1} INTERVAL AS A FUNCTION OF WAVE NUMBER CALCULATED FROM EXPERIMENTAL LINE INTENSITIES OF TUNGSTEN I AND TUNGSTEN II

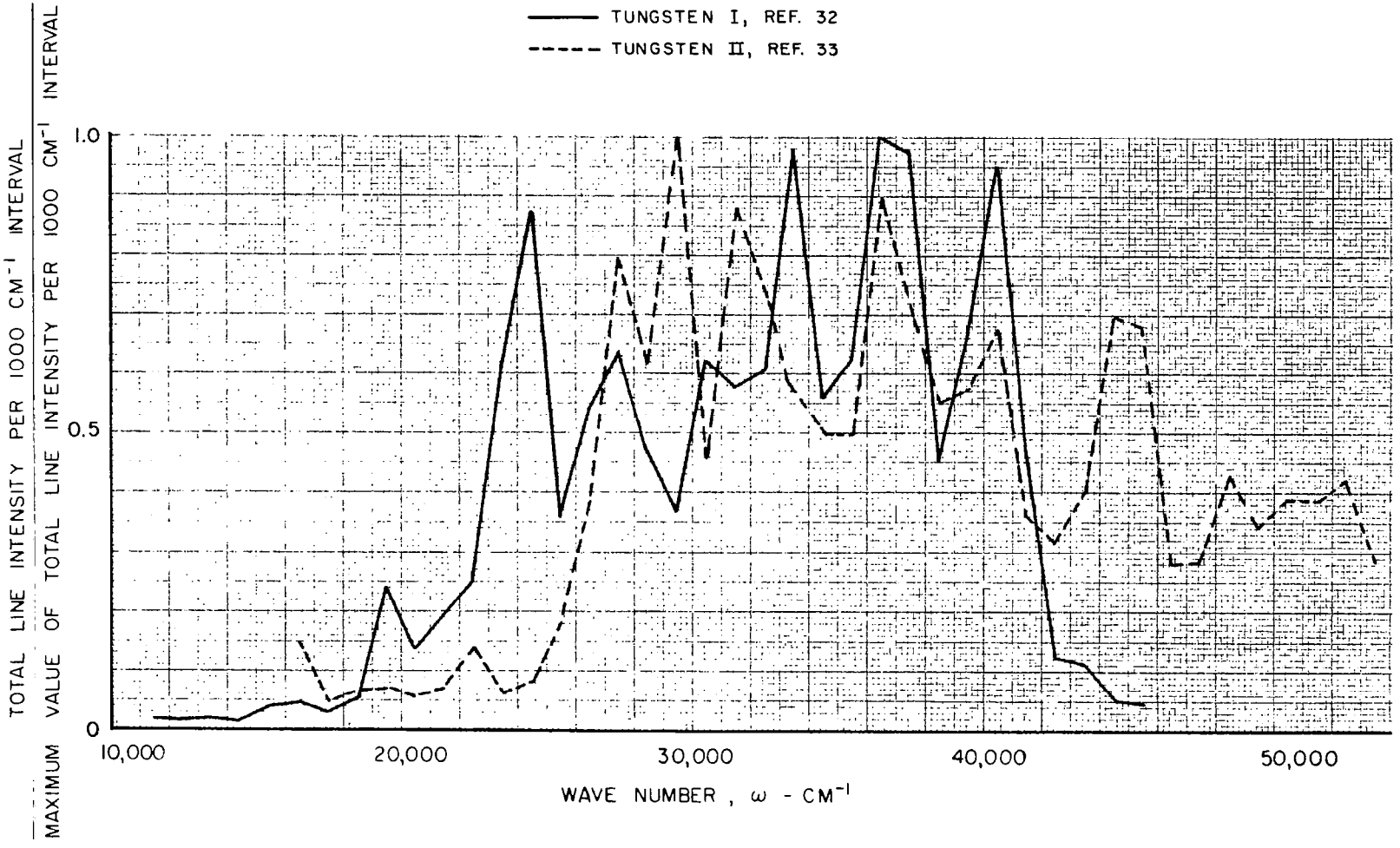

FIG. 33

COMPARISON OF ASSUMED OSCILLATOR STRENGTH DISTRIBUTIONS USED IN THE HEAVY-ATOM MODEL AS FUNCTIONS OF PHOTON ENERGY

"BAND" DISTRIBUTION $\frac{df_b}{dE}$, SEE EQ. (12)

"CONTINUUM" DISTRIBUTION $\frac{df_c}{dE}$, SEE EQ. (10)

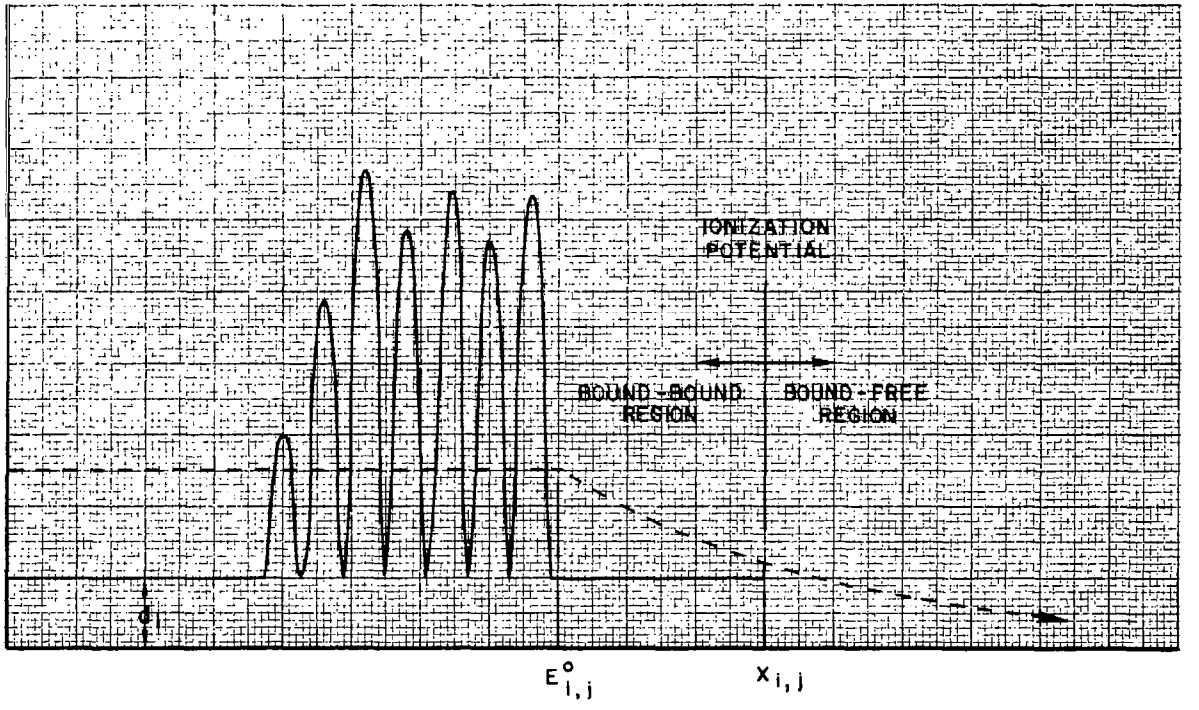

FIG. 34

COMPARISON OF DISTRIBUTION OF RELATIVE TOTAL LINE INTENSITY PER 1000 CM^{-1} INTERVAL CALCULATED FROM EXPERIMENTAL LINE INTENSITIES AND CALCULATED SPECTRAL ABSORPTION COEFFICIENT FROM HEAVY-ATOM MODEL

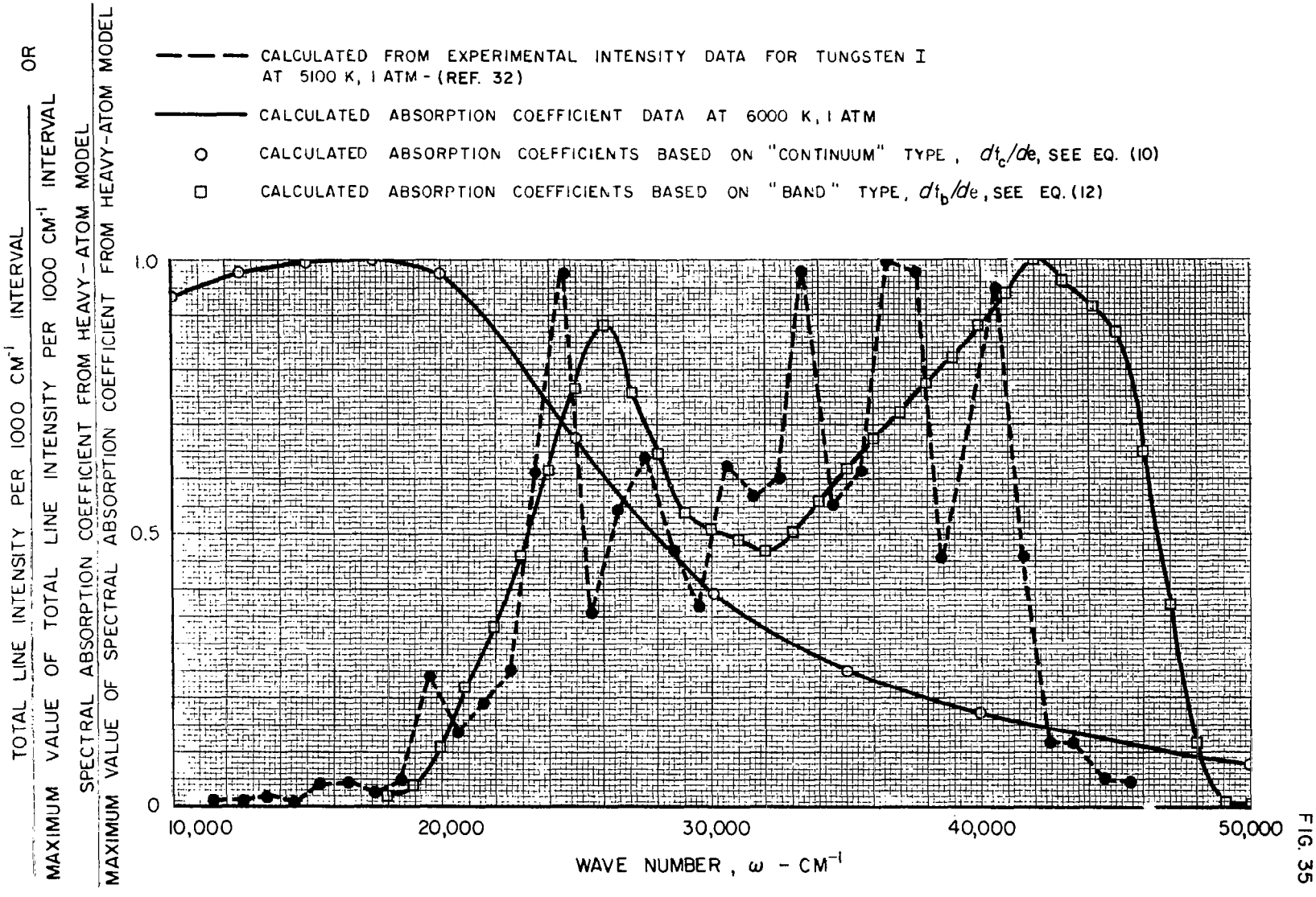

FIG. 35

COMPARISON OF THE EFFECT OF WAVE NUMBER ON THE SPECTRAL ABSORPTION COEFFICIENT OF TUNGSTEN GAS FOR DIFFERENT OSCILLATOR STRENGTH DISTRIBUTIONS USED IN HEAVY-ATOM MODEL

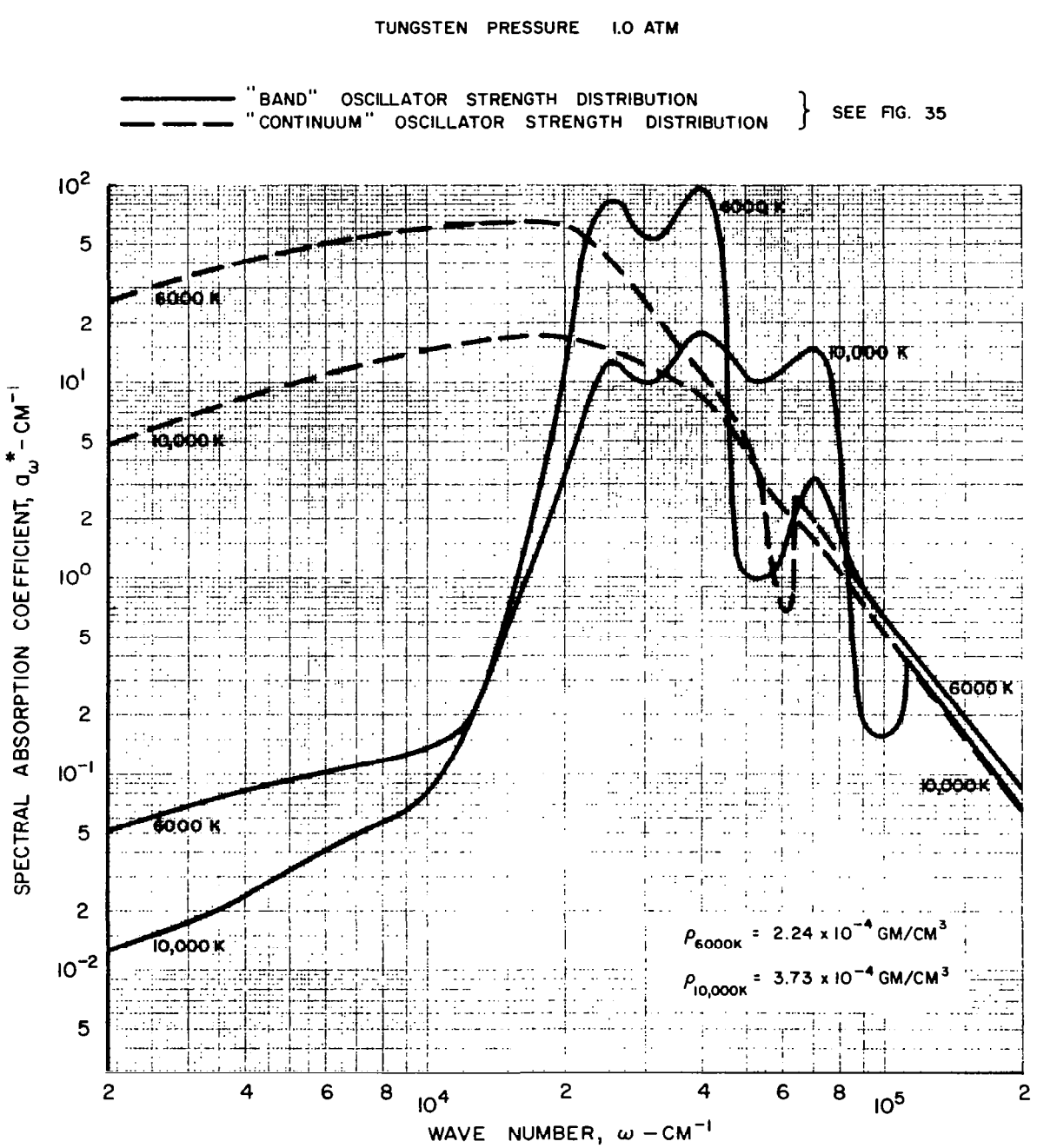

FIG. 37

COMPARISON OF THE EFFECT OF TEMPERATURE ON THE ROSSELAND MEAN OPACITY OF TUNGSTEN GAS FOR DIFFERENT OSCILLATOR STRENGTH DISTRIBUTIONS USED IN THE HEAVY-ATOM MODEL

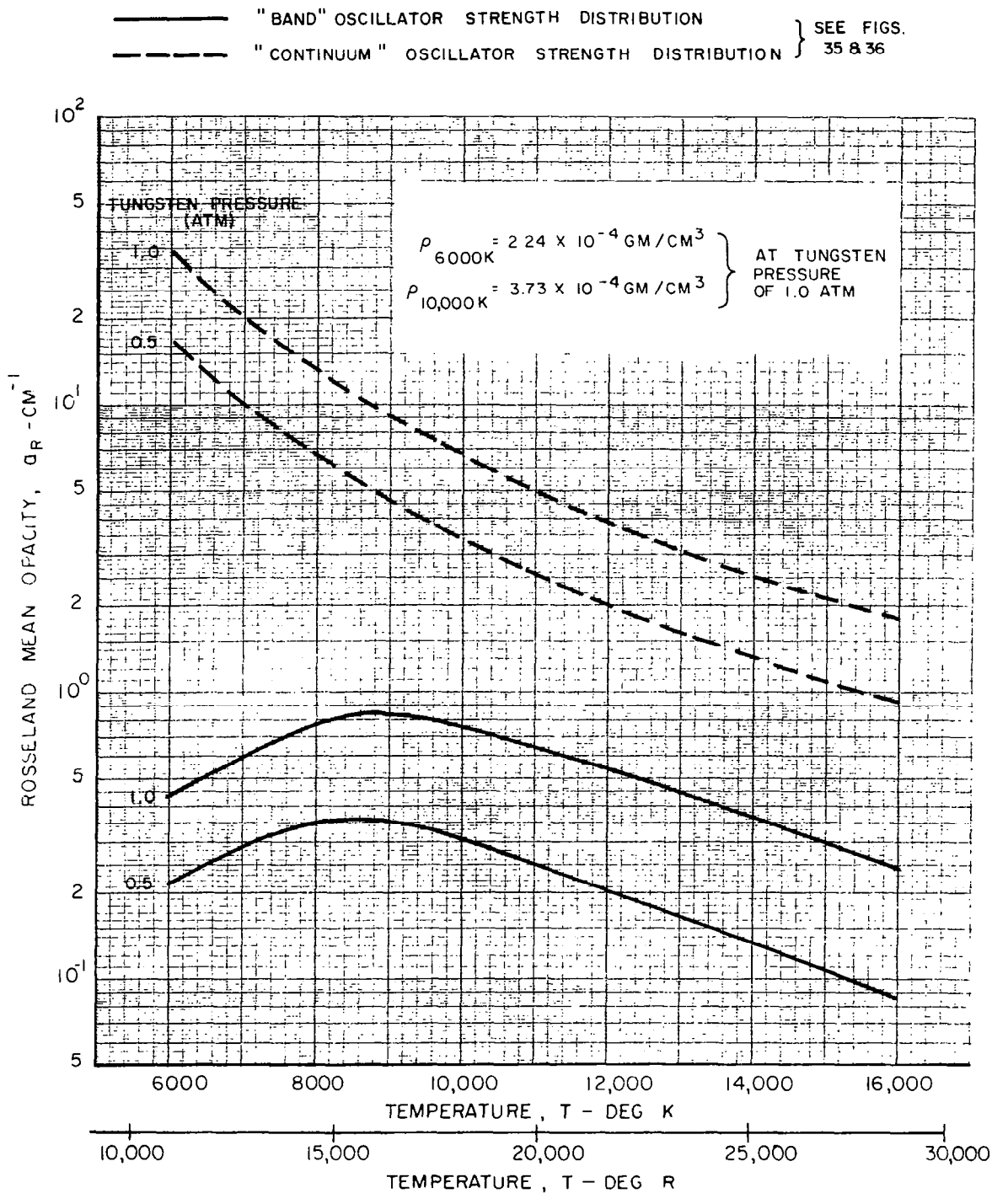

FIG. 38

LOCAL AVERAGE SPACING IN 1000 CM^{-1} INTERVALS FROM EXPERIMENTAL LINE STRUCTURES OF IRON I, SILICON I AND URANIUM I

$$S = \frac{1}{\text{NUMBER OF LINES PER 1000 } CM^{-1} \text{ INTERVAL}}$$

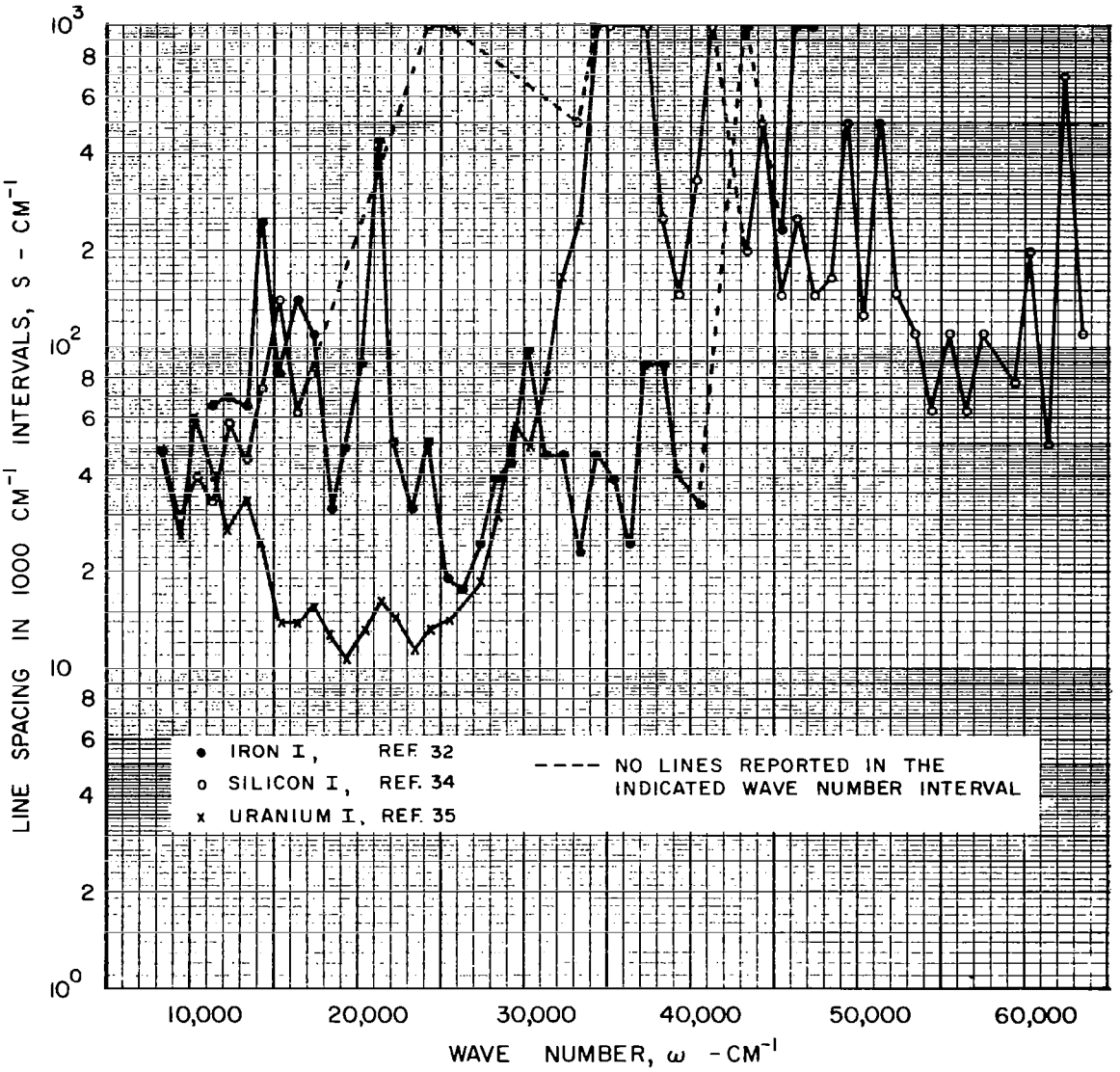

FIG. 39

LOCAL AVERAGE SPACING IN 1000 CM^{-1} INTERVALS FROM EXPERIMENTAL LINE STRUCTURES OF NIOBIUM I AND NIOBIUM II

REF. 36

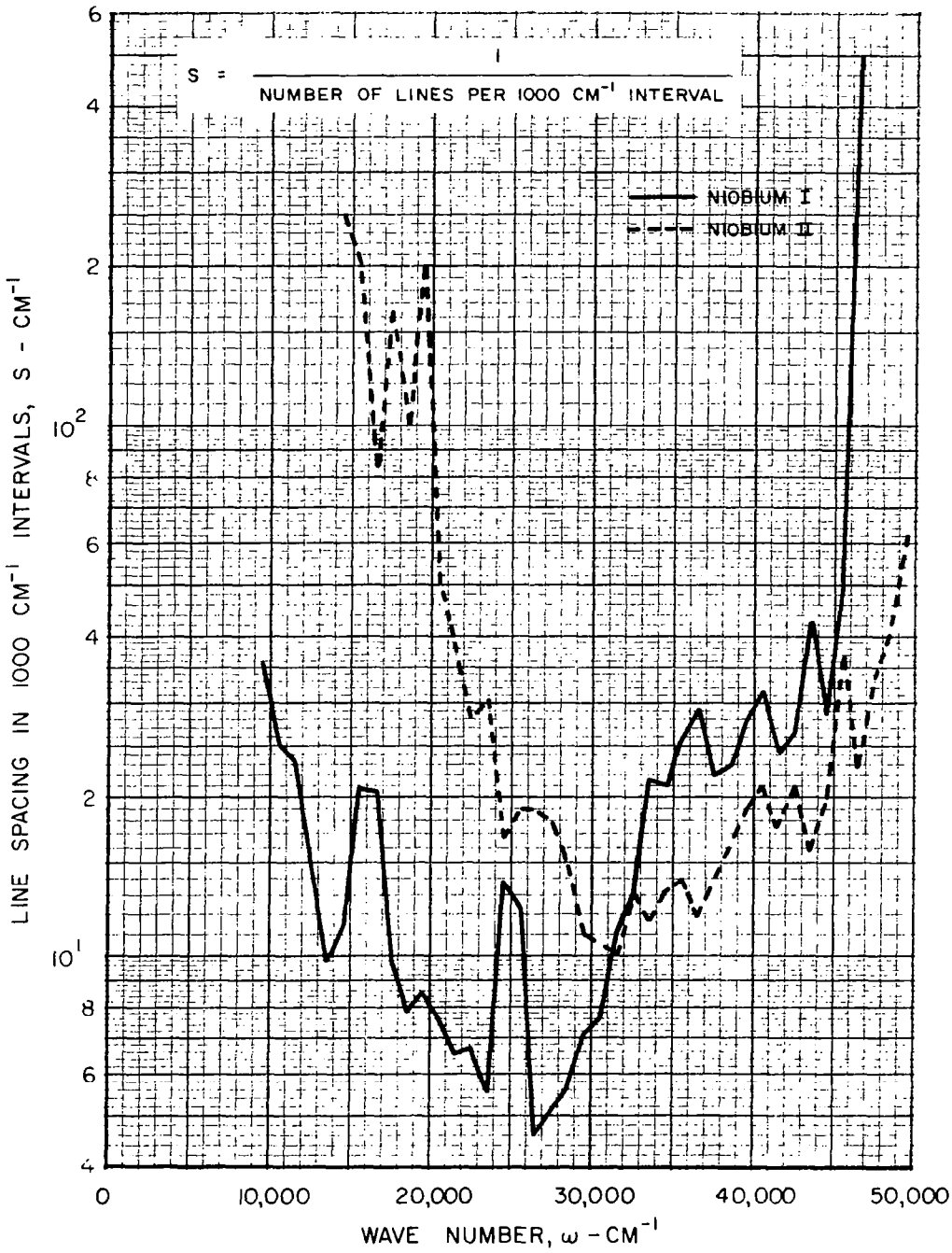

FIG. 40

LOCAL AVERAGE SPACING IN 1000 CM^{-1} INTERVALS FROM EXPERIMENTAL LINE STRUCTURES OF VANADIUM I AND VANADIUM II

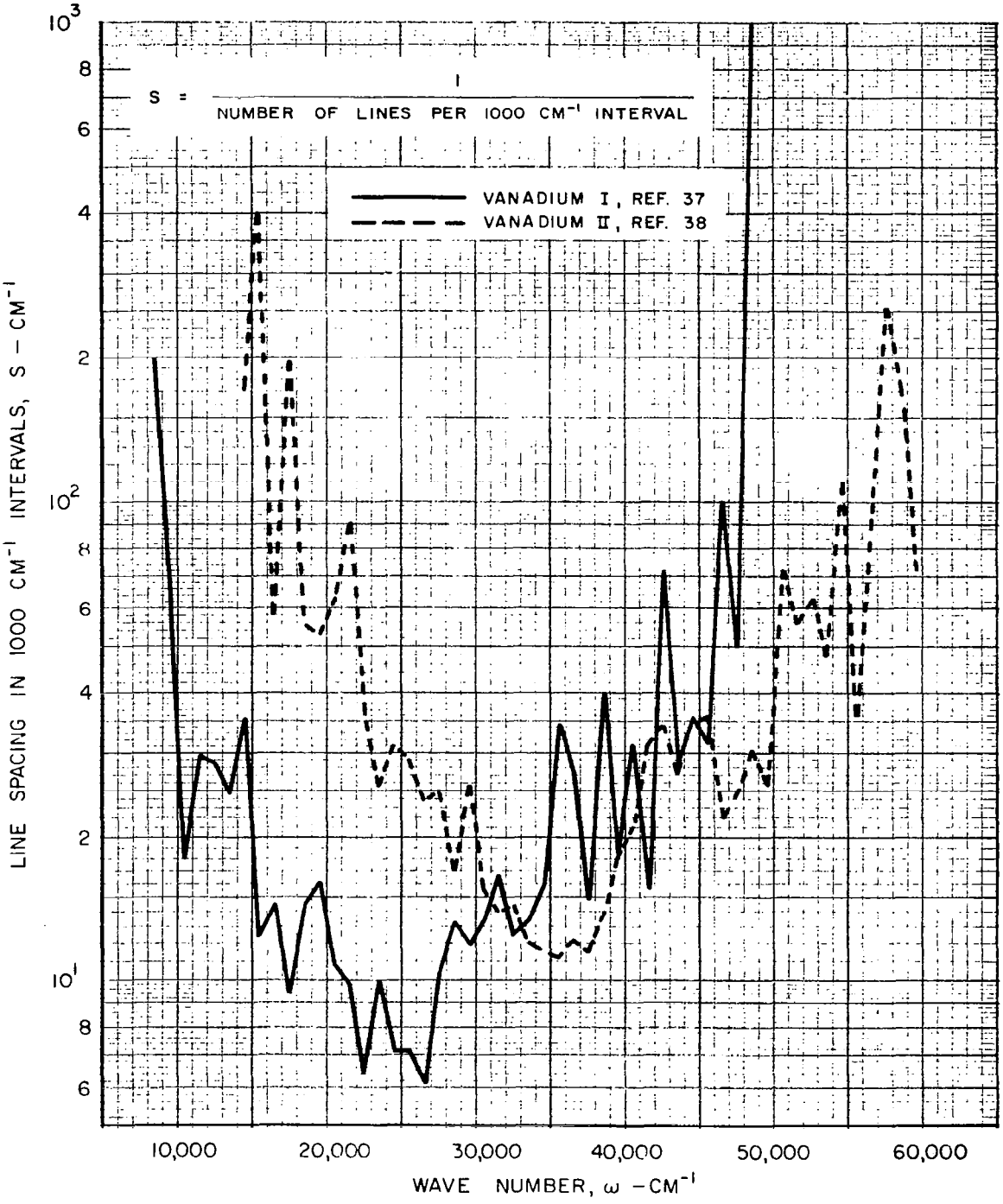

RELATIVE TOTAL LINE INTENSITY PER 1000 CM^{-1} INTERVAL AS A FUNCTION OF WAVE NUMBER CALCULATED FROM EXPERIMENTAL LINE INTENSITIES OF IRON I

REF 32

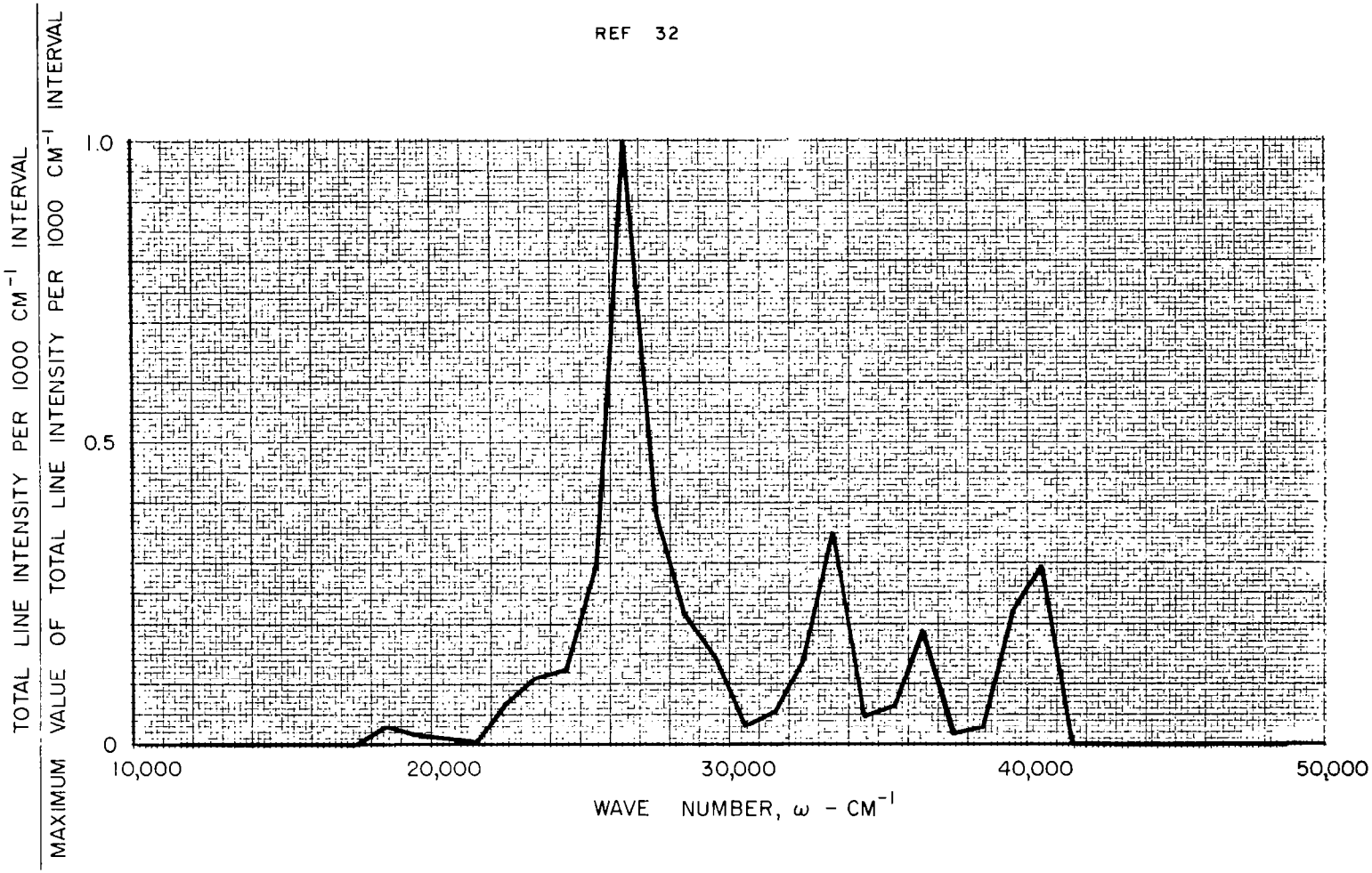

FIG. 41

RELATIVE TOTAL LINE INTENSITY PER 1000 CM^{-1} INTERVAL AS A FUNCTION OF WAVE NUMBER CALCULATED FROM EXPERIMENTAL LINE INTENSITIES OF SILICON I

REF. 34

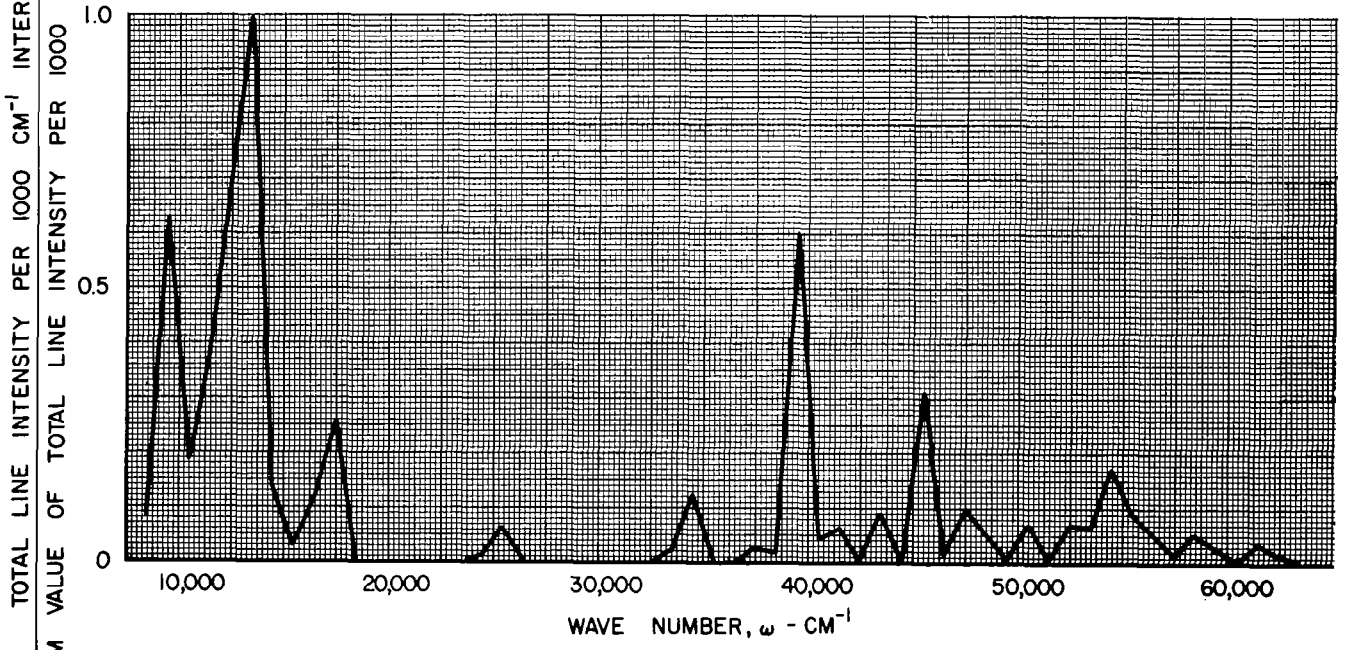

FIG. 42

RELATIVE TOTAL LINE INTENSITY PER 1000 CM^{-1} INTERVAL AS A FUNCTION OF WAVE NUMBER CALCULATED FROM EXPERIMENTAL LINE INTENSITIES OF URANIUM I

REF. 35

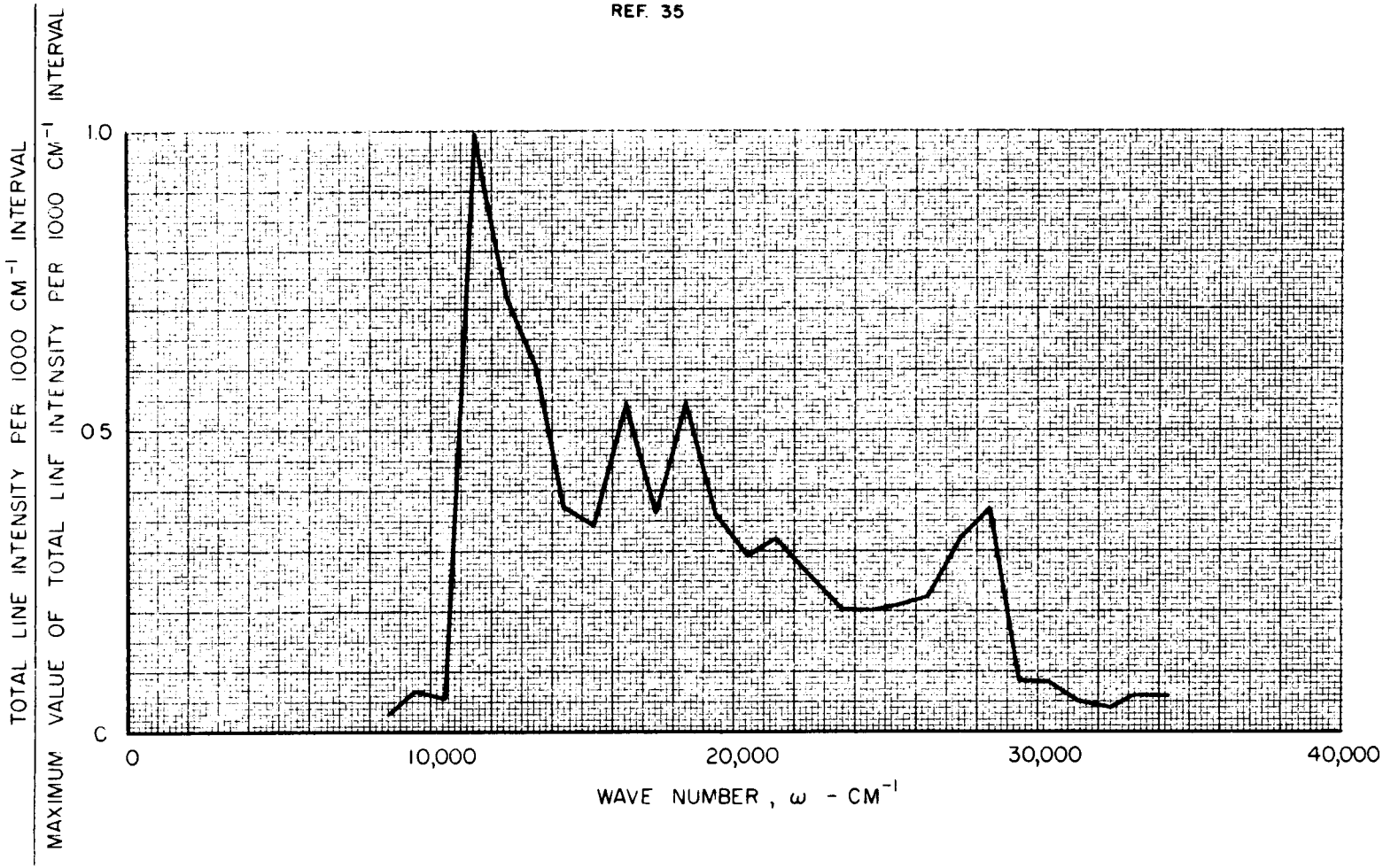

FIG. 43

RELATIVE TOTAL LINE INTENSITY PER 1000 CM^{-1} INTERVAL AS A FUNCTION OF WAVE NUMBER CALCULATED FROM EXPERIMENTAL LINE INTENSITIES OF NIOBIUM I AND NIOBIUM II

REF. 36

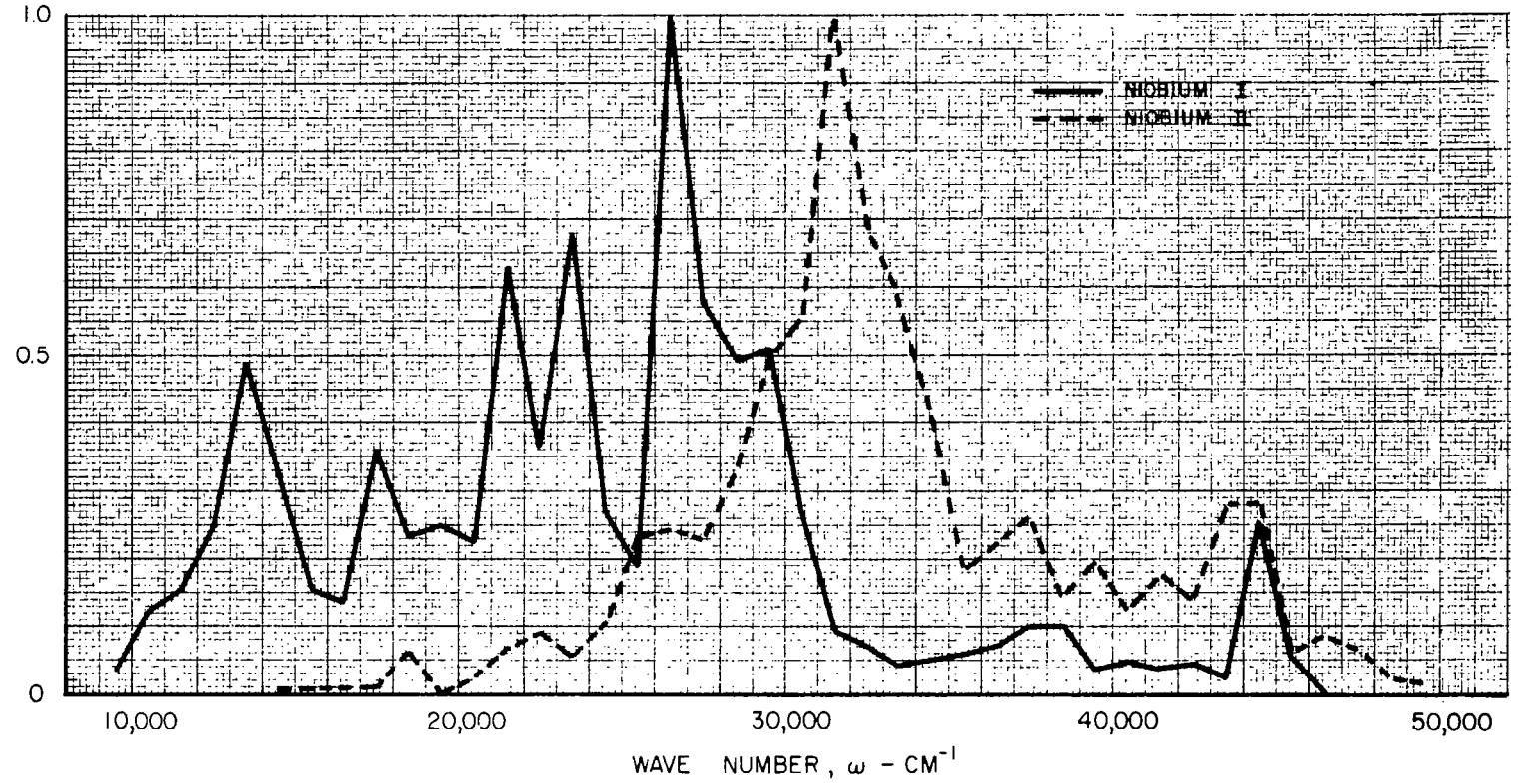

FIG. 44

RELATIVE TOTAL LINE INTENSITY PER 1000 CM^{-1} INTERVAL AS A FUNCTION OF WAVE NUMBER CALCULATED FROM EXPERIMENTAL LINE INTENSITIES OF VANADIUM I AND VANADIUM II

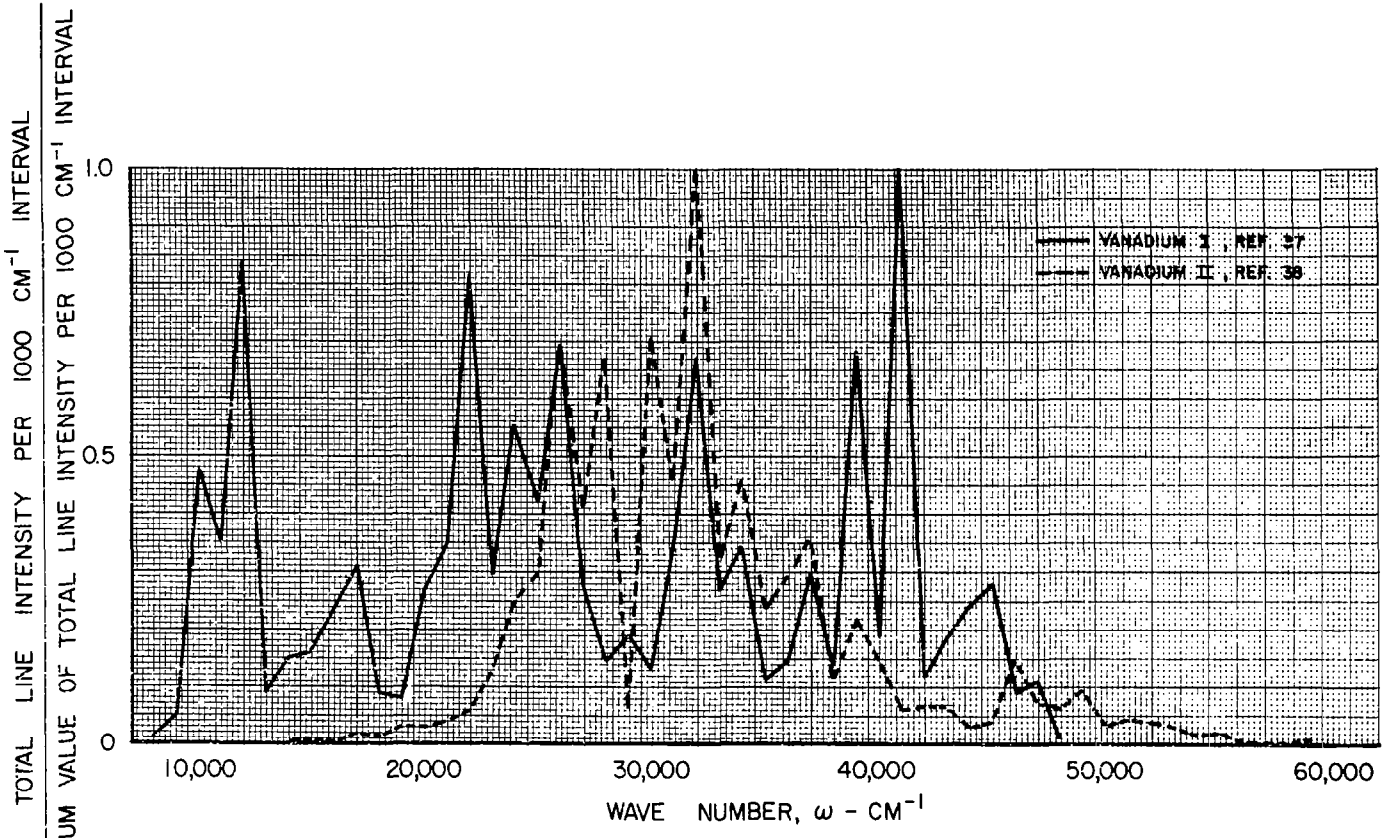

FIG. 45